Lignin First Biorefinery Approach and Lignin Valorization

Von der Fakultät für Mathematik, Informatik und Naturwissenschaften der RWTH Aachen University zur Erlangung des akademischen Grades einer Doktorin der Naturwissenschaften genehmigte Dissertation

vorgelegt von

Leonie Schoofs, Master of Science

aus

Xanten

Berichter: Prof. Dr. Walter Leitner

PD Dr. Holger Klose

Tag der mündlichen Prüfung: 15.09.2025

Diese Dissertation ist auf den Internetseiten der Universitätsbibliothek verfügbar.

Sworn Declaration

I, Leonie Schoofs hereby declare under oath that this dissertation and the content presented therein are entirely my own work and have been independently generated as the result of original research. Specifically, I declare:

1. This work was completed entirely while in candidature for a doctoral candidate at this faculty and university.

2. If any part of this dissertation was previously used for an academic degree or other qualification at this or any other institution, it has been clearly indicated.

4. Whenever other publications, either my own or those of third parties, were consulted, they have been explicitly cited.

5. All substantial sources of support have been acknowledged.

6. Whenever any part of this dissertation is based on collaboration with others, I have clearly indicated which contributions were made by others and which were made by myself.

7. Parts of this work have been published. A comprehensive list of all publications arising from this work, including a clear specification of my individual contributions, is provided on the following page.

Aachen,

The practical work of this thesis was performed from March 2020 to May 2024 at Forschungszentrum Jülich (FZJ) under the supervision of Dr. Philipp Grande and Dr. Holger Klose.

Parts of this work have been presented at conferences or published in scientific journals.

"*Fractionation of Lignocellulosic Biomass using the OrganoCat Process*" L. Schoofs, D. Weidener, U. Schurr, H. Klose, P.M. *Grande, J. Vis. Exp*., **2021,** *172, e61933* (doi:10.3791/61933-v)

My specific contributions include: study design: 30%; laboratory work: 100%; data processing and interpretation: 10%; manuscript drafting and revision: 80%.

"*Processing lignocellulose to extract lignin with designed properties*" ACS Spring Meeting 2022, San Diego, USA, 21. March 2022. Talk

My specific contributions include: study design: 90%; laboratory work: 80%; data processing and interpretation: 90%; presentation design and delivery: 100%.

"*Structural Changes of Lignin during OrganoCat Processing*" L.Schoofs, B. Thiele, T. Langletz, S. Herres-Pawlis, A. Jupke, P. M. Grande, H. Klose, *Energy Fuels,* **2023**, *38, 5*, 4192–4202. (doi:10.1021/acs.energyfuels.3c03673)

My specific contributions include: study design: 80%; laboratory work: 90%; data processing and interpretation: 90%; manuscript drafting and revision: 70%.

"*Lignocellulose Treatment Using a Flow-Through Variant of OrganoCat Process*" L. Schoofs, D. Weidener, W. Leitner, H. Klose, P. M. Grande, ChemSusChem, **2024** (doi:10.1002/cssc.202401063)

My specific contributions include: study design: 90%; laboratory work: 90%; data processing and interpretation: 90%; manuscript drafting and revision: 50%.

"*Time-Resolved Analysis of Lignocellulose Extraction in a Biphasic OrganoCat Flow-Through System"*, L. Schoofs, H. Klose, P.M. Grande, manuscript in preparation

My specific contributions include: study design: 90%; laboratory work: 90%; data processing and interpretation: 80%; manuscript drafting and revision: 30%.

Acknowledgements

I would like to express my sincere gratitude to everyone who supported me throughout this research journey.

First, I would like to thank Prof. Dr. Walter Leitner, my first examiner, for his guidance and valuable feedback throughout the course of this project. I would also like to thank Prof. Ulrich Schurr, head of the Institute for Plant Science (IBG-2) of Forschungszentrum Jülich, for welcoming me to his institute and his support.

At IBG-2, my deepest gratitude goes to my second examiner, Dr. Holger Klose, the head of the 'Alternative Biomasses and Biorefinery Concepts (ABB)' group, for his valuable feedback, support, and encouragement throughout my research. I also want to thank my daily supervisor, Dr. Philipp M. Grande, for his continuous guidance, constructive feedback, and fruitful discussions. I am also grateful to my colleagues from the ABB group, particularly the laboratory assistants Dagmar Drobietz, Tom Hübner, and Benedict Ohrem for their instrumental help with analytics, as well as the apprentices Vanessa Ploeger and Annika Ruers for their contributions. Special thanks to my PhD peers Jimena Martinez Diaz, Jane Mademann, and Dr. Sophie Weber for their ongoing support, advice, and many coffee chats. I am also grateful to Dr. Björn Thiele for his expertise and work on Py-Gc-Ms measurements.

At IET-1, I sincerely thank Dr. Hermann Tempel and Dr. Hans Kungl for their collaboration on the electrospinning of lignin project, and especially Victor Selmert for his hands-on experimental contributions. I would also like to acknowledge William von Westarp and Tim Langletz at RWTH Aachen for their essential support with SEC and HSQC-NMR analytics.

During my research stay at the University of British Columbia (UBC), I am grateful to Prof. Shawn Mansfield and his group for providing poplar samples, hosting me, and the opportunity to conduct experiments in their labs. Special thanks to my office colleagues, Sydne Guevara and Melike Karaca-Bulut, for their warm welcome and support. I would also like to thank Prof. Scott Renneckar and his group for their help with vacuum drying, analytics, and electrospinning equipment and Muzaffer A. Karaaslan for his invaluable assistance. I am also thankful to Deutscher Akademischer Austauschdienst (DAAD) for awarding me the scholarship that enabled me to carry out research in Canada for five months.

Finally, I wish to express my deepest gratitude to my family for their unwavering support throughout my life and to my friends and loved ones for their constant encouragement, patience, and belief in me.

Abstract

The transition to renewable resources requires efficient and sustainable methods for the valorization of lignocellulosic biomass. Lignin, a complex and variable component of lignocellulose, presents challenges for full utilization due to its structural heterogeneity, which can limit its applications to low-value energy recovery. This thesis investigates an acid-catalyzed biphasic fractionation process to optimize lignin extraction from various plant sources and enhance the product yield, quality, and application potential.

By conducting a comprehensive biomass screening of ten different plant types, including hardwoods, agricultural waste products, and grasses, correlations between lignocellulose structure and extraction behavior were established. This thesis found that plants with similar structural properties exhibited comparable extraction efficiencies and product qualities, enabling potential plant selection for tailored lignin applications.

A semi-continuous flow-through (FT) OrganoCat process was developed to provide insights into the fractionation kinetics and reaction dynamics, revealing that temperature significantly affects both lignin and sugar extraction. The time-resolved analysis further clarified the sequential release of lignin and sugars, shedding light on the structural organization of lignocellulose in different plant species. Furthermore, the research explored electrospinning as a method for lignin valorization, focusing on how structural attributes, such as the syringyl/guaiacyl (S/G) ratio, influence fiber formation. Eucalyptus lignin, with its higher S/G ratio, demonstrated superior electrospinning performance, suggesting the feasibility of producing carbon nanofibers from lignin for advanced materials.

The findings presented in this thesis offer a basis for selecting optimal biomass and process conditions to achieve specific product goals, thereby advancing the utility of lignocellulosic biomass in sustainable material production. This work contributes to the broader field of renewable resources by laying a foundation for improved biorefinery designs, with implications for materials science, sustainable energy, and bioeconomy.

Kurzbeschreibung

Der Übergang zu erneuerbaren Ressourcen erfordert effiziente und nachhaltige Methoden zur Verwertung von lignozellulosehaltiger Biomasse. Lignin, eine komplexe und strukturell variable Komponente der Lignozellulose, stellt aufgrund seiner Heterogenität eine Herausforderung für eine vollständige Nutzung dar und wird daher oft auf Anwendungen mit geringem Mehrwert, wie die Energiegewinnung, beschränkt.

Diese Arbeit untersucht einen säurekatalysierten, biphasischen Fraktionierungsprozess um die Ligninextraktion aus verschiedenen Pflanzenarten zu optimieren und die Ausbeute, Qualität und Anwendungspotenziale der Produkte zu verbessern. Durch ein umfassendes Biomassenscreening von zehn verschiedenen Pflanzentypen konnten Zusammenhänge zwischen der Struktur der Lignozellulose und dem Extraktionsverhalten festgestellt werden. Die Studie zeigt, dass Pflanzen mit ähnlichen strukturellen Eigenschaften vergleichbare Extraktionseffizienzen und Produktqualitäten aufweisen, was eine gezielte Auswahl von Pflanzen für maßgeschneiderte Ligninanwendungen ermöglicht.

Eine semi-kontinuierliche Durchflussvariante des OrganoCat-Prozesses (FT) wurde entwickelt, um Einblicke in die Fraktionierungskinetik und Reaktionsdynamik zu gewinnen. Dabei zeigte sich, dass die Temperatur sowohl die Lignin- als auch die Zuckerextraktion stark beeinflusst. Zeitaufgelöste Analysen verdeutlichten die schrittweise Freisetzung von Lignin und Zuckern und lieferten neue Erkenntnisse über die strukturelle Organisation der Lignozellulose in verschiedenen Pflanzenarten. Darüber hinaus wurde Elektrospinning als Methode zur Ligninvalorisierung untersucht, wobei der Fokus darauf lag, wie strukturelle Merkmale wie das Verhältnis von Syringyl- zu Guaiacyl-Einheiten (S/G-Verhältnis) die Faserbildung beeinflussen. Eukalyptuslignin, das ein höheres S/G-Verhältnis aufweist, zeigte bessere Eigenschaften im Elektrospinning und demonstriert so, welches Lignin für die Herstellung von Kohlenstoffnanofasern für fortschrittliche Materialien geeignet ist.

Die in dieser Arbeit gewonnenen Erkenntnisse bieten eine Grundlage für die Auswahl optimaler Biomasse- und Prozessbedingungen, um spezifische Produktziele zu erreichen und die Nutzung von Lignozellulose in der nachhaltigen Materialproduktion voranzutreiben. Die Arbeit leistet einen wichtigen Beitrag im Bereich der erneuerbaren Ressourcen, indem sie eine Grundlage für verbesserte Bioraffineriekonzepte schafft.

Table of Contents

1 Introduction 1
1.1 Motivation 1
1.2 Lignocellulose 3
1.2.1 Cellulose 3
1.2.2 Hemicellulose 4
1.2.3 Lignin 5
1.2.4 Interactions between hemicellulose, cellulose and lignin 7
1.3 Plant biomass as resource for biorefineries 8
1.4 Biorefineries 10
1.4.1 The OrganoCat process 12
1.4.2 Flow through biomass fractionation 14
1.5 Biomass fractionation and lignin depolymerization mechanisms 17
1.6 Lignin valorization 17
1.6.1 Electrospinning of lignin 19
2 Aim of the Thesis 22
3 Results and Discussion 23
3.1 Assessing lignin diversity 23
3.1.1 Biomass selection for inter-species comparison 23
3.1.2 Fractionation efficiency for different biomass materials 28
3.1.3 Lignin structure analysis and comparison 32
3.1.4 Molecular size of the extracted lignin 39
3.1.5 Impact of lignin structure on delignification and lignin quality 43
3.1.6 How Biomass Properties Affect Fractionation and Lignin Quality 45
3.2 Investigation of intra-species differences 47
3.2.1 Poplar sample selection 48
3.2.2 Fractionation yields 49
3.2.3 Lignin structure evaluation 52
3.2.4 Thermal properties of the extracted lignin 54
3.2.5 Conclusions on the impact of intra-species lignin content and structure differences on biomass fractionation 56
3.3 Flow through OrganoCat variation 58
3.3.1 Establishing the reaction 59
3.3.2 Assessing the flow through process setup 59
3.3.3 Exploring reaction variables using Design of Experiments (DOE) 64
3.3.4 Upscaling the FT OrganoCat 74
3.4 Time-resolved lignin and sugar fractions for mechanistic and structural process analysis 76

3.4.1 Time resolved yields at different process temperatures 76
3.4.2 Compositional Analysis of pulp 79
3.4.3 Time resolved structural analysis of lignin 81
3.4.4 Compositional Analysis of extracted sugars 84
3.4.5 Detailed examination of sugar extraction within 20 minutes 89
3.4.6 Comparing FT extraction patterns of beech and miscanthus 92
3.4.7 Comparing hemicellulose hydrolysis of miscanthus and beech 94
3.5 Electrospinning of selected OrganoCat lignin 99
3.5.1 Electrospinning of poplar OrganoCat lignin 99
3.5.2 Selection of lignin source for electrospinning 101
3.5.3 Electrospinning of OrganoCat lignin from different biomass sources 102
3.5.4 Conclusions for the electrospinning of OrganoCat lignin 105
4 Summary, Conclusion and Outlook 107
5 Materials and Experimental procedures 110
5.1 Chemicals 110
5.2 Plant material 110
5.3 High pressure laboratory equipment 111
5.4 Analytical methods 112
5.5 Biomass pretreatment 119
5.6 Statistical analysis 122
6 References 125
7 List of Figures and Tabels 132
8 Appendix 137
8.1 Principal component analysis 137
8.2 Sugar composition, biomass material screening 138
8.3 Additional HSQC-NMR Spectra 139
8.4 Py-GC-MS 140
8.5 Correlations between lignin parameters 143
8.6 Full ANOVA for DOE 144
8.7 Time resolved sugar yields, beech 146
8.8 Time resolved sugar yields, miscanthus 149

Abbreviation index

Abbreviation	Full description
2FI	two factor interaction
2-MTHF	2-Methyltetrahydrofuran
ABSL	acetyl bromide soluble lignin
AIR	alcohol insoluble residue
ANOVA	analysis of variance
Ara	Arabinose
ASC	alcohol soluble components
CrC	crystalline cellulose
dAIR	destarched alcohol insoluble residue
DMF	dimethylformamide
DOE	design of experiments
FDCA	2,5-furandicarboxylic acid
FT	flow through
Fuc	fucose
FZJ	Forschungszentrum Jülich
Glc	galactose
GlcA	galacturonic acid
Glu	glucose
GluA	glucoronic acid
GM	glucomannan
HMF	5-hydroxymethylfurfural
HPAEC-PAD	high-performance anion exchange chromatography with pulsed amperometric detection
HPLC	High-Performance Liquid Chromatography
HSQC-NMR	2D ^{1}H-^{13}C- heteronuclear single quantum correlation nuclear magnetic resonance spectroscopy
IC	Ion chromatography
KL	Kraft lignin
LCC	lignin carbohydrate complex
Man	mannose
MeGlcp-Xylan	O-acetyl-4-O-methylglucuronxylan
OA	oxalic acid
P	Pearson coefficient
p	significance (*p*-value)
PA	phosphoric acid

PAHBAH	4-hydroxybenzhydrazine
PCA	principal component analysis
PEO	polyethylene oxide
PS	polystyrene
Py-GC-MS	Pyrolysis-Gas Chromatography-Mass Spectrometry
RFC	reductive catalytic fractionation
Rha	rhamnose
RSM	response surface methodology
SEC	size exclusion chromatography
THF	tetrahydrofuran
wt%	weight percentage
XG	xyloglucan
Xyl	xylose

1 Introduction

1.1 Motivation

With fossil fuel depletion and the accelerating climate crisis, renewable feedstock represents the best path towards a sustainable, low-carbon economy. This shift is not merely a choice, but a necessity for ensuring a sustainable, low-carbon economy that can support future generations.[1]

In today's industrial landscape, fossil fuels continue to dominate as the primary source of energy and materials, contributing to significant carbon dioxide (CO_2) emissions and accelerating climate change.[2] As the world faces multiple challenges, environmental and political, the availability and price of fossil fuels, along with their environmental impact, drive the move to renewable sources—not just in the energy sector but also in the production of materials in the chemical industry. Within the EU Bioeconomy Strategy, one if the main goals is to reduce dependence on non-renewable, unsustainable resources.[3] Lignocellulosic biomass offers a compelling alternative, providing a vast reservoir of renewable carbon that can be transformed into clean fuels and value-added chemicals.[4–6]

Historically, the processing of lignocellulose, the cell wall material of plants, has focused on cellulose for pulp and paper production. However, modern biorefinery concepts aim to holistically utilize the entire lignocellulosic structure.[7,8] Among its components, lignin is the largest source of aromatic compounds, presenting opportunities for applications ranging from the medical field to fuel production. Nevertheless, due to its complex structure, lignin has been challenging to process and is often underutilized.[9] Currently, of the estimated 100 million tons of lignin produced worldwide each year, less than 2% are sold with the rest mainly being burned for energy recovery in the production process.[10]

The inherent inhomogeneity of plant cell walls complicates effective utilization of lignocellulosic biomass. Depending on the plant type and growing environment, the complex interplay of cellulose, hemicellulose, and lignin varies, significantly influencing the processing yields and quality of the fractionated products. Structural molecular differences, particularly in hemicellulose and lignin add to the diversity.[5,11,12]

This thesis aims to deepen the understanding of biorefinery concepts designed to fractionate lignocellulose from diverse sources into product streams. A variety of plant materials have

been used to investigate how a plant's chemical structure and the subsequent processing conditions affect the quality of the resulting lignin and sugars. Particular emphasis was placed on lignin, with the goal of preserving most of its native structure during processing. The structural differences in the extracted lignin were analyzed in detail and assessed for their potential applications, with electrospinning for carbon nanofiber production serving as a prime example of valorization. A flow-through process concept was employed to gain further insights into the kinetics of biomass disintegration, enabling a detailed assessment of the lignocellulosic structure, particularly the complex interplay between hemicellulose and lignin.

Understanding the influence of plant source selection on lignin valorization, the process of converting lignin into valuable products rather than discarding it as waste, is vital for developing efficient biomass processing technologies. By enhancing the quality of lignin, this work aims to contribute to a knowledge-based bioeconomy, where resources are used holistically, waste is minimized, and resources are continually repurposed. Such advancements not only offer sustainable alternatives to fossil-derived products, but also support broader environmental goals, fostering a more resilient economy that respects the finite nature of our planet's resources.

1.2 Lignocellulose

Lignocellulosic biomass plays an important role in the production of sustainable materials. Lignocellulose accounts for approximately 70% of the plant biomass on earth, making it the most abundant renewable resource available. Lignocellulosic biomass originates from non-edible plant residues in agriculture, forests, and energy crops. It is a renewable, inexpensive and abundantly available resource.[13]

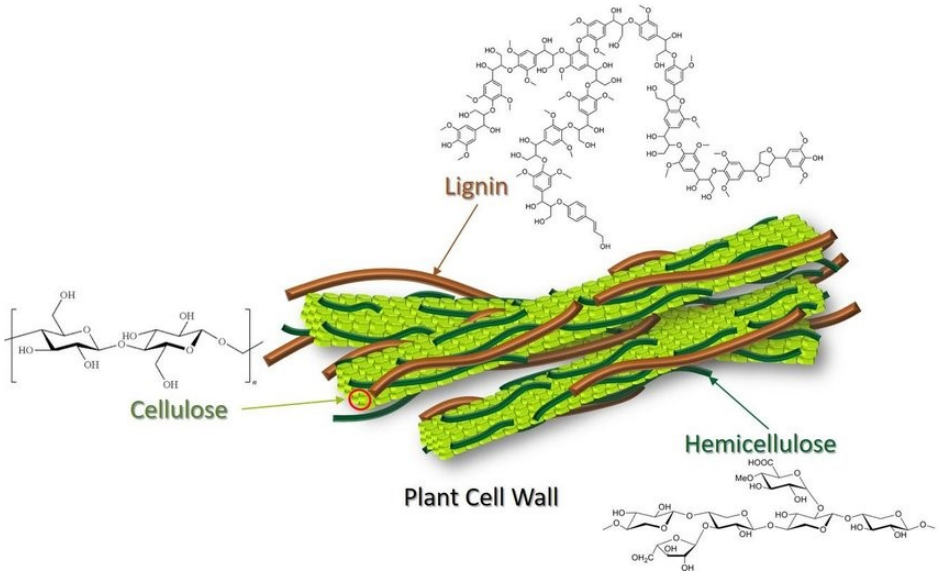

Figure 1: Schematic depiction of the structure of lignocellulose as found in the plant cell wall with examples of the molecular structures of its components.

Lignocellulose consists primarily of cellulose, lignin, and hemicellulose. Additional constituents, such as pectin, proteins, waxes, and minerals are present in varying proportions. Cellulose, hemicellulose, and lignin form a complex three-dimensional network that provides the plant with its recalcitrance towards degradation and structural integrity (Figure 1).[14]

1.2.1 Cellulose

Cellulose is, at 25-55wt%, the predominant component in lignocellulose.[6,12] It is a linear polysaccharide composed of β-1,4-linked D-glucose monomers. Its primary function is to provide structural support to plant cell walls. Multiple cellulose polymer strands align parallel to form microfibrils.[15] The cellulose macromolecules contain hydroxyl groups that create hydrogen bonds both within and between molecules, leading to the formation of diverse crystalline structures with ordered arrangements. Additionally, amorphous regions exist in cellulose microfibrils where the crystalline structure has not formed or has been disrupted.[16]

1.2.2 Hemicellulose

The cellulose fibers are embedded in a matrix of hemicelluloses, which make up 20-40wt% of the biomass.[6,12] Hemicellulose serves various functions, but it primarily connects the cellulose fibers and binds to lignin. It is an amorphous and branched polysaccharide composed of different pentoses and hexoses. The most common sugars in hemicellulose are D-xylose, D-mannose, D-glucose, D-galactose, L-arabinose, galacturonic acid and glucuronic acid. Unlike cellulose, hemicelluloses comprises shorter chains with a degree of polymerization value between 80-200 and can be hydrolyzed easier by weak acids or bases.[17]

The composition of hemicelluloses exhibits significant variability among species, developmental stages, and morphological locations; however, it can be characteristic of specific plant types and species. Hardwood hemicellulose is typically categorized into three main classes based on its structural properties. The primary hemicellulose component in hardwood is O-acetyl-4-O-methylglucuronxylan (MeGlcp-Xylan) (15-30%). Its core structure is composed of β-D-xylanopyranose with 4-*O*-methyl-α-D-glucuronic acid attached as a side group. The molar ratio of glucuronic acid to xylose ranges from 1:4 to 1:16 depending on the extraction and purification methods used. The main xylose chain also features acetyl substituents. The second most common hemicellulose in hardwoods, comprising 2-5%, is glucomannan (GM). This linear polymer is made up of β-D-glucose and β-D-mannose units. The ratio of glucose to mannose varies between 1:1 and 1:2, based on the hardwood species. Some mannose residues in GM can be O-acetylated. Xyloglucan (XG) is found in the primary cell walls of hardwood, with higher concentrations in dicots and lower concentrations in monocots. Its main chain is composed of D-glucose, and approximately 75% of the glycosyl residues have D-xylose substitutions on their backbone.[18]

Arabinoxylan is the primary hemicellulose in *gramineae* (grasses). Its structure comprises a linear backbone of D-xylose units, with individual L-arabinose units attached as lateral branches. Studies have demonstrated that arabinosyl groups in grass cell walls undergo acetylation to varying degrees by ferulate and *p*-coumarate. Furthermore, *gramineae* plants contain another hemicellulose, mixed-linkage glucan (β-(1→3, 1→4).glucan), which is composed of linear chains of glucosyl residues without substitutions or branches.[18]

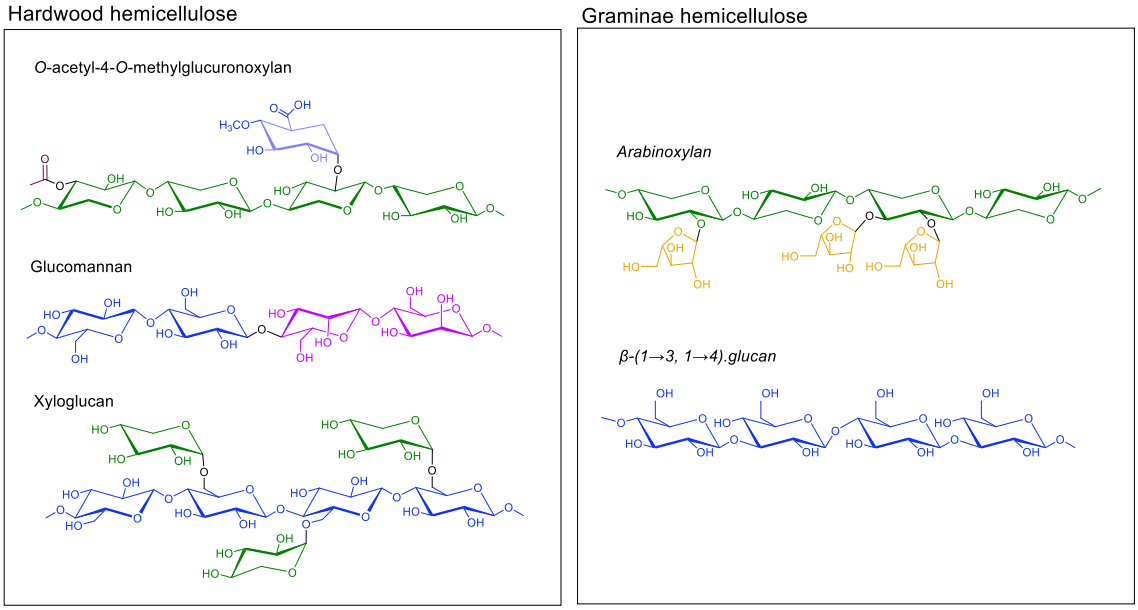

Figure 2: Example structures of the most common hemicellulose structures found in hardwoods and *Gramineae* (grass) cell walls.

1.2.3 Lignin

Lignin is primarily present in secondary plant cell walls and constitutes 10-30% of the biomass.[6,12] The proportion of lignin within a plant can vary significantly and is influenced by factors such as the plant species, the type of tissue being measured, and its developmental stage. Lignin is essential for maintaining the structural integrity, strength, and water impermeability of plants, as well as providing resistance against microbial attac. Additionally, it acts as a binding agent to hold adjacent cells together in the outermost layer of plants.[17,19] Lignin is a cross-linked amorphous macromolecule synthesized through oxidative radical polymerization of phenylpropane monomers, known as monolignols. The three most common monolignols are coniferyl, sinapyl, and *p*-coumaryl alcohols, which form guaiacyl (G), syringyl (S), and *p*-hydroxyphenyl (H) subunits, respectively. They are characterized by the number of methoxy side groups on the phenolic ring, as depicted in Figure 3.[17]

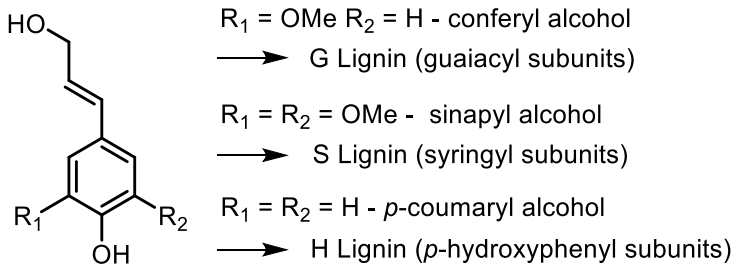

Figure 3: Chemical structure of the three main subunits of lignin: conferyl alcohol, synapyl alcohol, and *p*-coumaryl alcohol.

The quantity, molecular weight, and composition of lignin can vary depending on the plant species and the specific part of the plant or developmental stage. Lignin from gymnosperms, such as pine and other conifers, primarily comprise of G-lignin with up to 5% H-lignin and minimal S-lignin subunits. G- and S-lignin are more prevalent in angiosperms, including hardwoods such as poplar and beech, with significantly lower levels of H-lignin. A notable distinction between monocots and dicots is the proportion of H-lignin, with monocots containing 4-15% H-units and dicots containing only trace amounts.[19] By employing bioengineering techniques, it is possible to favor the production of a specific lignin subunit (S/G/H).[17,20]

The process of polymerization of monolignols in cell walls is initiated through dehydration and subsequent oxidation, leading to the formation of a free radical that can randomly couple with another monolignol or lignin oligomer. This results in the creation of a polymer with diverse bonds, primarily carbon-carbon (C-C) or ether bonds. The most prevalent bond in lignin is the aryl ether bond, which lies between the β-C atom of the propenyl chain and the phenyl hydroxy group (β-*O*-4). This bond makes up 40-60% of the bonds in lignin and can be cleaved relatively easily.[17] Other commonly found linkages in lignin are the phenylcoumaran (β-5) and resinol (β-β) structures, which include direct C-C coupling (Figure 4).

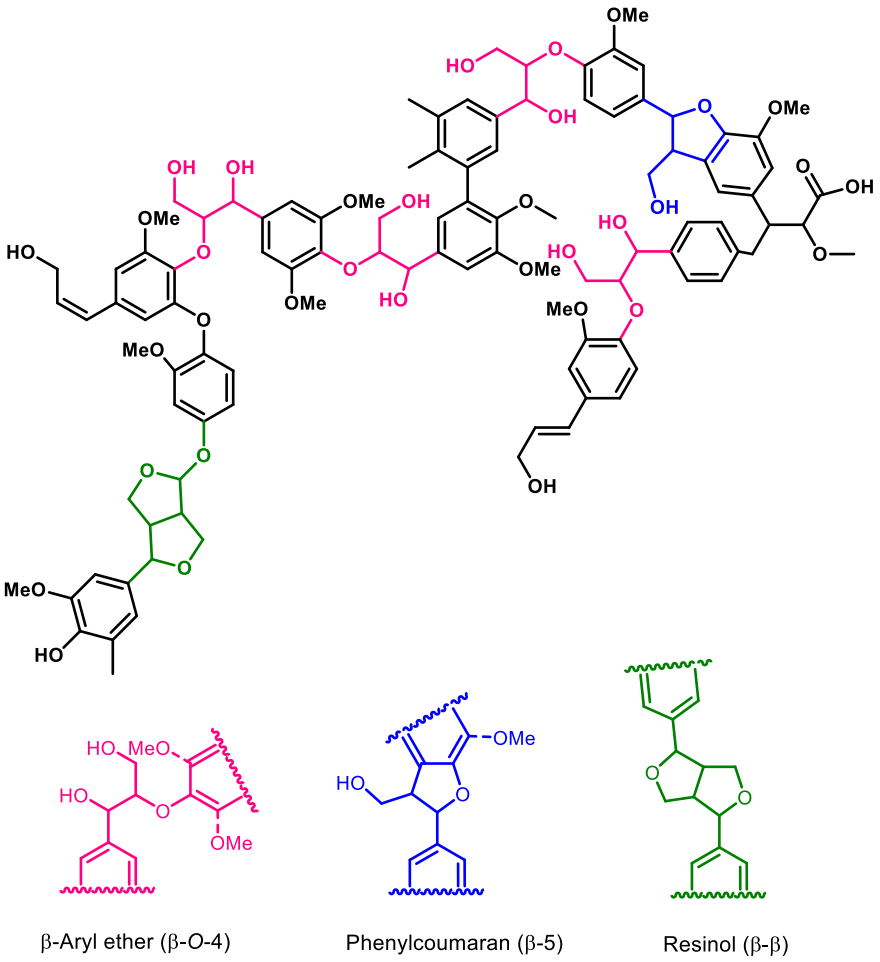

Figure 4: Example structure of a small lignin molecule with the three most commonly found linkages. The linkages are β-aryl ether (β-*O*-4), phenylcoumaran (β-5), and resinol (β-β).

1.2.4 Interactions between hemicellulose, cellulose and lignin

The interactions between the polysaccharides hemicellulose and cellulose, and the aromatic polymer lignin are complex, and establishing a comprehensive understanding remains the subject of ongoing research. However, elucidating the nature of lignocellulose interactions could potentially lead to enhancement of the fractionation process.

Xylans can occur in two different three-dimensional (3D) structures. Simmons *et al.* suggested that a mayor portion of xylan, which typically forms a three-fold helical screw in solution, flattens into a two-fold helical screw ribbon to closely adhere to the hydrophilic surface of cellulose microfibrils within the cell wall.[21] For the connection between lignin and xylan however, research conducted by Wang *et al.* demonstrated that lignin displays numerous electrostatic interactions with the polar motifs of xylan and preferentially binds to it in a three-fold or distorted two-fold helical screw configuration.[22] Further investigations examined the difference the in carbohydrate–lignin interface and molecular structure of lignocellulose

biomass between grass, hardwood, and softwood. These studies revealed that lignin primarily binds to three-fold xylan in a non-flat conformation through non-covalent bonds, with direct connections also existing between lignin and the junctions of cellulose surface and flat-ribbon xylan, possibly due to molecular crowding.[23] Based on these findings, a 3D model of secondary cell walls in various lignocellulosic biomass types has been proposed, as illustrated in Figure 5. This proposed model of secondary cell walls suggests that lignin preferentially binds to three-fold xylan in a non-flat conformation via non-covalent bonds (hydrogen bonds), with the three-fold xylan not closely bound to cellulose. The three-fold domain connects to the two-fold flat-ribbon region, which covers the smooth surface of cellulose microfibrils. In woody plants, lignin and carbohydrates are more thoroughly mixed compared to grass, resulting in lignin binding to both three-fold and two-fold xylans, as well as cellulose microfibrils.[23]

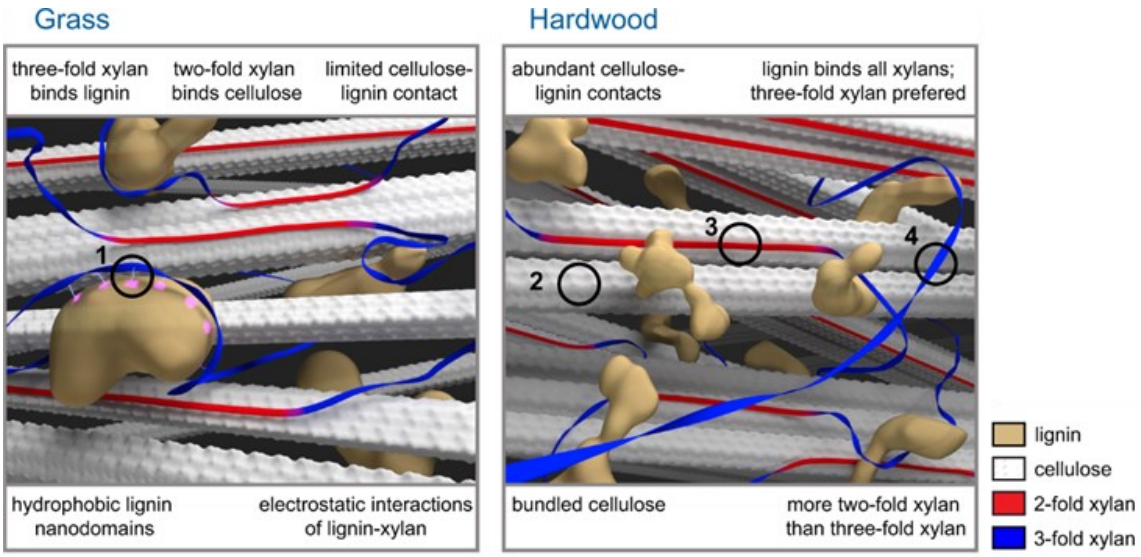

Figure 5: Model of cellulose, hemicellulose, and lignin interactions in hardwoods and grasses. Adapted from Kirui *et al*..[23]

Lignin can be chemically bound to carbohydrates to form lignin carbohydrate complexes (LCCs). While further research is needed in this area, there is evidence suggesting the presence of α-ether bonds between lignin and hemicellulose.[24] LCCs mainly play a role in woods. In hardwoods, 47-66% of all lignin moieties are bound to carbohydrates, mainly hemicellulose.[25]

1.3 Plant biomass as resource for biorefineries

When selecting plant material for large-scale biorefinery applications, several essential factors must be considered to maximize efficiency, sustainability, and profitability. As described above, the structural characteristics of the lignocellulose, such as lignin content, cellulose

crystallinity, and hemicellulose composition, significantly influence the yield, ease of processing, and quality of end products. These characteristics dictate how easily the biomass can be broken down and converted into various bio-based chemicals, fuels, and materials.[26]

Beyond structure, economic, environmental, and ethical considerations are crucial for biomass selection. From an economic perspective, biomass sources should be locally abundant and affordable, reducing costs associated with transportation and cultivation.[27] Environmentally, sustainable biomass should have a minimal ecological footprint, ideally requiring limited water, fertilizers, and pesticides. It is also critical that selected biomass does not compete with food crops for land to avoid contributing to food insecurity—known as the "food versus fuel" issue.[28]

Biomass sources should be fast-growing and renew quickly to ensure a steady year-round supply for continuous processing. Additionally, resilient biomass types that withstand climate stress contribute to the sustainability of biorefineries by reducing reliance on inputs such as irrigation and fertilizers The plants should have high resilience to environmental stressors such as heat, drought, and soil variability, making them well-suited for the climate challenges present in many agricultural regions.[29] Finally, ethical considerations include ensuring that biomass cultivation supports local communities and ecosystems without disrupting their natural biodiversity. Choosing species that can be grown on marginal or degraded lands, for instance, can help meet these ethical goals while also reclaiming unproductive land for sustainable use .[30]

Trees have long served as a primary lignocellulosic resource, particularly in the pulp and paper industry, due to their high biomass yield and well-established supply chains. Softwoods, such as pine (*Pinus spp.*) and Douglas fir (*Pseudotsuga menziesii*), grow relatively quickly and dominate woody biomass sources in the Northern Hemisphere. Their high guaiacyl (G) lignin content and low hemicellulose acetylation make them more resistant to acidic fractionation, posing challenges for efficient processing.[31] Hardwoods, including beech (*Fagus spp.*) and eucalyptus (*Eucalyptus spp.*), also benefit from established forestry practices and are well suited for biorefinery applications. Their lower lignin content and shorter cellulose fibers enhance processability compared to softwoods, making them advantageous for bio-based chemical and fuel production.[32,33]

Fast-growing grasses, such as switchgrass (*Panicum virgatum*), are promising feedstocks for biorefineries due to their adaptability to marginal lands and minimal input requirements.[34] Emerging energy crops, including *Sida hermaphrodita* and *Silphium perfoliatum*, are currently under research for their high yields over prolonged periods with minimal management needs, which may support efficient, sustainable biorefinery operations. [35]

Agricultural waste products offer a cost-effective means of advancing circular bioeconomy. Byproducts like sugarcane bagasse and nut shells, produced by the food industry, not only help reduce waste but also provide high-lignin biomass that can be leveraged for bioenergy production.[36–38]

Poplars are among the fastest growing trees in temperate forests. Therefore, pulping and papermaking practices for Populus species have a long history. *Populus trichocarpa* has been identified as particularly suited for biomass fractionation because of its amenability to genetic modification, which can enhance solubilization and conversion to biofuels without the need for pretreatment. E.g. monolignol ferulate conjugates were engineered into poplar trees, which resulted in the introduction of unique ester bonds in the lignin backbone. Those bonds are more reactive than the dominant natural ether bonds under acidic or alkaline conditions and “unzip” readily during chemical processing. This new, so called zip-lignin biomass showed increased yields during kraft pulping.[39] Genomic tools can also be used to alter lignin content and composition in poplar, which has been used to assess the impact on cell wall lignin on recalcitrance.[40] Due to the widespread distribution of poplar trees, natural variations exist that exhibit differences in structural characteristics, such as the S/G ratio. These variations within a single species can be utilized to examine how changes in lignin structure affect biomass fractionation.[41]

1.4 Biorefineries

Various methodologies have been developed for the fractionation of biomass components in industrial settings.[6] The predominant focus of these approaches is to extract the cellulose, given its crucial role in the pulp and paper sector, whereas lignin is typically regarded only as a byproduct.

At present, the fractionation process most widely used for the pulp and paper industry is the Kraft process. In this process, wood chips are cooked at 170 °C in an alkaline solution of sodium

hydroxide and sodium sulfide. Lignin and hemicelluloses are solubilized and exit the reactor as an aqueous stream with 15wt% solid content (weak black liquor). The obtained cellulose-rich solid pulp was the primary product of this process. Lignin can be recovered using mineral acid or carbon dioxide, although this is infrequently performed. Typically, it is burned to recover process heat. Kraft lignin contains 1.5-3wt% sulfur in its structure and exhibits a higher percentage of refractory C-C linkages between its monomers due to recondensation. This characteristic renders the depolymerization of Kraft lignin challenging.[42] The average molar mass is reported to be below 10,000 Da, although the range is considerably broad (up to 180,000 Da) due to the severe process conditions.[43]

The sulfite process utilizes aqueous sulfur dioxide along with calcium, magnesium, or sodium as counter ions. The reactor operates at temperatures ranging from 120 to 180 °C for a duration of 1-5 hours. The primary reaction involves sulfonation of lignin through the introduction of sulfonic acid to the α-carbon atoms, resulting in its hydrolysis. The degree of sulfonation per monomer ranges between 0.4 and 0.7, rendering the lignin soluble over a broader pH range. The average molar mass of the lignosulfonate exceeds that of Kraft lignin. Prior to the advent of the Kraft process, the sulfite process served as the predominant pulping method; however, its significance has diminished.[42] Nonetheless, lignosulfonates continue to have important applications. In the *Borregaard* biorefinery in Norway, where 90% of woody biomass is converted into marketable products, lignosulfonates are transformed into vanillin. Another substantial application of lignosulfonates is in the concrete industry, where they function as dispersing and set retarding agents.[44]

The third biomass fractionation process, which has significant industrial applications, accounting for 5% of pulp production, is the soda pulping process. It is primarily utilized in biorefinery operations where biomass is converted into ethanol and other chemical compounds. The lignin and hemicellulose components are solubilized in an aqueous sodium hydroxide solution. This process predominantly uses agricultural waste from annual plants, which possess a lower lignin content compared to wood. Consequently, only 10-15% NaOH is required for delignification.[42] The reaction duration can be relatively brief (1.5 h), and the reaction temperature can range from 120-170 °C.[45] This process yields sulfur-free lignin, which exhibits a lower molar mass than Kraft lignin and lignosulfonates.[42]

Organosolv processes, which utilize low-boiling organic solvents in combination with water, represent an alternative method for lignin fractionation. These processes are not necessarily focused on cellulose as a product, thus enabling specific isolation of the three main components.[42] The resulting organosolv lignin is sulfur-free and less condensed, rendering it more suitable for technical conversion. Despite extensive research and pilot scale tests, the application of organosolv processes on an industrial scale is still limited.[46] Among the most developed organosolv processes are the Alcell and Organocell processes. Reaction conditions vary depending on the specific process. For instance, in the Alcell process, the biomass is subjected to treatment in a 1:1 ethanol and water solution at 190 °C for 1 h.[47] The organosolv processes are nevertheless considered one of the most promising approaches in integrated biorefineries, with potential for high-value utilization of all side-streams.[7]

1.4.1 The OrganoCat process

The OrganoCat process, developed by Domínquez de María *et al.* in 2011, belongs to the category of organosolv-like processes. Utilizing a two-phase system provides a method for performing single-step fractionation of cellulose, hemicellulose, and lignin under mild conditions. In a reactor with a 1:1 ratio of water and 2-methyltetrahydrofuran (2-MTHF), the biomass is subjected to treatment with oxalic acid (OA) as the catalyst. The catalytic depolymerization of hemicellulose subsequently leads to the disentanglement of lignocellulose, which facilitates the extraction of lignin into the organic phase, dissolution of depolymerized hemicellulose sugars in the aqueous phase, and retention of cellulose as a solid residue. The catalyst can be recovered through crystallization from the aqueous solution.[48]

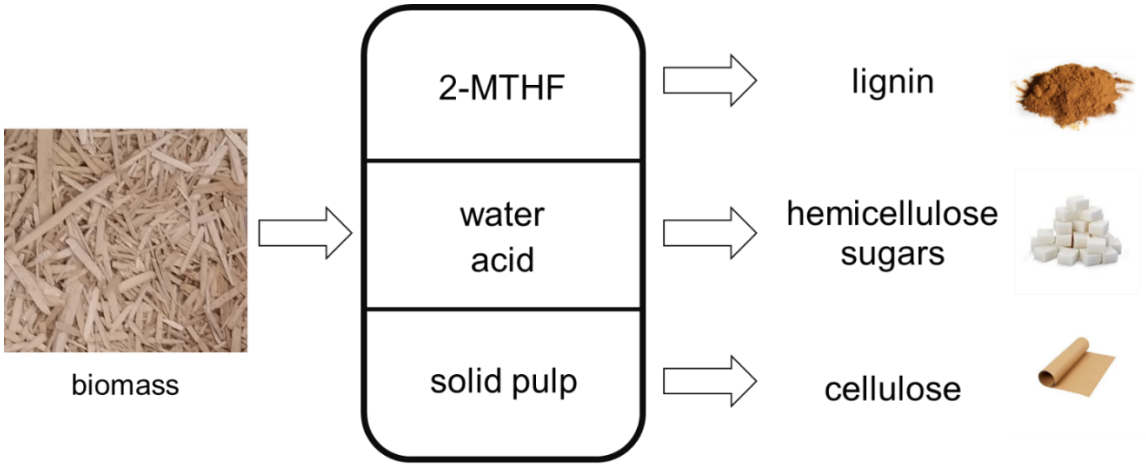

Figure 6: Schematic depiction of the OrganoCat process. Oxalic acid,[48] 2-5-furandycarboxylic acid,[49] and phosphoric acid[50] have been established as organic catalysts. 2-Methyltetrahydrofuran (2-MTHF) is used as organic solvent.

Energetic and economic analyses have demonstrated that the process requires high-value lignin yield and improved solvent recycling to be viable.[51] Consequently, the process was enhanced by reusing the aqueous and organic phases after filtration of the solid cellulose pulp. This approach achieved higher catalyst loadings in a repetitive-batch mode, thereby increasing the economic viability of the process. Up-scaling to a 3 L reactor was successfully demonstrated.[52] Although oxalic acid has proven to be a suitable catalyst, it has several disadvantages. The recovery of the catalyst from the reaction mixture by crystallization requires either cooling the reactor or evaporating water, both of which require significant energy input. Moreover, a substantial amount of oxalic acid is lost in the process due to thermal degradation. Therefore, the investigation of novel biogenic catalysts is essential for process optimization. 2,5-furandicarboxylic acid (FDCA) was identified as another effective catalyst in the OrganoCat process. FDCA exhibits high thermal stability and low solubility in water at room temperature, properties that can be utilized for recovery via pH-shift extraction. Similar to oxalic acid, it can be synthesized from the products of the OrganoCat biorefinery.[49] An alternative variation uses phosphoric acid (PA) as a catalyst. This procedure incorporates a pretreatment step, wherein the lignocellulosic biomass is combined with concentrated (65wt%) phosphoric acid for swelling at 80 °C for 1 h. Subsequently, the two-phase fractionation process is conducted to yield lignin, cellulose, and hemicellulose sugars, which may be directly processed to furfural using the same catalyst and solvent system.[50] Phosphoric acid is known to be able to cause the swelling of cellulose, and reducing crystallinity and making it more accessible to enzymatic degradation.[53] The incorporation of the swelling step with concentrated PA pre-processing reduced the solid residue from 64% to 50% and increased the yield of lignin from 8% to 10%. Additionally, the glucose release rate in enzymatic saccharification was almost three times higher for the processed pulps.[50]

In the aforementioned studies, lignin recovery in the OrganoCat process was achieved through the evaporation of the organic solvent. An alternative approach was investigated wherein lignin was recovered from the 2-MTHF phase of the OrganoCat process via antisolvent precipitation. This method not only potentially reduces the process energy required for solvent recovery but also enables the fractionation of lignin by controlling the quantity of antisolvent. As the amount of antisolvent increases, the molecular weight and the quantity of β-*O*-4 linkages in the obtained lignin fractions decrease. High precipitation yields were

obtained using *n*-pentane and *n*-hexane. *n*-Pentane is the preferred solvent for minimizing energy and antisolvent consumption. However, neither solvent is optimal from an ecological perspective; therefore, further investigation of non-hazardous, bio-based solvents could lead to an optimization of the procedure.[54]

Various biomass sources, including beech wood, mate tea, reed, and spruce[52], as well as sida, silphium, miscanthus, and szarvasi[55], have been examined in the OrganoCat process using oxalic acid as a catalyst. For the process employing FDCA as a catalyst, beech wood has been extensively investigated.[49,54] Furthermore, a study has been conducted to assess the impact of different biomass types on processability with OrganoCat.[56] Multiple biomass sources, namely pineapple, beech wood, eucalyptus, maize cobs, miscanthus, rapeseed, sida, silphium, sugarcane bagasse, and szarvazi, have been examined both in their raw form and after OrganoCat processing with oxalic acid and FDCA catalysis for 3 h. The FDCA-catalyzed OrganoCat process was conducted at 140, 150, and 160 °C. Consistent with previous studies, it was demonstrated that a higher quantity of β-*O*-4 linkages correlates with a higher lignin yield, indicating the influence of ether cleavage on the extraction process. The S/G ratio of biomass was found to be negatively correlated with pulp degradability. G units can form more cross-linked lignin due to additional C-C bonds and may thus function as a physical barrier for extraction. Consequently, a high S/G ratio and lignin content resulted in a high residual pulp. Additionally, a significant negative correlation was observed between the xylan acetylation degree and enzymatic pulp degradability and lignin yield.[56]

1.4.2 Flow through biomass fractionation

The chemical industry often employs continuous processes as the most cost-effective and energy-efficient approach in most applications, given their ability to minimize downtime, enhance productivity, and provide superior process control. In the realm of holistic biomass fractionation processes, most studies have centered on batch methods, as they are easier to develop and test, particularly on a laboratory scale. Additionally, the scale-up of batch processes is more straightforward.[57] A potentially optimal reactor design for biomass fractionation employs continuous countercurrent flow, which ensures steady product output and facilitates the seamless integration of downstream processes such as pulp washing. Nevertheless, this design presents certain challenges, including considerations of particle size,

safe handling of organic solvents, high-pressure requirements, and transport of biomass particles.

A considerable amount of research on the biomass valorization field has been devoted to the continuous processing of depolymerizing soluble lignin.[58] The number of publications on semicontinuous biomass fractionation has been growing in recent times, with many researchers advocating for a method that involves keeping the biomass stationary in the reactor while pumping solvents through it.

Following the early research on hydrothermolysis by O. Bobleter *et. al*.[59] in the 1980s using a flow-through approach, Bhagia *et al.* further explored the technique 2016 by comparing batch and flow-through fractionation of poplar through liquid hot water treatment and extremely dilute acid.[60] Simultaneously, Machmudah *et al.* examined the extraction of lignin from Japanese rice straw using hot compressed water in a flow-through reactor system at temperatures ranging from 170 to 230 °C. This process allowed for the thermal softening of the rice straw, which facilitated the removal of lignin through depolymerization reactions.[61]

Since 2018, various groups have focused on producing lignin monomers by combining biomass fractionation with reductive catalytic fractionation (RCF) of lignin. Anderson *et al.* developed a methanol RCF biomass fractionation using semi-continuous flow-through reactors to extract and depolymerize lignin. This method separates the lignin solvolysis and fractionation by packing biomass and the Ni/C catalyst into separate beds, which allows for the control of both processes individually.[41,62] Brandner *et al.* introduced a method for producing native-like lignin from poplar biomass using flow-through solvolysis with methanol at 225 °C. The flow-through system ensures rapid exposure of solubilized lignin to catalysts, thereby preventing condensation, but also achieves monomer yields comparable to those from batch processes.[63] The group later extended the system developing a multi-pass-flow-through system that allows for better solvent-to-biomass ratios while maintaining reaction efficiency.[64] Kramarenko *et al.* used β-zeolite as catalyst to assist flow-through fractionation that yields high amounts of lignin monomers.[65]

A research team led by Z. Wang published a rapid flow-through fractionation process for poplar using aqueous formic acid (72wt%) at 130 °C, which preserves a significant number of aryl ether bonds within the lignin. This process can be completed in as little as 15 minutes.[66]

The development of this process was advanced by adding *p*-toluenesulfonic acid, resulting in 40% of the available lignin being produced with nearly complete retention of β-*O*-4 linkages within 15 minutes.[67] Adding an acid hydrotrope enabled low reaction temperatures (below 98 °C) and yields of up to 80%, resulting in lignin with a high molecular weight, low T_g, and a pink color. [68]

Biomass processing at atmospheric pressure was successfully accomplished by Cai *et al.* through the employment of a solution containing 50% maleic acid, which effectively preserved 80% of the native β-*O*-4 linkages.[69]

Variations in organosolv biomass fractionation have also been studied in flow through variants. Zijlstra *et al.* examined an ethanosolv flow through variation that utilized walnut shells as feedstock. While the reaction time for this variation was longer than other flow through approaches at 5 h, most of the lignin was extracted within the first 2 h.[70] Smit *et al.* presented a semicontinuous aqueous acetone organosolv fractionation for lignocellulosic biomass at 140 °C, utilizing a countercurrent flow design that reduces the residence time of solubilized sugars and lignin. A percolating reactor design with six fixed solid bed positions and liquid exchange between reactors was proposed.[71]

Overall, the utilization of a semicontinuous flow through method for biomass fractionation has shown promise in providing a viable option, as it allows for the extraction of lignin and sugars with reduced residue times, which in turn leads to less degradation and condensation. The use of this flow through variation has been shown to increase β-*O*-4 retention when compared to batch processing and often results in higher fractionation yields and shorter process times. Additionally, the direct depolymerization of lignin into its monomers is a relatively straightforward process.

Flow-through pretreatment at the laboratory level can serve as an effective method for elucidating the breakdown processes that take place during aqueous pretreatments. The ongoing extraction of soluble components from plant material offers valuable insight into the sequence of component removal and their effects on the characteristics of the remaining solid matter. These findings can be contrasted with the outcomes of batch pre-treatments conducted under comparable conditions.[60]

1.5 Biomass fractionation and lignin depolymerization mechanisms

The mechanism of β-*O*-4 cleavage in aqueous acidic media has been extensively studied. Although slightly different nuances have been reported, the most suggested mechanism for the acidic cleavage of aryl ether bonds in lignin suggests that the acidic proton plays a major role. Protonation of the hydroxyl group at the α-carbon is the first and limiting step of the cleavage reaction. Next, dehydration occurs at the α-carbon and deprotonation occurs at the β-carbon, which forms a carbocation and/or enol-ether intermediate. After hydroxylation at the β-carbon, the β-*O*-4 ether bond is cleaved. Another approach includes the initial oxidation of the α-carbon hydroxy group, which allows the cleavage of the β-*O*-4 linkage under mild conditions with formic acid.[72] Nevertheless, due to the complexity of lignocellulose, many aspects of the fractionation and extraction mechanism are still unknown.

It remains unclear whether the β-*O*-4 cleavage during lignin extraction is necessary for the extraction process or merely a byproduct of the reaction conditions. Moreover, the role of hemicellulose in the extraction process has not been definitively established. The question arises as to whether a certain degree of hemicellulose dissolution is essential for extraction. As research on lignin-carbohydrate complexes continues to evolve, their role in biomass recalcitrance remains under investigation. Numerous factors that increase and decrease biomass recalcitrance have been identified; however, contradictory effects have been reported for various lignin properties, such as S/G ratio, molecular weights, and polydispersity (Figure 7).[73]

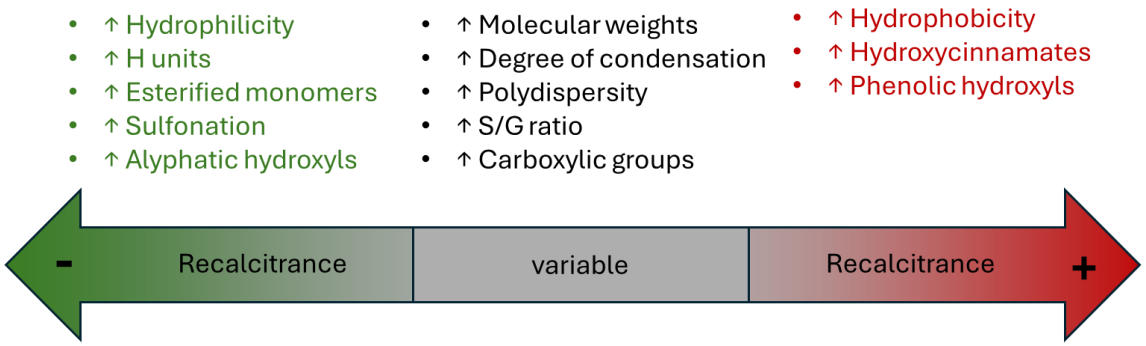

Figure 7: Recalcitrance factors of lignin properties on biomass cell wall fractionation, adapted from Ragauskas *et al.*.[73]

1.6 Lignin valorization

Lignin constitutes approximately one-third of lignocellulosic biomass and is generated in substantial quantities as a byproduct in the pulp and paper industry and in second-generation

ethanol biorefineries. However, most lignin applications, such as combustion for energy recovery, are of low value. Technical lignins can be concrete additives increasing fluidity and strength, used in epoxy resins with self-healing properties and in polyurethanes replacing toxic polyols and increasing flame retardancy. Mesoporous carbon generated from lignin has been investigated as an excellent biobased adsorber and in electrodes of batteries and supercapacitors.[74,75] To maximize economic efficiency and achieve a circular bio-based economy, it is imperative that all side streams of lignocellulosic biomass be valorized to their highest potential value.

Higher-value applications of lignin are achievable by utilizing the rich structure of lignin; the more specific the product structure, the higher is the application value (Figure 8). Lignin can be converted into biofuel or basic chemicals such as phenol; however, the highest value is derived from transforming it into fine chemicals and specialty products such as carbon fibers.[7]

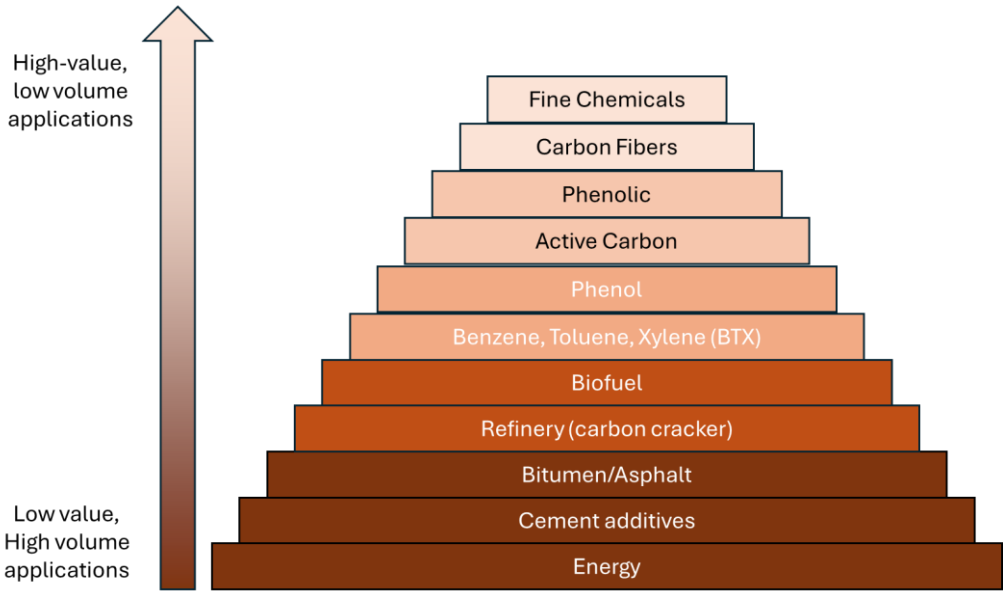

Figure 8: Schematic hierarchy of lignin applications from low to high values. Adapted from Margarida Martins *et al.*.[7]

Recent advancements in biorefinery techniques have enabled the preservation of a greater proportion of the native lignin structure, thereby facilitating higher-value applications. However, the sole commercialized high-value application of lignin is the production of vanillin through catalytic oxidative depolymerization. One approach to lignin valorization involves the depolymerization of lignin into simple aromatic units and their subsequent utilization as base chemicals for fuel additives or polymers. While this method allows lignin products to

substitute fossil-derived chemicals in existing manufacturing processes, it necessitates several cost-intensive and energy-intensive steps.[76]

An alternative approach to lignin valorization involves utilization of existing polymer structures. Extensive research has been conducted on applications that exploit the inherent properties of lignin. In these applications, the variation in lignin structure among plant species presents a challenge; however, it can also be advantageous to select an appropriate lignin source. Researchers have investigated the antimicrobial properties of lignin for use in food packaging products, agricultural applications, and medical materials such as wound dressings.[77] Furthermore, lignin has been examined for potential applications in electrical materials and as a component in 3D printing polymers.[78,79]

1.6.1 Electrospinning of lignin

Polyacrylonitrile (PAN) is currently the standard material for carbon fibers and carbon nanofibers. As it is derived from fossil resources and relatively expensive, there exists a demand for cost-effective and renewable alternatives such as lignin.[80] Carbon fibers from pure lignin were initially commercialized on a small scale in the 1970s; however, PAN-derived fibers developed more rapidly and resulted in superior materials. Hardwood lignin can be melt-spun, whereas softwood lignin lacks thermal stability. Narrower molecular weight distribution facilitates more effective thermal pretreatment. The glass transition temperature T_g must be significantly below the decomposition/crosslinking temperature while remaining sufficiently high for oxidative thermostabilization. Combining softwood and hardwood lignins can also yield improvements. Research indicates that increased alkoxy contents and/or carbon contents contribute to improved lignin-based carbon fibers. Additionally, plasticizing with polyethylene oxide can enhance fiber spinning.[80]

Carbon nanofibers with extremely small diameters have been known for a long time. They are typically produced through electrospinning, a process in which electrostatic forces draw a fine jet of solution into a thin fiber (Figure 9).

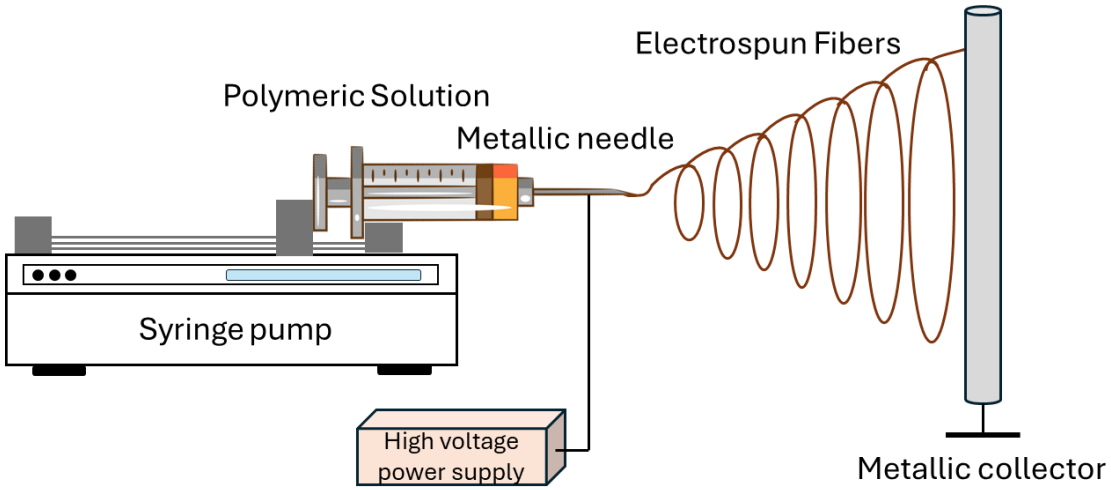

Figure 9: Schematic of basic electrospinning setup.

Carbon nanofibers derived from lignin were first reported in 2007 and have undergone further development over the past decade. However, the production of uniform carbon nanofibers from pure lignin remains challenging due to its comparatively lower molecular weight, nonlinear structure, and anionic charge in solutions.[81] Lallave *et al*. fabricated filled and hollow nanofibers from pure Alcell lignin with ethanol (1:1).[82] Alternative approaches have employed at least a minimum amount of additives, such as poly(ethylene oxide), to enhance the spinnability of lignin.[83] Refined lignosulfonate and Kraft lignin were electrospun with 50% PAN and carbonized at 1300 °C to produce nanofibrous webs suitable for use as anodes in sodium ion batteries. PAN serves as a necessary binder polymer to ensure the spinnability of lignin with low molecular weight and high polydispersity.[84] The binding of lignin and cellulose yielded carbon nanofibers exhibited high flexibility and thermal stability. This presents the possibility of developing a fully biobased composite.[85] Recently, Parot *et al.* successfully electrospun pure lignin nanofibers from organosolv softwood lignin. Uniform fibers were obtained by optimizing the process parameters. The incorporation of $FeCl_3$ facilitated a reduction in the minimum fiber diameter to 200 nm and inhibited fiber fusion on the collector.[86]

The heterogeneous nature of the lignin structure significantly affects its material characteristics. The composition of monomer units and their connections within the macromolecule are related to the linearity of the polymer chains and the quantity of functional groups. These aspects, along with the molecule size, are also affected by the extraction method employed. Collectively, these lignin attributes determine crucial spinning parameters, including solubility and viscosity.

The influence of the lignin source on the production of carbon nanofibers has been investigated little to date. Du *et al.* conducted a comparative study of hardwood (poplar), softwood (pine), and grass (corn stalk) organosolv lignin in co-spinning with PAN. Poplar-based lignin carbon nanofibers exhibited superior performance in terms of tensile strength, surface area, and specific capacitance and demonstrated favorable characteristics for use in supercapacitor electrodes. Structural analysis revealed that a high proportion of S units and β-*O*-4 linkages, which are predominantly found in hardwoods, is advantageous for fiber morphology. This lignin is hypothesized to possess a more linear structure with fewer branches, which is conducive to enhancing polymer alignment during the spinning process.[87] García-Fuentevilla *et al*. utilized Kraft lignins from diverse sources and cellulose acetate to produce electrospun nanostructures. Notably, hardwood lignins derived from eucalyptus and poplar demonstrated suitability for spinning, potentially attributable to their more linear structure.[88]

2 Aim of the Thesis

The transition towards sustainable, renewable resources necessitates the holistic valorization of lignocellulosic biomass. The complex, structurally variable nature of lignocellulose, particularly the composition of lignin, poses challenges for its full valorization, often limiting its applications to low-value energy recovery. The extraction of lignin while preserving its structural features enables high-value applications.

This thesis aims to enhance lignocellulose pretreatment and fractionation via an acid-catalyzed biphasic process, exploring the impact of plant species, lignocellulose composition, lignin structure, and fractionation conditions on product yields, sugar composition, and lignin structure to support sustainable material and chemical production. It also investigates lignin and sugar extraction mechanisms to improve fractionation and deepen understanding of plant structure. This thesis has three main objectives:

1. **Plant biomass recalcitrance towards lignin extraction**: A comprehensive analysis compares diverse plant materials with contrasting structural and compositional properties to examine how their diversity affects lignin extraction efficiency and the resulting configuration of the extracted lignin. This objective aims to leverage plant selection to control lignin properties for optimized downstream applications. (Chapter 3.1 and 3.2)

2. **Process Dynamics through Flow-Through Fractionation**: A flow-through variant of the fractionation process is employed, utilizing statistical experiment design (DOE) and time-resolved analysis of product streams to identify key parameters influencing hemicellulose and lignin extraction. This objective seeks to uncover mechanistic insights into the kinetics of sugar and lignin release, advancing the development of continuous and scalable lignocellulose biorefining. (Chapter 3.3 and 3.4)

3. **Lignin Valorization through Electrospinning**: Selected plant-based lignin samples are evaluated for their suitability in electrospinning, with a focus on how different lignin structures impact fiber formation and stability. This approach provides insight into the potential of lignin as a renewable feedstock for advanced material applications. (Chapter 3.5)

3 Results and Discussion

3.1 Assessing lignin diversity

Utilizing lignocellulosic biomass as a renewable resource entails dealing with feedstock that is subject to regional availability, economic factors, and highly variable growth conditions. But at the same time, the specific configuration of cellulose, hemicellulose, and lignin, can exhibit significant variations in structure. Those differences can be caused by genetic variation and are large between species, depend on the tissue that is utilized (e.g. leaves vs stem) and can change with environmental factors such as drought and nutrient availability.[17] Nevertheless, these differences can also present significant opportunities for producing specific products with reduced reliance on chemical processing. Instead of breaking down the biomass into its smallest components and then reconstructing molecules from there, the natural plant structure, which can be tailored through breeding and growth conditions, can be utilized to save time and energy.[89] The objective of this chapter is to assess the impact of compositional diversity on the processability of biomass in the OrganoCat process and on the properties of the extracted lignin. This information will enable the identification of an appropriate lignin for further valorization.

3.1.1 Biomass selection for inter-species comparison

Material from ten different plants was selected for comparison, as shown in Table 1. Each material exhibits potential as a renewable resource for diverse reasons, such as availability, growth rate, and ability to grow on marginal soils. Wood has traditionally been used for building materials, pulp, and paper production. Beech, a common hardwood found in temperate Eurasia and North America, is commonly employed for biomass fractionation processes due to its widespread availability.[33,48] Eucalyptus, the most widely planted species of hardwood, is native to Australia and can be produced at a low cost while also tolerating water shortages well.[32] Softwoods, such as spruce, were not included in this study as they exhibited low processability for the OrganoCat process in previous research, despite typically having a high lignin content.[52] Perennial grasses, which grow more quickly than woods, can be harvested multiple times and have been identified as valuable feedstocks for biorefineries due to their high yields. *Miscanthus x giganteus* (miscanthus) and *Agropyron elongatum* (szarvasi) are known as examples of such grasses.[90] *Silphium perfoliatum* (silphium), a tall-growing flower that can be harvested for up to 15 years, and *Sida hermaphrodita* (sida), a

herbaceous species belonging to the Malvaceae family, have recently gained attention as energy crops.[35,91,92] Common agricultural crops like maize and rapeseed are also utilized for bioenergy production.[93] Residual products from other processes such as sugarcane bagasse and walnut shells, which are byproducts of food production, have demonstrated potential in biorefineries.[37,38]

Table 1: Overview of plant biomass materials used for inter-species comparisons.

Material (trivial name)	binominal name of the origin species	notable traits
beech	*Fangus sylvatica*	Hardwood
eucalyptus	*Eucalyptus spp.*	Hardwood
miscanthus	*Miscanthus x giganteus*	Grass, perennial
szarvasi	*Elymus elongatus*	Grass, perennial
maize	*Zea mays*	Grass, common agricultural crop
sugar cane bagasse	*Saccarum officinarum*	Grass, perennial, agricultural waste product, pre-processed for sugar extraction
sida	*Sida hermaphrodita*	Malvacae
silphium	*Silphium perfoliatum*	Perennial
rapeseed	*Brassica napus*	Common agricultural crop
walnut shells	*Juglans regia*	Agricultural waste product

Plant materials differ in their composition and structure. To determine the composition of the biomasses used for OrganoCat processing, established procedures for wet chemical analysis of the components were employed.[55] These included examining the alcohol soluble components (ASC), starch content, amount of crystalline cellulose, acetylation, lignin content, and fraction of hydrolysable hemicellulose sugars. A flow scheme of the steps included in the wet chemical analysis can be found in the experimental section (Figure 45). Table 2 shows the determined composition of the materials, relative to the raw material weight.

Table 2: Composition of selected plant biomass determined by wet chemical analysis. Lignin content, acetylation, crystalline cellulose, and hemicellulose sugar were determined after extraction of the alcohol soluble components and destarching. Results of those measurements are calculated to represent the percentage of full biomass weight. All experiments were conducted in triplicates, standard derivation is given in brackets. Data is sorted by lignin content.

	alcohol soluble components (ASC)	starch	lignin (ABSL)	acetylation	crystalline cellulose (CrC)	hemi-cellulose sugars
	[%]	[%]	[%]	[%]	[%]	[%]
walnut shells	0.0 (0.0)	5.1 (0.8)	28.7 (3.2)	4.4 (0.5)	29.7 (3.9)	14.9 (3.0)
sugar cane bagasse	1.4 (0.2)	2.1 (0.3)	26.1 (1.2)	3.5 (0.7)	45.8 (1.7)	23.9 (2.5)
eucalyptus	1.0 (0.2)	5.9 (1.4)	25.4 (1.3)	3.3 (0.4)	47.1 (3.8)	13.8 (2.3)
miscanthus	0.0 (0.0)	10.8 (1.4)	21.7 (2.2)	2.4 (0.6)	41.5 (4.2)	21.6 (3.2)
sida	4.2 (1.0)	12.7 (9.4)	21.0 (1.3)	4.2 (0.3)	37.0 (2.5)	14.6 (2.1)
beech	0.8 (0.3)	16.6 (2.3(	20.4 (1.7)	4.2 (0.6)	37.6 (1.7)	18.8 (2.9)
rapeseed	3.3 (0.2)	14.8 (0.1)	18.9 (1.8)	3.3 (0.3)	33.7 (4.4)	11.2 (1.2)
szarvazi	9.8 (0.1)	12.9 (1.7)	15.9 (1.2)	1.7 (0.2)	31.3 (3.5)	18.8 (2.4)
maize	18.3 (3.4)	20.2 (3.9)	12.6 (1.2)	1.6 (0.4)	22.2 (3.1)	18.0 (0.7)
silphium	20.8 (0.3)	35.4 (1.6)	5.8 (0.6)	1.5 (0.5)	16.8 (0.9)	8.2 (1.2)

Eucalyptus, walnut shells, and sugar cane bagasse possess the highest ABSL lignin content, making them promising candidates for high lignin extraction yields. However, the extraction process is influenced by various factors, such as hemicellulose accessibility, lignin structure, and lignin accessibility, which do not guarantee the highest amounts of lignin will be extracted from these plants. Previous OrganoCat fractionation results showed that almost no lignin was extracted from eucalyptus, while szarvasi delivered the highest lignin yield with 19.4wt% of the initial biomass.[56]

The hemicellulose sugar profile is distinct for each plant. As depicted in Table 2, sugar cane bagasse, miscanthus, and szarvasi display the highest levels of overall hemicellulose sugars. Table 3 shows the composition of the different pentoses and hexoses found in the sugar analysis.

Table 3: Composition of hemicellulose sugars after TFA hydrolysis determined by high-performance anion exchange chromatography with pulsed amperometric detection (HPAEC-PAD). Sorted by xylose yield. Values are expressed as a percentage of total biomass weight.

	Fuc [%]	Rha [%]	Ara [%]	Glc [%]	Glu [%]	Xyl [%]	Man [%]	GlcA [%]	GluA [%]
silphium	0.1	0.5	1.7	1.7	1.1	9.0	1.0	3.2	0.3
rapeseed	0.1	0.3	0.5	0.5	0.5	10.0	0.6	0.9	0.2
eucalyptus	0.0	0.2	0.1	0.3	2.6	10.2	0.5	0.8	0.0
sida	0.1	0.4	0.4	0.5	1.4	12.5	0.8	1.5	0.1
walnut shells	0.0	0.2	0.2	0.4	0.4	13.6	0.0	0.7	0.0
beech new	0.0	0.4	0.4	0.6	2.1	17.4	0.8	1.0	0.0
szarvazi	0.0	0.0	2.4	0.3	0.9	19.5	0.9	0.2	0.1
miscanthus	0.0	0.0	1.9	1.1	2.1	19.7	0.0	0.3	0.0
sugar cane bagasse	0.0	0.0	1.8	0.3	2.3	20.0	0.0	0.3	0.0
maize	0.0	0.0	3.2	0.7	2.6	21.0	1.1	0.3	0.2

Xylose is the predominant sugar in the hemicellulose of all plants, whereas the amounts of other sugars vary depending on the plant in question. Walnut shells had the highest xylose content and the lowest levels of other residual sugars, while Silphium exhibited the lowest xylose content in this fraction. Glucose can be found in all plants in varying amounts. Different glucan structures were found in all hemicellulose samples. The grasses maize, Miscanthus, sugar cane bagasse, and szarvasi have a high content of arabinose, as arabinoxylan is the domination hemicellulose in grasses.[18] Arabinose is found in very low quantities in beech, eucalyptus, walnut shells, and sida.

To obtain information on the lignin structure in plants, the biomass was analyzed following the methodology outlined by Pauly *et al*. [94], which employs a protocol that dissolves the plant cell wall while minimizing destruction (Table 4).

Table 4: HSQC-NMR analysis of lignin in unprocessed biomass

	S	G	H	S/G	β-*O*-4	β-β	β-5
beech	58.0	39.6	2.4	1.5	70.5	10.7	5.0
eucalyptus	57.9	37.8	4.2	1.5	67.6	9.0	1.2
walnut shells	39.7	46.2	14.1	0.9	53.7	9.1	1.1
sida	57.3	40.3	2.4	1.4	69.2	10.6	1.3
silphium	24.2	43.8	32.0	0.6	40.2	5.5	0.9
szarvasi	17.5	66.9	15.6	0.3	27.2	2.3	1.2
miscanthus	21.8	67.6	10.6	0.3	30.7	3.4	7.7
sugar cane	17.5	64.5	18.0	0.3	27.6	1.2	1.2
rapeseed	35.9	52.4	11.7	0.7	63.0	8.0	7.5
maize	11.1	51.5	37.4	0.2	11.3	0.1	0.6

Principal component analysis (PCA) of the biochemical data was conducted to cluster plants based on their chemotypes. Normalized data from the wet chemical analysis (ASC, starch, CrC, ABSL lignin, and hemicellulose sugars) was included along with the results of the HSQC-NMR characterization of lignin (S/G ratio, β-*O*-4, β-β, and β-5 linkages). The detailed composition of hemicellulose sugars was not included as the focus of this chapter focuses on lignin interactions rather than the influence of sugars. The first two principal components accounted for 81.6% of the variance in the set (PC1: 52.0%; PC2: 29.6%). The rotated component matrix (Appendix 8.1) revealed that PC1 mainly represented the biomass composition data, whereas PC2 was dominated by lignin analysis.

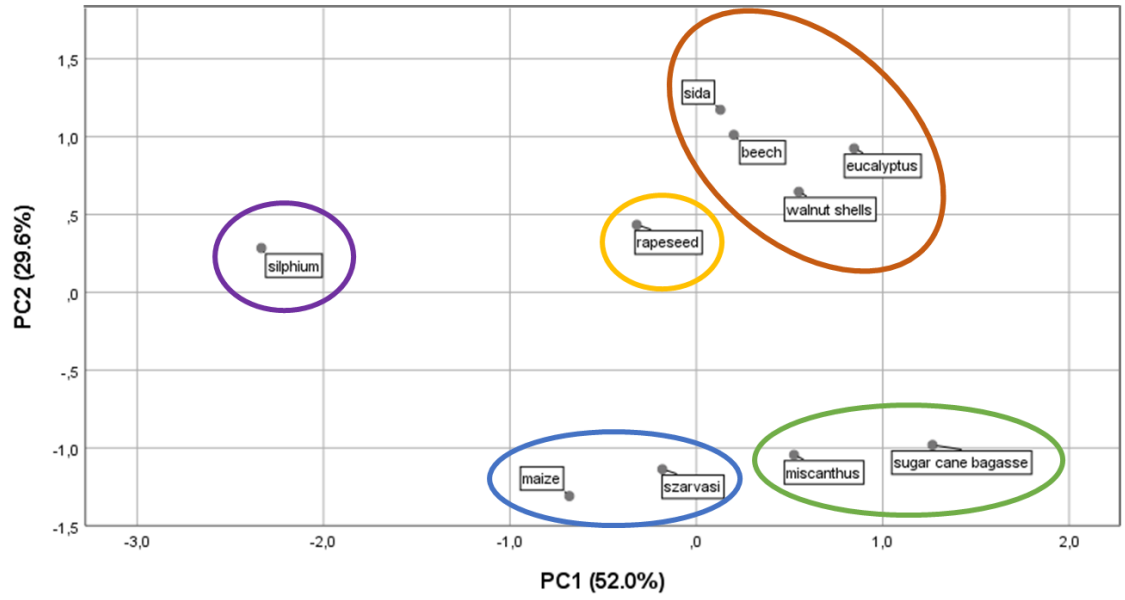

Figure 10: Principal component analysis (PCA) of normalized unprocessed biomass data. Included data: alcohol soluble components, starch, crystalline cellulose, ABSL lignin, hemicellulose sugar content, and acetylation.

The results of the hierarchical analysis showed clustering of plants based on their characteristics in the PCA (Appendix 8.1). Beech and eucalyptus, two hardwoods, were found to be part of the same cluster as walnut shells and sida, a plant known for its hard, pithy, brown stems with low moisture content that remain in the field at the end of the growing season.[92] These shared qualities led to the formation of a 'woody materials' group. The compositions of these four biomasses were similar, as they all contained high amounts of lignin. Lignin itself had a relatively high S/G ratio and a significant proportion of β-*O*-4 and β-β linkages per 100 monomer units.

The grasses maize, szarvasi, miscanthus, and sugarcane bagasse exhibit similarities in their lignin structure, primarily represented in PC2. All four grasses possess a higher G lignin content and relatively low levels of β-*O*-4 and β-β linkages. Based on PC1, these grasses were divided into two clusters, with maize and szarvasi containing significant amounts of starch and ASC. Miscanthus has a comparable amount of starch but almost no alcohol soluble components. Sugarcane bagasse, which has already been processed, contains very little starch or ASC. Additionally, the amounts of lignin and crystalline cellulose are lower in maize and szarvasi than in miscanthus.

Rapeseed and silphium were separated from the other clusters in the PCA of unprocessed biomass. Both have medium S/G ratios and high β-β linkages in their lignin, which results in similar PC2 values. However, in terms of wet chemical composition, as represented in PC1, silphium stands out as having more than 50% of starch and alcohol soluble components in total, while the composition of rapeseed is similar to that of other grasses, especially szarvasi.

3.1.2 Fractionation efficiency for different biomass materials

Fractionation experiments were performed following the previously described PA OrganoCat procedure.[50] This OrganoCat version was chosen as it combines the thermal stability of the catalyst, as seen in the FDCA variation,[49] with the high yields and retention of ether linkages, as seen in the OA variation.[52] Lignin yield and solid residue were determined gravimetrically while the hydrolyzed sugars were calculated from their concentrations measured in the aqueous phase. The fractionation products of all ten plant biomasses are shown in Figure 11.

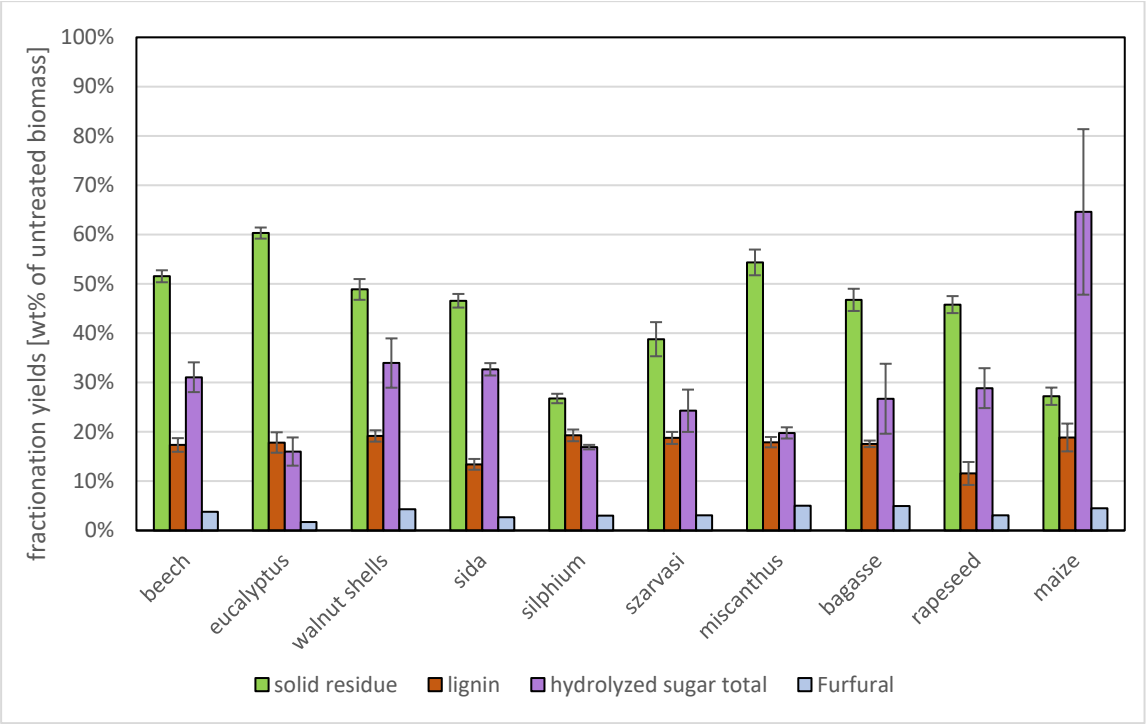

Figure 11: Fractionation yields after PA OrganoCat processing. The solid residue and lignin content were determined gravimetrically after drying. The hydrolyzed sugar concentration was measured using HPAEC-PAD and extrapolated to the total yield. Furfural concentration was measured in ^{1}H-NMR and similarly calculated to represent the total yield. All yields are given in wt% of the unprocessed biomass.

The yield of solid residue differs significantly among the biomasses, with eucalyptus, beech, and miscanthus exhibiting the highest mass retention (over 50%). In contrast, maize and silphium had the lowest solid residue retentions of only 27%. These plants contain substantial amounts of ASC and starch, which, along with lignin and hemicellulose sugars, are removed during fractionation.

The amount of solid residue does not correlate with the amount of hemicellulose sugars or crystalline cellulose in the unprocessed biomass. However, the amounts of starch (Pearson coefficient $P = -0.768$) and alcohol soluble residues ($P = -0.941$) show significant ($p < 0.05$), negative correlations with solid residue. ASC could be extracted into the organic phase, and the starch is depolymerized to glucose, which can be found in the sugar hydrolysate fraction after processing. The amount of solid residue also correlates with the proportion of lignin in the unprocessed biomass ($P = 0.814$, $p < 0.05$) confirming the influence of lignin on lignocellulose recalcitrance.[56]

Pentose sugars can be converted to furfural and 5-hydroxymethylfurfural (HMF). Under the selected process conditions, the process yielded between 1.7% (eucalyptus) and 5% (miscanthus) furfural derivates. Earlier studies have shown that furfural production is heavily

dependent on the reaction time and temperature. Up to 56% of furfural could be produced from beech wood at 175 °C in 60 min.[50] Furfural can be a desired product as it can be used as a platform chemical.[6]

The total yield of hydrolyzed sugars exceeds the amount of hemicellulose sugars found in the unprocessed material for beech, walnut shells, sida, rapeseed, and maize. Upon closer examination of the sugar composition (full dataset in Appendix 8.2), it becomes evident that there is a higher-than-anticipated proportion of glucose in the aqueous phase in most plants, particularly in maize, where the glucose hydrolyzed by the OrganoCat process exceeded the glucose found in the wet chemical analysis (TFA hydrolysis) by 47wt% of the unprocessed material. This additional glucose is likely released from starch and/or the dissolution of amorphous cellulose. The catalyst phosphoric acid is known to cause the swelling of cellulose transforming it into its amorphous state, but can also dissolve cellulose depending on the concentrations and reaction conditions employed.[95]

The lignin yield among various plants falls within a narrow range, with an average of 12% (rapeseed) to 19% (walnut shells, szarvazi, silphium, and maize). Testing parametric statistical variance analysis (Kruskal Wallis), it was revealed in the post hoc analysis that a significant statistical difference ($p < 0.05$) solely exists between the lignin yield of rapeseed and silphium. A substantial range of available lignin was observed in the unprocessed biomass, varying from 6% (silphium) to 29% (walnut shells). Nonetheless, no linear correlation (Pearson) was found between the available lignin in the biomass and the lignin yield. This indicates that lignin availability alone does not determine the amount of lignin that can be extracted from the plant. Instead, lignin and biomass structure also play a crucial role in determining the extraction efficiency.

When processing szarvasi, maize, and silphium, the lignin yield was higher than that determined by the ABSL method. All three contain comparably higher amounts (10%, 18%, and 20%, respectively) of ASC. A part of the ASC could be extracted into the organic phase during the OrganoCat extraction process, adding to the dried organic extract weight, which was defined as lignin yield. Furthermore, part of the dried organic extract of maize and silphium was insoluble in acetone after a few weeks of storage, indicating the polymerization of some of its components. Spectroscopic analysis of the organic extracts of these plants via

HSQC-NMR showed some signals that could not be assigned to lignocellulosic compounds (Figure 13, Appendix 8.2), adding to the hypothesis that non-lignin components are extracted into the organic phase.

To further investigate the relationship between lignin, sugar extraction, and biomass structure, the pulp was assessed using wet chemical analytical techniques. ASC and starch are easily extracted during the OrganoCat processing and therefore cannot be determined in the pulp material. Similarly, acetylation was not detected in the pulp. The results were adjusted to correspond with the pulp yield to facilitate the comparison of the extraction efficiency.

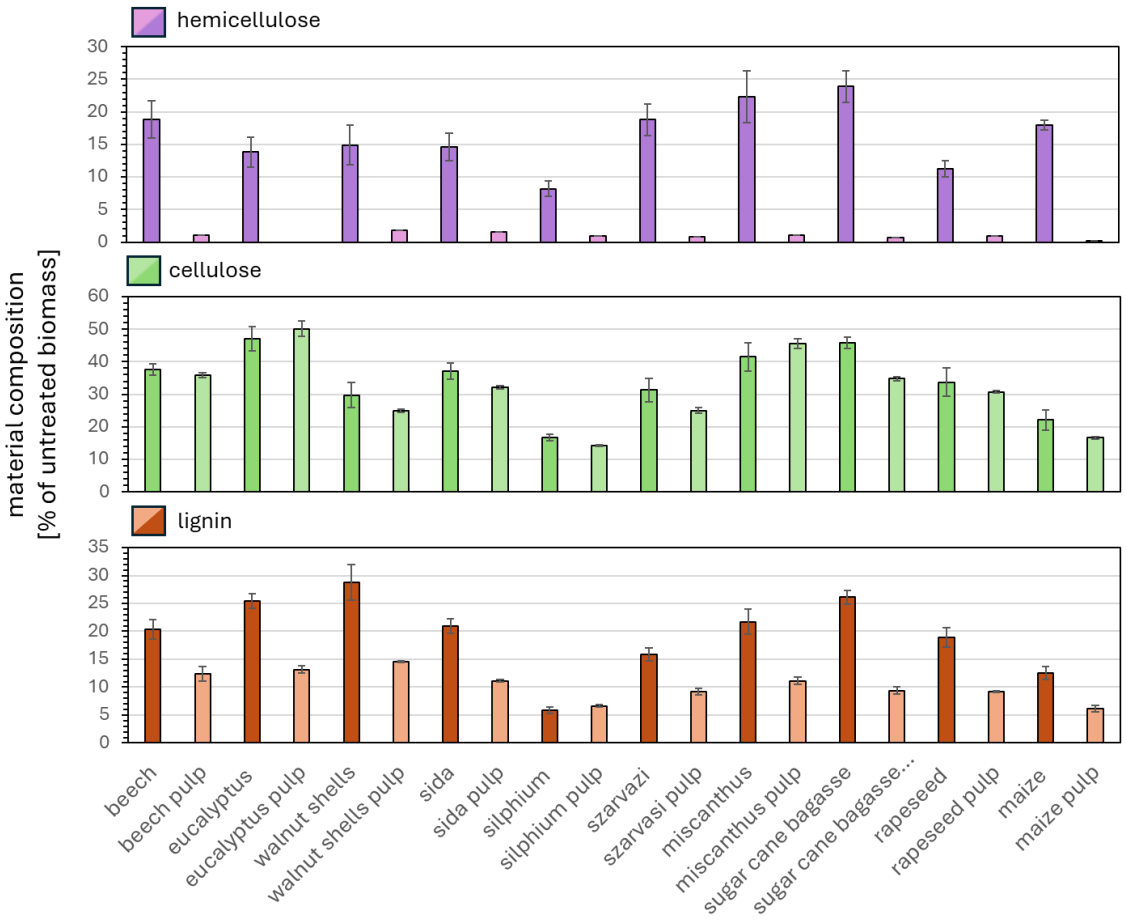

Figure 12: Wet chemical analysis results of solid residue in comparison with the compositional analysis of the unprocessed material. The pulp results were adjusted to the corresponding yields for direct comparison.

As depicted in Figure 12, cellulose content decreased minimally or remained unchanged (beech, eucalyptus, miscanthus) as intended for the process aimed at yielding predominantly cellulosic pulp. The removal of readily hydrolysable hemicellulose sugars was virtually complete, with only negligible traces remaining. Together with the sugar yields, which mostly reach the amount expected from the source material analysis, it can be concluded that

hemicellulose extraction is nearly complete. In addition, acetylation was no longer detected. Delignification proportions ranged from 40% (beech) to 65% (bagasse), with Silphium representing a noteworthy exception.

The low lignin content in silphium does not seem to decrease in pulp, despite the substantial amount of lignin (17wt%) obtained from the organic phase. The HSQC-NMR analysis confirmed the presence of lignin in the dried organic extract of Silphium (Appendix 8.3), although it also displayed several unidentified signals. This leads to the suspicion that the organic extract of silphium is not pure lignin but contains impurities. The high amount of ASC in silphium may contribute to these, as some ASC could be extracted into the organic phase due to similar polarity. Literature suggests that the lignin content in silphium is high (21%[96], 25%[97]). In the dAIR of the silphium sample used in this work, the measured lignin content was 13.3wt%. It is possible that the plant material used had a lower lignin content either because of the early growth stage or other environmental conditions. Silphium lignin extraction is not commonly reported in literature. In a catalyst-free organosolv extraction, a lignin yield of 15.7% was achieved, which is comparable to the OrganoCat extraction yield achieved here.[97]

In general, the composition of pulp in all ten plants exhibits a greater degree of similarity following OrganoCat processing. Almost all hemicellulose sugars were removed, while the crystalline cellulose content remained unchanged, and the lignin content in the pulp fell within the range of 19-29%. This suggests that to effectively utilize cellulose, an additional lignin removal step may be necessary.

3.1.3 Lignin structure analysis and comparison

3.1.3.1 Monomer unit analysis

The chemical structure of lignin has a significant influence on its processing characteristics, including reactivity, viscosity, and extraction efficiency. Therefore, lignin was examined in the unprocessed biomass for monomer composition and linkages. The extracted lignin was also analyzed for monomer composition and linkages, in addition to its molecular size.

The two-dimensional ^{1}H-^{13}C-heteronuclear single quantum correlation nuclear magnetic resonance spectroscopy (HSQC-NMR) provides a detailed insight into the structure and composition of lignocellulosic materials. For solubilizing the plant materials and pulp, a

procedure of ball milling as described by Pauly *et al.* was used.[98] The extracted, dried lignin could be directly solubilized for HSQC-NMR.

Maize was chosen for further investigation because of its high concentration of alcohol-soluble components (ASC). The unprocessed maize biomass, maize pulp, and organic extract of maize were analyzed using HSQC-NMR and are shown in Figure 13.

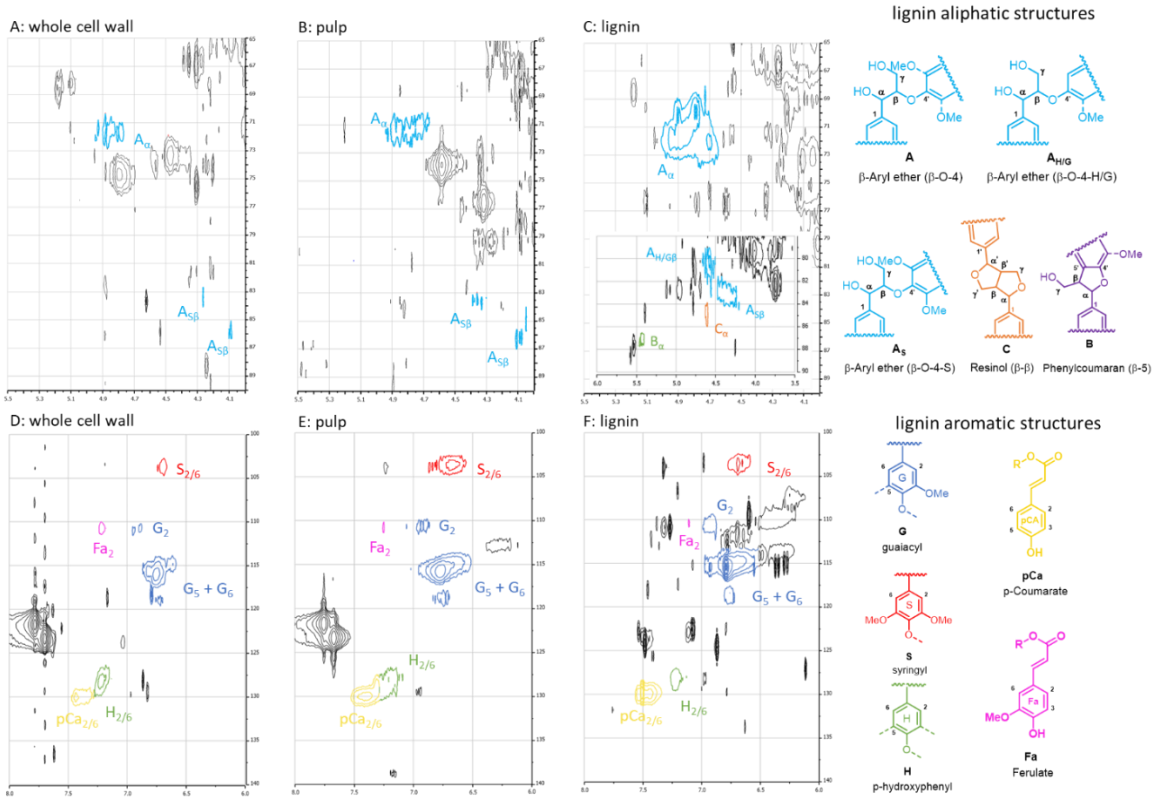

Figure 13: Partial 2D HSQC-NMR spectra of whole cell wall (A and D), pulp (B and E), and lignin after OrganoCat extraction (C and F) of maize. The top three spectra: relevant lignin aliphatic region (δ_H = 4.0 – 5.5 ppm, δ_C = 65 – 90 ppm). The bottom three spectra: lignin aromatic region (δ_H = 6.0 – 8.0 ppm, δ_C = 100 - 140 ppm).

Comparing the spectra, the lignin remaining in the maize pulp showed a reduction in β-*O*-4 linkages to approximately one-third of that in the untreated biomass (Figure 13, Table 5). However, the extracted lignin displayed only a minor reduction in β-*O*-4 linkages. This suggests that most of the ether linkages are cleaved within lignocellulose, which may disentangle lignin from hemicellulose and cellulose and enhance its solubility in 2-MTHF. The extraction of certain molecular sizes or proportions of β-*O*-4 linkages might be favored in the organic solvent, resulting in a similar level of ether linkages in the extracted lignin across different plants. Once extracted, only a small amount of acid catalyst was present in the organic phase, thereby reducing further cleavage of the lignin fragment. There is only a slight increase in β-β and β-5 units in the extract which might be within the margin of error. Those linkages are

usually neither cleaved nor created through condensation under the employed process conditions.[99]

The S/G ratio of maize lignin increased in the pulp but decreased in the extracted lignin. In maize, it appears that G-rich lignin is favored for extraction. In the unprocessed plant, 58% of the monomer units were identified as H units. However, this percentage is most likely an overestimation, as the *p*-hydroxyphenyl content of maize reported in literature is typically lower. The H-units may be overestimated due to the overlap of the 2/6 signal of *p*-hydroxyphenyl with the 3/5 correlation peak of phenylalanine, although the expected amount in the whole cell wall is very low. Additionally, the *p*-coumarate signal, which is particularly found in grasses, may also overlap with the 2/6 signal of H-units, as shown in Figure 13D, E.[100,101]

Solvents such as DMSO or THF, which exhibit medium polarity, are commonly known to effectively solubilize lignin.[102] According to the models developed by Petridis *et al.,* the solvent-lignin interaction is independent of lignin monomer composition when using THF:water mixtures.[103] Beckham *et al*.[102] suggested that high G content is favorable for extraction. The miscibility gap between 2-MTHF and water leads to the formation of a biphasic system in the OrganoCat process, which differs from the THF:water mixtures.

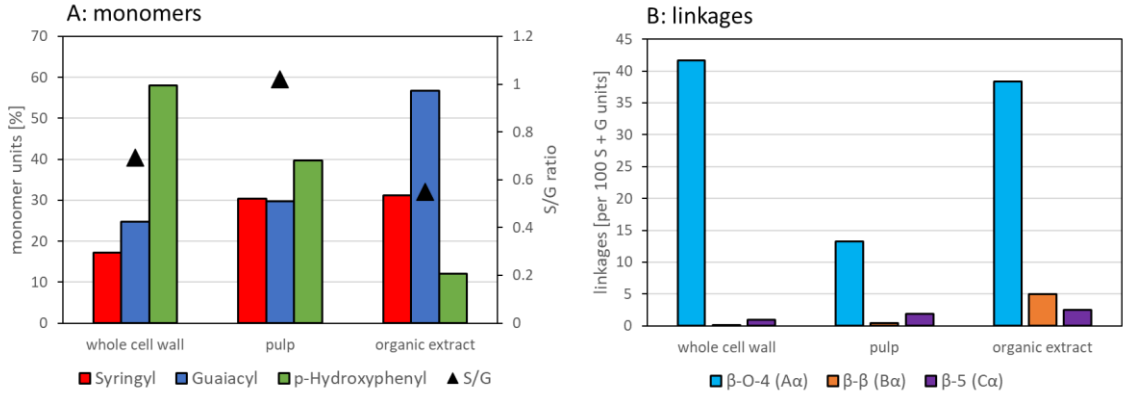

Figure 14: A: Monomer composition [%] determined by HSQC-NMR analysis of unprocessed maize, maize pulp, and extracted maize lignin. B: Proportions of β-*O*-4, β-β, and β-5 linkages per 100 S + G units determined by HSQC-NMR analysis of unprocessed maize, maize pulp, and extracted maize lignin.

Analogous to maize, the unprocessed biomass and extracted lignin of all plant species were examined by HSQC-NMR.

Table 5: Monomer unit composition [%] (Syringyl S, guaiacyl G, *p*-hydroxyphenyl H) for the ten selected plant species determined by HSQC-NMR. Measurements of the extracted lignin were conducted for a minimum of three technical repetitions, and the averages are shown with standard deviations in brackets.

	unprocessed plant [%]			extracted lignin [%]		
	S	G	H	S	G	H
beech	58.9	38.6	2.5	69.7 (0.8)	29.9 (0.7)	0.4 (0.1)
eucalyptus	58.6	37.1	4.3	72.0 (0.1)	27.6 (0.2)	0.4 (0.1)
walnut shells	45.0	39.0	16.0	61.3 (1.0)	34.9 (1.2)	3.8 (0.2)
Sida	58.9	38.6	2.5	54.4 (0.9)	43.4 (0.9)	2.2 (0.1)
Silphium	31.6	26.5	41.9	38.3 (0.8)	49.1 (0.4)	12.7 (0.4)
Szarvasi	23.0	56.5	20.5	25.9 (2.7)	61.3 (5.6)	12.8 (8.2)
Miscanthus	29.8	55.7	14.4	37.9 (1.7)	52.4 (0.3)	9.8 (1.9)
sugar cane bagasse	30.9	37.2	31.8	41.2 (1.3)	39.0 (0.6)	19.7 (1.1)
rapeseed	38.5	48.9	12.6	53.7 (3.0)	41.9 (2.8)	4.4 (0.8)
maize	17.2	24.8	58.0	31.2 (0.6)	56.7 (1.2)	12.1 (1.8)

Unlike the S and G units, the H units before and after extraction did not match but were considerably higher in the unprocessed biomass (Table 5). Due to the presence of overlapping signals, it was hypothesized that the H-units in the unprocessed plants were overestimated. Consequently, in the subsequent analysis, the linkages were only calculated in relation to the S and G units.

Furthermore, in addition to utilizing HSQC-NMR as an analytical tool, Pyrolysis-Gas Chromatography-Mass Spectrometry (Py-GC-MS) was employed to assess the monomer composition (Table 6). HSQC-NMR and Py-GC-MS are well-established methods for lignin analysis; however, their results depend partly on the intricate structure of the particular lignin. While HSQC-NMR analysis is complicated by overlapping peaks and interfering signals, the Py-GC-Ms method presents the challenge of assigning the numerous components produced by the pyrolysis reaction to their corresponding structural sources. Additionally, both methods can be subject to errors resulting from the presence of secondary non-lignin components.

Table 6: Monomer unit composition [%] (Syringyl, Guaiacyl, *p*-hydroxyphenyl) for the ten selected plant species determined by Py-GC-Ms.

	unprocessed plant [%]			extracted lignin [%]		
	S	G	H	S	G	H
beech	54.4	41.3	4.2	53.6	39.5	6.9
eucalyptus	54.4	41.2	4.4	58.6	36.9	4.5
walnut shells	46.0	46.0	8.0	41.5	42.9	15.5
Sida	38.8	50.6	10.6	37.2	47.0	15.7
Silphium	22.6	32.4	45.0	18.0	25.4	56.6
Szarvasi	19.7	56.5	23.8	14.3	51.0	34.8
Miscanthus	24.1	48.0	27.9	23.8	45.3	30.9
sugar cane bagasse	27.1	39.1	33.8	26.5	35.0	38.5
rapeseed	40.8	53.7	5.5	42.7	47.6	9.7
maize	19.4	44.7	35.9	15.4	40.7	43.9

*averages and standard deviations (brackets), determined by measuring three technical replicates.

The S/G ratios determined by both HSQC-NMR and Py-GC-MS are listed in Table 7.

Table 7: S/G ratios of lignin in unprocessed material and in extracted lignin. Comparison of the HSQC-NMR and Py-GC-MS results.

	NMR S/G unprocessed	NMR S/G extracted*	Py-GC-MS S/G unprocessed	Py-GC-Ms S/G extracted
beech	1.53	2.33 (0.08)	1.68	1.35
eucalyptus	1.58	2.62 (0.02)	1.70	1.57
walnut shells	1.15	1.76 (0.09)	1.15	0.96
Sida	1.52	1.25 (0.05)	1.00	0.79
silphium	1.20	0.78 (0.31)	0.91	0.71
Szarvasi	0.41	0.43 (0.02)	0.38	0.28
miscanthus	0.54	0.72 (0.03)	0.55	0.53
sugar cane bagasse	0.83	1.06 (0.04)	0.76	0.77
rapeseed	0.79	1.29 (0.15)	0.99	0.90
maize	0.69	0.55 (0.00)	0.48	0.38

*averages and standard deviations (brackets), determined by measuring 3 technical replicates.

No apparent pattern was observed in the variation of the S/G ratio before and after extraction, which could indicate a mechanism for the value shift during processing. Based on the HSQC-NMR results, the S/G ratio for beech, eucalyptus, walnut shells, miscanthus, bagasse, and rapeseed increased, whereas that of sida, silphium, and maize decreased, and szarvasi remained unchanged. HSQC-NMR analysis of the extracted lignin showed good reproducibility. Regarding the Py-GC-MS results, all S/G ratios, excluding bagasse, decreased. In contrast, sugar cane bagasse remained unaltered.

There are several possible reasons for the change in the lignin S/G ratio between the untreated biomass and the extract. Although demethoxylation of S to G is chemically possible,

it is unlikely to occur under the given reaction conditions. This explanation cannot account for the measured increase in S/G in some plants when HSQC-NMR was used. Another possibility is that the extractable lignin under the applied conditions is distinct from residual lignin that is still attached to the cellulosic fibers. However, it is unclear whether these more accessible parts are primarily composed of S or G, as these appear to vary among different plant species.

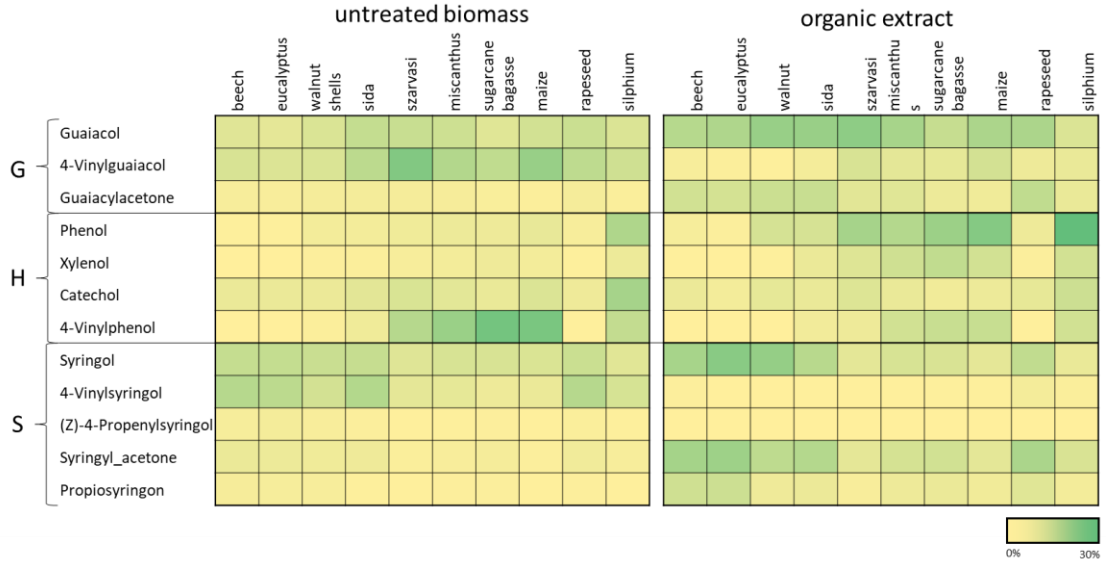

Figure 15: Heatmap of the relative proportions of Py-GC-MS components in untreated biomass and extracted lignin. The full dataset can be found in Appendix 8.4

A systematic review of the measured pyrolysis components revealed more information about the structural changes (Figure 15). The absence of carbohydrates in the extracted lignins resulted in higher concentrations of methoxylated and ethoxylated compounds. Polysaccharides, particularly xylan, can act as a hydrogen donor for the elimination of aromatic substituents by replacement with hydrogen.[104] The interactions between lignin and polysaccharides at higher temperatures can significantly impact the pyrolysis products.[105] In untreated plant material, there is a higher concentration of 4-vinyl products from S, G, and H compared to extracted lignin. This is consistent with the higher levels of β-*O*-4 linked units in the untreated material. Certain types of plant materials, such as beech, eucalyptus walnut shells, and sida, showed a higher concentration of 4-vinylsyringol, while szarvasi, miscanthus, sugarcane bagasse, and maize contained higher levels of 4-vinylguaiacol and 4-vinylphenol. Less common monomer units, such as *p*-coumarate and ferulate, contribute to the formation of these pyrolysis products.[106]

A comparison of the pyrolysis products with chemical lignin features (ABSL lignin in pulp, ABSL lignin in untreated biomass, and delignification) revealed a few correlations. The Pearson coefficients for all combinations are presented in appendix 8.4.

Notably, phenol content was negatively correlated with the lignin content of the untreated material (Pearson coefficient $P = -0.799$, $p < 0.05$), lignin content of the pulp ($P = -0.721$, $p < 0.05$), and delignification ($P = -0.772$, $p < 0.05$). Syringol ($P = 0.857$, $p < 0.05$) and methylsyringol ($P = 0.844$, $p < 0.05$) exhibited a positive correlation with the lignin remaining in the pulp. While phenol is a product formed after the elimination of aromatic substituents, syringol and methylsyringol still retain their aromatic substitutions.[105] Guaiacols and syringols rapidly convert to catechols and phenols when the pyrolysis temperature is increased to 400–450 °C and secondary pyrolysis reactions take place with sufficient H-donors available.[104] Interestingly, silphium lignin demonstrated a remarkable abundance of catechols and phenols after pyrolysis of the untreated biomass, unlike other biomasses where these products were only observed in the pyrolysis of extracted lignin.

Further investigation into the relationships between lignin, carbohydrates, and other components in future studies may help elucidate additional molecular parameters that can explain lignin extraction or retention.

3.1.3.2 Interunit linkage analysis

Subsequently, the linkages between the monomer units were analyzed using HSQC-NMR. The β-*O*-4 ether linkage is the most prevalent type of linkage. It is highly susceptible to cleavage, making it a prime candidate for post-processing depolymerization reactions.[75] In addition, the resinol (β-β) and phenylcoumaran (β-5) linkages were quantified. These linkages include C-C bonds and therefore require more energy to break than the β-*O*-4 linkage.[107] The values are reported relative to 100 S+G units in Table 8.

Table 8: Proportion of ether (β-*O*-4), resinol (β-β,) and phenylcoumaran (β-5) linkage proportion in unprocessed biomass and extracted lignin, per 100 S+G units measured by HSQC-NMR- For the extracted lignin, three technical replicates were measured. Averages are given with standard derivation in brackets.

	unprocessed biomass [per 100 S+G units]			extracted lignin [per 100 S+G units]		
	β-*O*-4	β-β	β-5	β-*O*-4	β-β	β-5
beech	72.3	10.9	5.1	19.2 (0.9)	9.8 (0.2)	2.3 (0.2)
eucalyptus	70.6	9.4	1.3	25.1 (3.3)	9.7 (0.5)	2.0 (0.1)
walnut shells	62.5	10.6	1.3	16.2 (0.9)	8.1 (0.1)	2.7 (0.1)
sida	70.9	10.8	1.4	21.4 (2.2)	6.9 (0.3)	2.6 (0.1)
silphium	59.2	8.1	1.4	23.3 (2.9)	7.2 (1.4)	1.4 (0.2)
szarvasi	32.2	2.8	1.5	22.2 (3.3)	3.7 (0.3)	2.0 (0.3)
miscanthus	34.4	3.8	8.6	14.5 (1.4)	3.5 (0.2)	2.4 (0.1)
sugar cane bagasse	33.7	1.5	1.5	14.2 (2.4)	1.6 (0.2)	1.2 (0.1)
rapeseed	71.4	9.1	8.5	22.7 (3.1)	9.1 (0.4)	3.0 (0.2)
maize	18.1	0.1	1.0	17.4 (1.7)	2.3 (0.3)	1.1 (0.1)

Differences in the proportion of β-*O*-4 linkages among untreated plants are evident. In the woody plant group with beech, eucalyptus, walnut shells, and sida, as well as in rapeseed and sugarcane bagasse, a high proportion of 70-80 linkages per 100 monomer units was observed. Silphium exhibits an even higher β-*O*-4 linkage proportion, at 90 linkages per 100 S+G units. Szarvasi, miscanthus, and maize have noticeably fewer β-aryl linkages, at 40-50 per 100 S + G units.

In the extracted lignin, ether linkages were significantly reduced in plant materials that initially contained a high amount of these linkages, while they were only slightly reduced in those with fewer linkages. Minor variations between experiments can be attributed to biological variance in the sample or slight fluctuations in reaction conditions, such as temperature and pressure. Following processing, there is no statistically significant difference in the β-*O*-4 linkages between the plants (Kruskal-Wallis, post hoc, $p > 0.05$). Thus, it can be concluded that processing uniformly reduces the variety of β-*O*-4 linkages. The β-β and β-5 linkages remained mostly unchanged throughout processing.

3.1.4 Molecular size of the extracted lignin

The molecular weight distribution of lignin is a crucial property for processing, as it affects material properties, such as processability, mechanical strength, and morphological phase behavior. The most common method for measuring lignin size is size exclusion chromatography (SEC), which is a standard method for determining polymer weight. However,

the SEC of lignin is challenging because of its wide size distribution and its macromolecular structure. A wide size distribution results in a high polydispersity index (PDI), and the values for weight and number averages do not represent the actual size distribution of the molecules. Additionally, SEC is a relative analytical method where values are calculated referring to a standard polymer of known size, in this case, polystyrene (PS). Various functional groups cause lignin to behave differently from PS in the solvent dimethylformamide (DMF), so the relation to the standard is not accurate, and the absolute values should be viewed with care. Nevertheless, SEC can be used to compare different lignins, and the structural differences between lignins from different plants add another component of insecurity to the measurements. Different proportions of functional groups and branching also influence the hydrodynamic radius of lignin, and therefore, the SEC results. Lignin from different types of biomass with the same molecular weight might have different retention times and different values reported.[108] Due to these reasons, the full chromatograms of the different extracted lignins are shown here before comparing mass average (M_w), number average (M_n) and PDI.

According to the results of NMR analysis, certain dried lignin fractions contain a substantial quantity of non-polymeric molecules. To remove residual acid, solvents, and secondary plant metabolites, lignin was purified by redissolving in acetone and precipitating in water. The results of this removal are illustrated in Figure 16, which displays the SEC chromatograms of beech lignin before and after precipitation. The precipitation process was effective in eliminating most of the small molecules in the range of 100-120 Da. This includes phosphoric acid, which has a molecular mass of 98 g/mol. Additionally, it was observed that the distribution of larger molecules also decreases towards the end of the curve, indicating that some very large molecules were also removed during the resolution of the dried extract in acetone before precipitation.

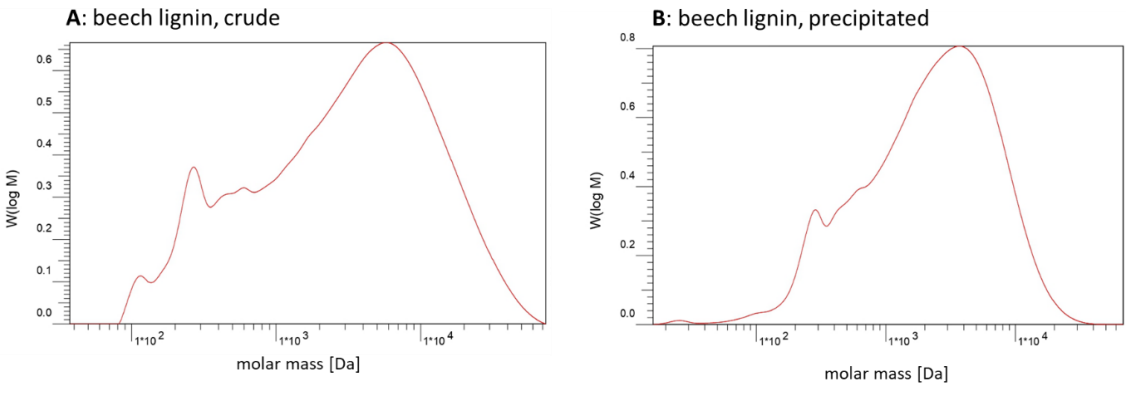

Figure 16: SEC chromatogram of PA OrganoCat beech lignin, A: Dried organic extract, B: After re-solving with acetone and precipitation in water.

The procedure exhibits good reproducibility as demonstrated by three replications of extracted maize lignin (Figure 17).

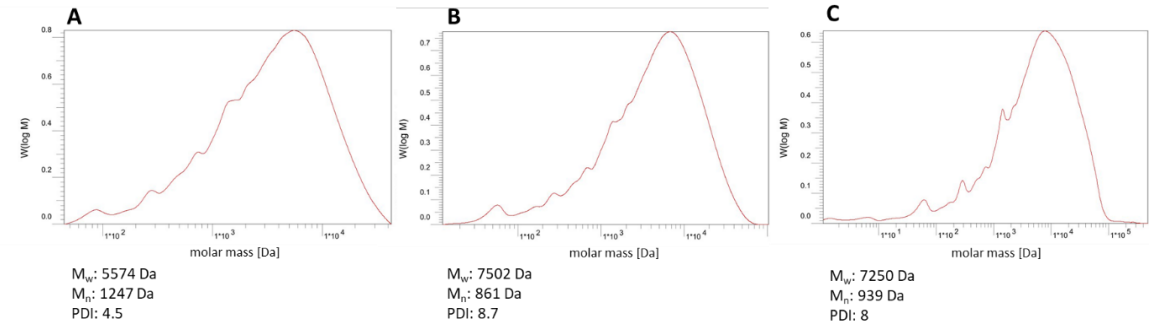

Figure 17: SEC chromatogram of PA OrganoCat maize lignin, three technical replicates.

The chromatograms obtained from the SEC analysis of all remaining plants are presented in Figure 18.

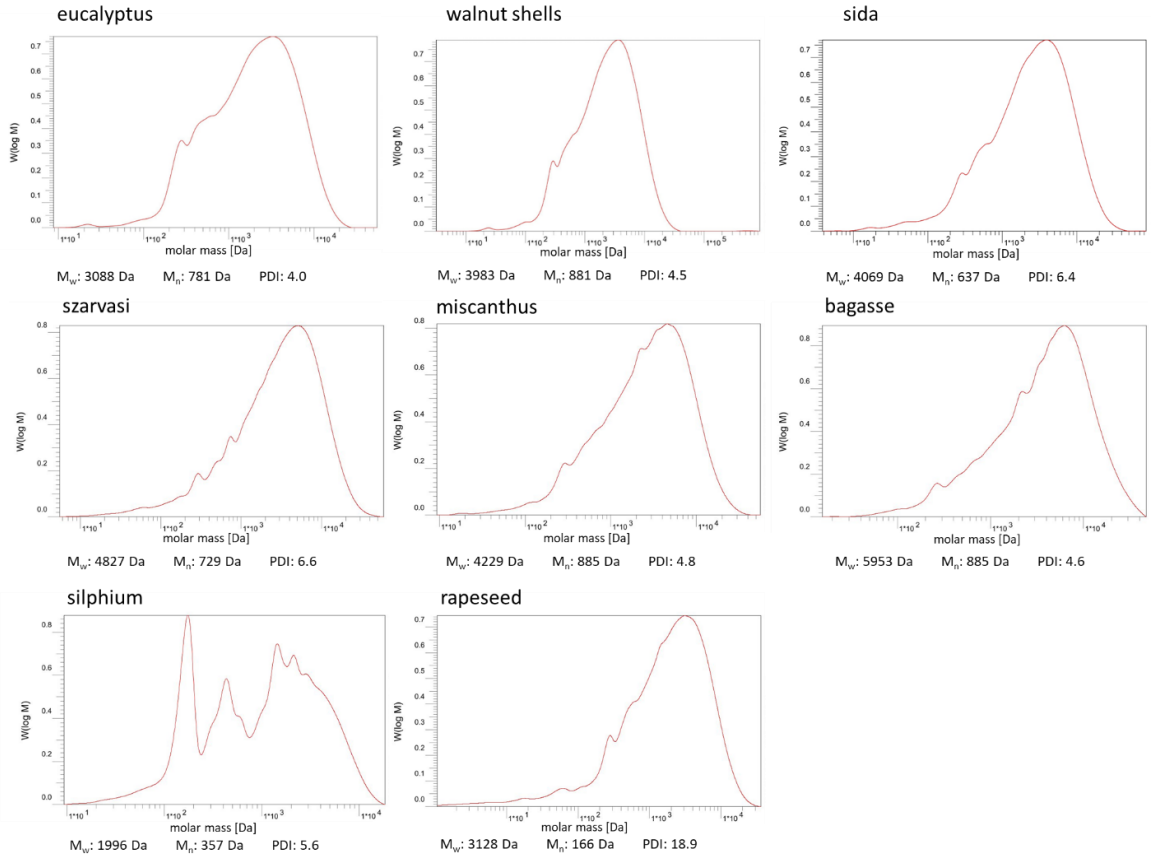

Figure 18: SEC chromatograms of PA OrganoCat lignin from eucalyptus, walnut shells, sida, szarvasi, miscanthus, bagasse, silphium, and rapeseed.

The lignin from all plants other than Silphium exhibits a somewhat similar weight distribution where the molecule size is distributed with a single main peak with a maximum in the range

of 3000-8000 Da. In addition, there appears to be a head with a lower molecular weight. In all chromatograms, a notable number of smaller molecules can be found, represented by a small peak present around 200-300 Da. In some spectra, such as those of szarvasi, maize, and beech, another peak around 700 Da suggests the existence of medium-sized molecules. The pattern might be attributed to extracted phospholipid, which have a reported molecular weight ranging between 800 to 900 Da.[109]

The chromatogram of silphium lignin presents a different appearance than the others. The measurements were repeated to ensure the accuracy of the results. Three main peaks were observed. The first one, which is the largest and most distinct, appears at approximately 150 Da. The second peak is visible at approximately 400 Da, whereas the third and broadest signal consist of three separate peaks that occur between 1500 and 3000 Da. Silphium can contain significant amounts of tannins, proteins and fats, which might make up the lower molecular weight molecules found.[91,110] The results align with previous observations on silphium, suggesting that the organic extract of silphium contains impurities in addition to lignin. The quantity of organic extract exceeds the available lignin in the material, and in the HSQC-NMR analysis, several signals were observed that are not attributable to lignin. A comprehensive analysis of the organic extract of silpium is necessary to confirm these findings.

Lignin molecular weight is typically described by the weight average (M_w), which is a more accurate and reproducible measure than the number average (M_n) due to the presence of smaller molecules in the lignin. However, as discussed above, the range of lignin molecules is broad, and the average does not fully represent the entire extract.

Table 9: SEC chromatography data for weight average (M_w) and number average (M_n) molecular mass of extracted lignin and polydispersity index (PDI).

	M_w [Da]	M_n [Da]	PDI
beech	3595	915	3.9
eucalyptus	3088	781	4.0
walnut shells	3983	881	4.5
Sida	4069	637	6.4
Silphium	1996	357	5.6
Szarvasi	4827	729	6.6
Miscanthus	4229	885	4.8
sugar cane bagasse	5953	1298	4.6
rapeseed	3128	166	18.9
maize*	6775 (855)	1016 (166)	7.0 (1.8)

*for maize, the average of three experiments and their corresponding measurements are shown to prove repeatability of results. Standard derivation in brackets.

The weight average of the PA OrganoCat lignin of the selected materials is measured to be 2000-7000 Da, which is well within the range measured with comparable biomass fractionation processes.[97] Material from beech, eucalyptus, walnut shells and sida seem to yield a slightly smaller lignin than material from the grass species szarvasi, miscanthus, sugar cane bagasse and maize.

The quotient of M_w and M_n, referred to as the polydispersity index (PDI), serves as a numerical representation of the size variation within a polymer. When the PDI is equal to 1, all polymer molecules possess equal dimensions, while a higher value indicates a greater variation in size. With PDI values of 3.9-7 most extracted lignins in this work fall into a range previously reported in literature[97] for similar biomass fractionation processes. Rapeseed is a unique case, exhibiting a notably high PDI of 18.9, which is indicative of an exceedingly small M_n value. Consequently, rapeseed lignin comprises a multitude of small molecules, possibly also containing impurities.

3.1.5 Impact of lignin structure on delignification and lignin quality

To investigate the relationship between structural features of lignin and fractionation efficiency by OrganoCat, multivariate data analysis was conducted (Figure 19).

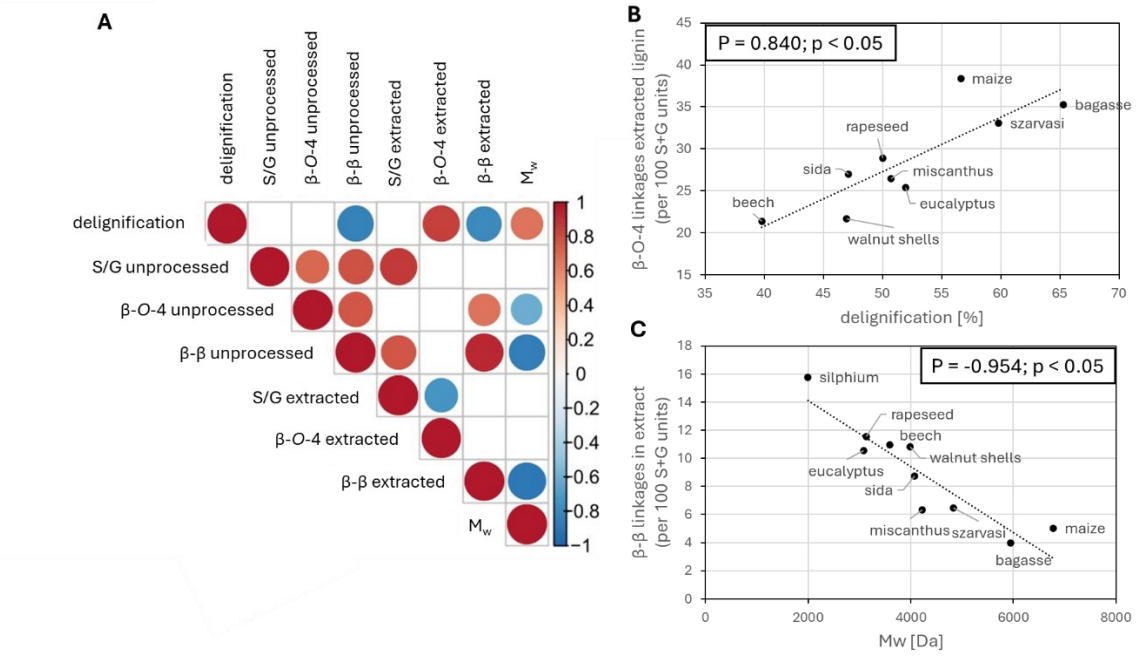

Figure 19: A: Schematic representation of Pearson correlation between delignification and lignin characteristics before and after processing measured by HSQC-NMR. The full dataset can be found in Appendix 8.5. B: Above: Graphical representation of the correlation between β-*O*-4 linkages of extracted lignin and delignification. Below: Graphical representation of the correlation between β-β linkages and molecular weight M_n.

The correlation between biomass delignification and the proportion of β-β linkages is negative in both native (Pearson coefficient P = -826, $p < 0.05$) and extracted (P = -791, $p < 0.05$) lignin, indicating that plants with more β-β linkages in lignin have a smaller proportion of lignin removed from the lignocellulose. However, a positive correlation with delignification is observed for β-*O*-4 linkages of the extracted lignin (P = 0.840, $p < 0.05$) and M_w (P = 0.746, $p < 0.05$), suggesting that plants with lower recalcitrance towards delignification need less ether linkage cleavage to achieve extraction. Grasses such as maize, szarvasi, and bagasse showed high delignification and a high proportion of β-*O*-4 linkages in the extracted lignin, indicating that their lignin is more easily accessible for this extraction. In contrast eucalyptus, and walnut shells showed lower delignification and a lower proportion of β-*O*-4 linkages. Interestingly, rapeseed and Miscanthus exhibited similar behavior to eucalyptus and sida, with mid-range delignification and ether linkages in the extract. Silphium was not considered in the correlation analysis for delignification as the quantification of lignin in this material was made difficult through the high amount of ASC resulting in a higher amount of lignin measured in pulp than in the untreated biomass.

There is no significant correlation of the proportion of native β-*O*-4 linkages with the β-*O*-4 linkages in extracted lignin, but there is a weak negative correlation with the M_w of the extracted lignin (P = -0.683, $p < 0.05$). Similarly, the M_w also demonstrates a negative correlation with the β-β linkages of native (P = -0.738, $p < 0.05$) and extracted lignin (P = -0.954, $p < 0.05$). This suggests that a higher number of β-ether and/or resinol structures per 100 S + G units result in smaller extracted lignin molecules. Since resinol linkages are frequently found at the beginning of lignin chains, lignins with a high amount of β-O-4 and β-β linkages likely have more chains, leading to smaller molecules when ether linkages are cleaved.[100]

The β-β linkage proportion and M_w in the extract correlate negatively (P = -0.954, $p < 0.05$). Only loose clustering with the previously defined plant groups can be observed. While miscanthus, szarvasi, sugar cane, and maize, have a low number of β-β linkages and a high molecular weight beech, eucalyptus, and walnut shells exhibit higher β-β linkage range but lower molar mass average. Sida is again found to be close to the woody biomasses, while silphium is at the extreme end with small molar mass and high β-β linkages. Rapeseed

appeared to be more similar to beech and eucalyptus as it has similar β-β linkages and molar mass as the woods.

3.1.6 How Biomass Properties Affect Fractionation and Lignin Quality

The separation of lignocellulose into its main components—cellulose, lignin, and hemicellulose—is governed by the interplay between the structural characteristics of the biomass and the conditions of the fractionation process. The OrganoCat process was applied to 10 different plant biomasses. These included various woods, grasses, and agricultural residues, allowing an investigation into how biomass composition and lignin structure influence processability.

Although the selected biomass materials varied significantly in native lignin content, the lignin extraction yields were similar across the samples. Materials with a high lignin content, such as walnut shells, did not necessarily result in higher lignin yields. This suggests that factors beyond total lignin content, such as lignin structure and the presence of other biomass components, play a significant role in the efficiency of extraction. A key observation was that, regardless of the initial proportion of β-*O*-4 linkages, the extracted lignin showed no significant ($p > 0.05$) variation in this structural feature. A reduction in β-*O*-4 linkage content was evident in the pulp, suggesting that larger lignin molecules were cleaved prior to extraction. The average molecular weight of the extracted OrganoCat lignin was relatively consistent, ranging from 2,000 to 6,800 Da.

Despite the general consistency in lignin extraction, variations in quality and efficiency were observed, highlighting the need to carefully select biomass for OrganoCat processing. The S/G monomer ratio, which is characteristic of a material, remained similar across all plant materials before and after fractionation. This observation underscores the robustness of the OrganoCat method in preserving fundamental lignin characteristics during the extraction. Consequently, the branching and accessible functional groups in the lignin can be different depending on the source material of the lignin. S rich lignin, such as that derived from hardwoods like beech and eucalyptus, is suspected to be more linear, while G-dominant lignin, found in grasses like szarvasi or miscanthus, is known as more branched.[111] These structural variations can influence downstream applications, such as the design of lignin-based materials or bio-refinery feedstocks. For example, linear lignins may be more suitable for fiber

production due to their reduced branching,[87,88,112] while in crosslinked polymer systems branched lignins might offer advantages.[113]

Processing plant materials with high ASC content, such as silphium, was found to present additional challenges. In the organic extract of silphium, non-lignin components were prominent, as indicated by unusual peaks in the SEC chromatogram, non-lignin-related signals in HQSC-NMR spectra, and the abundance of catechol and phenols in pyrolysis products. The extracted lignin exhibits reduced quality, with potential implications for its applicability in high-value material production. To address this, pre-processing steps to remove ASC or additional post-fractionation treatments could enhance lignin purity. Exploring the chemical nature of ASC and its interactions with the OrganoCat process may also yield strategies for improving overall process efficiency.

This chapter explored the influence of biomass composition and lignin structure on the fractionation process and lignin quality across a diverse range of plant materials. The findings highlighted how structural features such as the β-*O*-4 linkages, S/G monomer ratios, and ASC content impact lignin extraction efficiency and quality. While these comparisons among species provided valuable insights, they also revealed the complexity of predicting fractionation outcomes based solely on biomass composition. To further refine our understanding, the next chapter investigates variations within a single species, examining how cell wall characteristics influence the lignocellulose fractionation in the OrganoCat process and the chemical and physical properties of the extracted lignin.

3.2 Investigation of intra-species differences

While overall cell wall composition within a single species is typically consistent, subtle variations in specific features can arise due to genetic diversity, environmental conditions, or developmental factors. These intra-species differences, although less apparent than inter-species variation, can significantly influence biomass fractionation and lignin quality. For instance, genetic variants within a species may alter lignin monomer ratios, molecular weight distributions, or ether linkage proportion, all of which impact the efficiency of fractionation processes.[114] Similarly, environmental stressors such as drought or nutrient availability can induce changes in cell wall architecture, potentially affecting the accessibility and extractability of lignin.[115]

Studies have reported mixed results regarding the relationship between lignin structure and fractionation yields, largely due to the diverse processes applied. These processes often involve fundamentally different chemical mechanisms that influence lignin and lignocellulose fractionation in distinct ways, thereby limiting their comparability. Consequently, the variations in methodologies contribute to the observed inconsistencies in outcomes. Méchin *et al.* found that in maize, cell wall degradability was better predicted by syringyl units esterified with *p*-coumaric acid than by the S/G ratio, suggesting a focus for future research in poplar.[116] Studer *et al.* demonstrated that both S/G ratio and lignin content influenced sugar release during enzymatic hydrolysis after hot water pretreatment, with higher S/G ratios generally increasing sugar yields, although exceptions highlighted the roles of other factors.[117] Mansfield *et al.* reported that lignin content had a greater impact on bioethanol conversion yields than the S/G ratio in transgenic poplar, with low-lignin plants showing 15% higher conversion efficiency during steam explosion and organosolv pretreatments. High S-lignin plants, however, exhibited better cellulose recovery.[40]

Studies on genetically modified Arabidopsis further showed that S-lignin-rich tissues yielded more glucose than G-lignin-rich ones after liquid hot water pretreatment.[118]

Lignin structure, which is affected by both genetic factors and environmental conditions, is a crucial factor in the fractionation of lignocellulose. Therefore, it is essential to investigate the effects of intrinsic differences within a single species on this process to better manage future processes. Exploring these variations within a single species offers a unique opportunity to understand how inherent cell wall characteristics contribute to biomass recalcitrance.

Therefore, a set of natural variants of poplar was selected for fractionation in the OrganoCat process. The results of this chapter were obtained at the University of British Columbia (Vancouver) within the framework of academic exchange.

3.2.1 Poplar sample selection

A collection of native cottonwood poplars (*populus trichocarpa*) from the Pacific Northwest coastline (44-60° N), which has been planted and maintained at the common garden of the Totem Field, University of British Columbia, was used for sample selection. The harvest has been characterized before in multiple publications.[114,119,120] Nine exemplars of poplar, comprising specimens with high, medium, and low concentrations of total lignin as well as high, medium, and low S/G ratios, were selected for the OrganoCat process (Table 10).

Table 10: Selection of nine poplar accessions characterized by contrasting chemotypic properties, specifically focusing on total lignin content (including soluble and Klason lignin (insoluble), KL) and the S/G ratio was determined by thioacidolysis.[121] The data, originally obtained by Porth *et al.* and previously published[120], provides the foundation for the selection process.
Accessions were categorized into high, medium, and low values based on their lignin content and S/G ratio. One representative sample was selected from each combination of these chemotypic traits.

	Total lignin (soluble + insoluble) [%]	lignin content category	S/G	S/G category
BELA18-2	18.6	Low	2.0	Low
ALAA20-1	21.1	Medium	1.5	low
BULF11-4	27.2	High	2.2	low
MCHB19-1	18.0	Low	2.8	medium
LNZK28-2	21.3	Medium	2.7	medium
LILC26-1	24.2	High	2.7	medium
YALD27-4	17.6	Low	3.5	high
YALE27-3	21.1	Medium	3.8	high
WELC27-5	23.8	High	3.3	high

The 1 L Parr reactor located at the UBC necessitated upscaling of the reaction. Previously, an upscale of the OrganoCat fractionation had been reported, but only with oxalic acid and FDCA as catalysts.[52,122]

The OrganoCat process variation with phosphoric acid was selected for the experiments to maintain consistency with previous work carried out in this study. One of the challenges encountered in upscaling the PA OrganoCat process is the swelling pretreatment step at 80 °C. The reactor configuration does not allow temperature control without the addition of a liquid. Consequently, the swelling step is omitted. Previous research has indicated that while the

swelling step enhances enzymatic saccharification, it does not significantly affect the lignin yield, which is the primary focus of this chapter.[50]

The scale of the reaction was increased forty-fold, utilizing 20 g of biomass for each batch instead of 0.5 g. 200 mL each of 2-MTHF and 0.7 M aqueous H_3PO_4 were used for the liquid phases. The reaction duration was maintained at three hours, following the attainment of an internal temperature of 140 °C. The heating time was approximately 30 min, and the cooldown required 60 min until room temperature was reached. After separating the liquid phases from the pulp by filtration, the organic and aqueous phases were separated, and the aqueous phase was washed with 2-MTHF three times to ensure that the lignin was removed. The aqueous phase visibly lost its light brown color during this process. The organic solvent was removed using a rotary evaporator, and the lignin was fully dried using a high vacuum until weight consistency was achieved.

3.2.2 Fractionation yields

The experiments were conducted on all selected samples (Table 10) with triplicates for all except the high lignin content sample, which was performed twice due to insufficient material. The overall gravimetrically measured pulp and lignin yields exhibited minimal variation (Table 11). In the replicated experiments, no statistically significant differences ($p > 0.05$) were observed between the poplar variants in pulp and lignin yields.

Table 11: Fractionation yields after upscaled PA OrganoCat without swelling using selected poplar samples. Solid residue and lignin yield were determined gravimetrically after drying, residue (insoluble) lignin in pulp was determined using the Klason method. Delignification was calculated using the quotient of lignin in the biomass and pulp yield-corrected residue of lignin in the pulp.

	total KL [% of initial biomass]	S/G	Solid residue [wt% of initial biomass]	lignin yield [% of initial biomass]	Residue KL in pulp [% of pulp]	Deligni-fication [%]
BELA18-2	18.6	2.0	49.5	22.5	16.5	56.1
LILC26-1	24.2	2.7	47.5	21.5	16.0	68.7
MCHB19-1	18.0	2.8	49.3	22.6	16.7	54.4
WELC27-5	23.8	3.2	49.0	23.7	16.9	65.3
BULF11-4*	27.2	2.2	45.7	22.2	15.2	74.7
YALD27-4**	17.6	3.5	48.7 (1.4)	21.5 (0.4)	18.9 (0.9)	47.8
YALE27-3**	21.1	3.8	47.5 (0.8)	21.5 (0.1)	15.5 (0.6)	65.2
ALAA20-1**	21.1	1.5	48.2 (0.8)	21.9 (0.5)	15.1 (1.0)	64.0
LNZK28-2**	21.3	2.7	48.7 (0.5)	21.9 (0.1)	18.0 (0.1)	58.8

* average of duplicate experiments

** average of triplicate experiments, standard deviation given in brackets.

The comparability of these results with those of other plant materials is limited owing to variations in structure and composition. However, the upscaled OrganoCat process generally achieves high extraction yields. The solid residue obtained from the process (45–50 wt%) is slightly lower than that of beech (52%) in the small-scale PA OrganoCat. Using this setup, 21–24 wt% lignin was extracted from poplar, which is notably higher than the lignin yield from beech in the small-scale PA OrganoCat. Without performing a smaller-scale OrganoCat experiment on the same poplar sample, it is unclear whether this increased yield is due to structural differences between the materials or the greater severity of the upscaled process. It is important to note that the process time for the scaled-up PA OrganoCat is slightly longer because preheating and cooldown times were excluded from the calculation. Additionally, the mixing dynamics differ between the two systems, as a magnetic stirring bar was used in the small-scale setup, while a propeller stirrer was used in the upscaled process, potentially affecting the contact area between phases. The lignin yield among different poplar accessions shows less variation than the lignin content in the untreated material, indicating a delignification efficiency of 47–68%.

The obtained yield data shows that as the amount of lignin in poplar increases, the pulp yield decreases (Figure 20). This contradicts the observation of the previous OrganoCat fractionation experiments on different plants (Chapter 3.1) and many other lignocellulose fractionation processes, where increased lignin contents add recalcitrance.[123] Despite this,

the trend is not strong enough to show a significant correlation (Spearman coefficient ρ = -0.567, p = 0.111). Further experiments are required to confirm these observations.

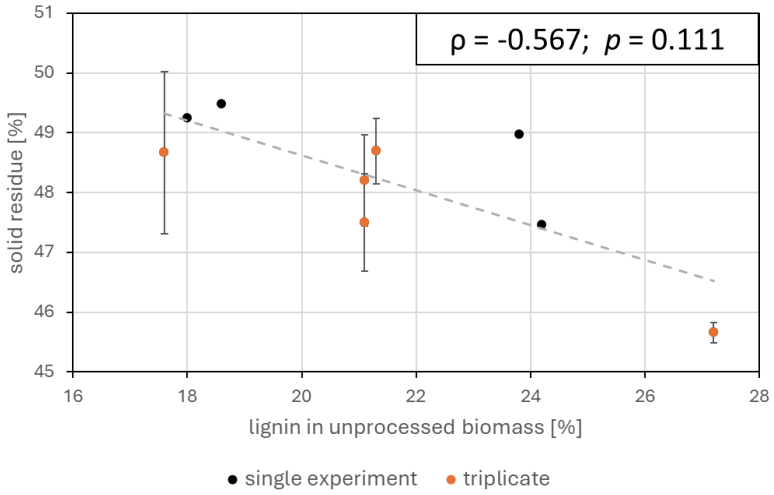

Figure 20: Comparison of solid residue and lignin content of unprocessed biomass. Average data points were used for Spearman correlation when repetitions were present.

The yields of extracted lignin, which range between 21.5–23.7wt% of the initial biomass, are marginally higher than the measured lignin content of the plant. Although the organic extract was dried under high vacuum, secondary plant metabolites, residual catalyst, and residual solvent could contribute to the lignin weight. Therefore, measuring the remaining lignin content in pulp can provide a better estimate of delignification.

The Klason lignin determination method quantifies lignin by hydrolyzing polysaccharide components of the sample and measuring the residual weight (insoluble lignin). Additionally, a smaller portion of lignin in the aqueous hydrolysate can be quantified using UV/Vis spectroscopy (soluble lignin). The pulp showed a low soluble lignin content (0.92–1.18 wt%), indicating that most of the easily soluble lignin (2.2–3.2 wt% in unprocessed poplar) had been extracted. Notably, the (insoluble) lignin content of the pulp showed less variation compared to the lignin content of the unprocessed plant, aligning with the homogenization observed during OrganoCat extraction across various plants (chapter 3.1).

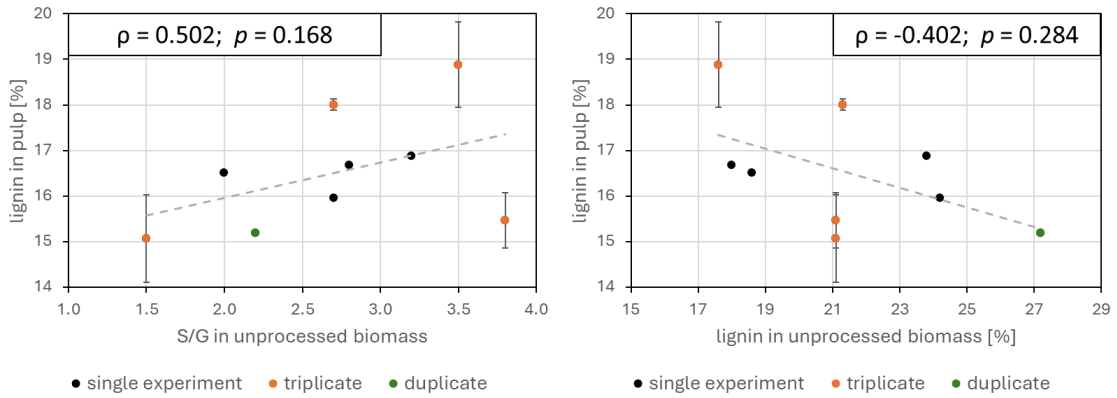

Figure 21: Comparison of the residual lignin content in pulp to the lignin content and S/G ratio of unprocessed poplar samples, utilizing average data points were used for Spearman correlation when repetitions were present.

When comparing the lignin content in the pulp to the S/G ratio in unprocessed poplar, no significant correlation ($p > 0.5$) was observed (Figure 21). However, a noteworthy trend emerged, wherein a higher initial lignin content in the pulp was associated with lower residual lignin content. It is possible that the more lignin-rich poplar varieties possess a type of lignin that is more readily removable.

To enhance the quality of the findings, it is recommended that a larger dataset be utilized through increased repetitions. To investigate the effect of poplar composition on OrganoCat yields, milder conditions should be employed. A smaller scale setup, as shown for the OrganoCat process by Martinez Diaz *et al.* would hereby allow for a higher throughput of samples.[124,125]

3.2.3 Lignin structure evaluation

The HSQC-NMR spectra were acquired to elucidate the structure of the extracted lignin. In the initial measurements, the spectra revealed the presence of several impurities in the lignin, as previously suspected. However, these byproducts were not further identified.

Two lignin samples were purified through the process of re-solving in acetone and subsequent precipitation in water, resulting in a more refined spectral analysis (Figure 22).

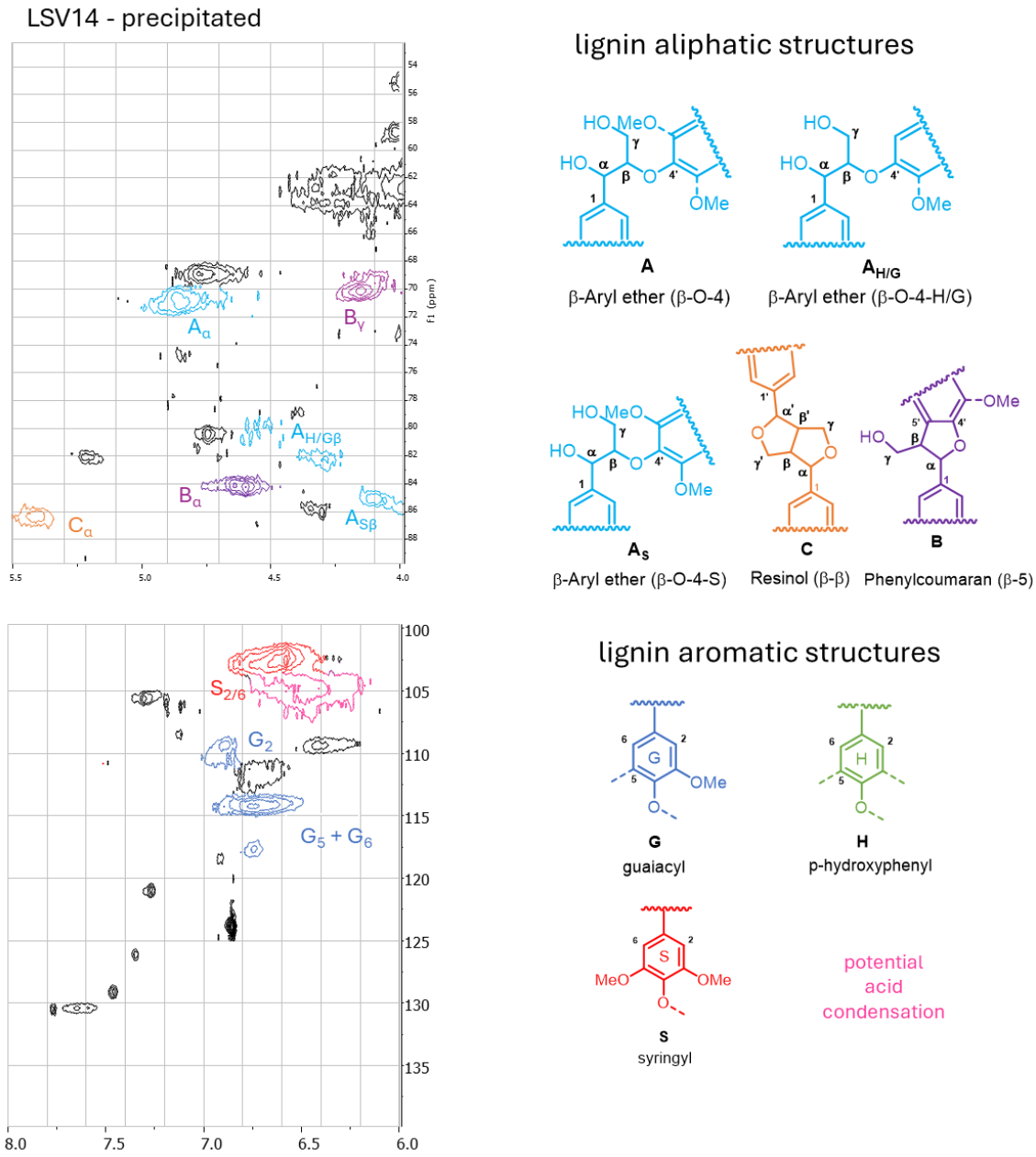

Figure 22: HSQC-NMR spectra of lignin extracted from ALAA20-1. The lignin was redissolved in acetone and precipitated in water to remove impurities prior to the measurement.

The HSQC-NMR spectrum presents all the signals needed to identify the lignin structure; however, additional signals, potentially stemming from condensation and side reactions, remain unknown. The signal adjacent to the $S_{2/6}$ peak is well-known to arise in acid fractionations and may indicate acid condensation on the S-lignin subunits.[126] In conclusion, the HSQC-NMR results suggest that the lignin is altered to a greater extent than desired. Employing milder reaction conditions, such as utilizing a less acidic catalyst, might produce more native lignin.

Table 12: S/G ratios of unprocessed samples determined by thioacyoilysis; β-*O*-4, β-β, β-5 linkages of extracted lignin; H, G, and S units of extracted lignin; S/G of extracted lignin, all determined by HSQC-NMR. Ppt = samples precipitated for cleanup.

Sample	S/G unprocessed	ß-*O*-4 [%]	ß-ß [%]	ß-5 [%]	H [%]	G [%]	S [%]	S/G
ALAA20-1	1.5	12.3	15.4	2.6	0.4	17.1	82.5	4.8
ALAA20-1 ppt	1.5	16.6	12.6	4.5	0.8	21.6	77.6	3.6
BULF11-4	2.2	13.4	16.4	2.6	1.2	17.9	80.9	4.5
LNZK28-2	2.7	13.7	15.1	3.0	1.4	21.9	76.7	3.5
YALD27-4	3.5	16.1	13.6	3.3	0.5	26.2	73.3	2.8
YALE27-3	3.8	15.7	14.6	2.9	0.6	17.7	81.7	4.6
YALE27-3 ppt	3.8	16.8	12.7	4.0	1.1	22.6	76.3	3.4

Analysis of the integrals revealed a higher S/G ratio than previously measured, and it did not align with the S/G ratio in the unprocessed poplar. One reason for this could be the different methods used to determine the S/G ratios. Thioacidolysis was used for the unprocessed samples, whereas lignin analytics were performed via HSQC-NMR. However, HSQC-NMR analysis itself also revealed some difficulties. The quantified signals $S_{2/6}$ and G_2 were affected by condensation reactions, such as acid condensation, as observed in Figure 22; thus, these integrals may not accurately represent the monomer structure. The accuracy of the results may be compromised because quantification of the linkages is relative to the monomer units. However, the cleanup of lignin by precipitation did not significantly affect the quantification of monomer units and linkages. The resinol signal was as strong as the β-*O*-4 signal, indicating significant cleavage of ether linkages and potentially some degree of condensation.

3.2.4 Thermal properties of the extracted lignin

The thermal behavior of lignin is a relevant characteristic for some lignin applications, such as melt spinning and carbonization. To further compare the extracted lignins, the glass transition temperature (T_g) of lignin with high, medium, and low S/G ratios was determined using dynamic scanning calorimetry (DSC). Prior to the measurements, all lignins were dried in a vacuum oven at 40 °C for a minimum of 24 h.

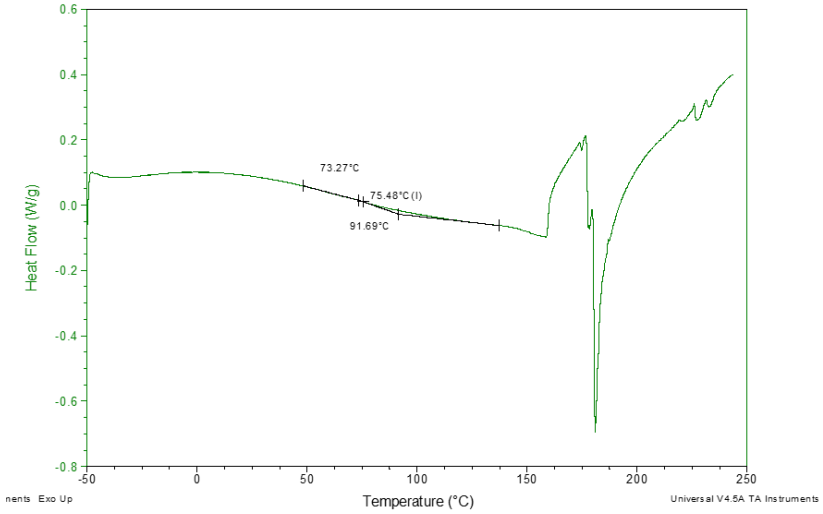

Figure 23: DSC graph of lignin of YALE27-3, dried organic extract.

Measurements of raw lignin (Figure 23) revealed a slow early onset glass transition. The T_g values determined for the raw lignin samples were–75-79 °C. Moreover, the abruptly changing signal that begins after 120 °C during the first heating cycle and then at 150 °C, the maximum temperature of cycle 1, in the second cycle, indicates the presence of evaporating or decomposing components in the sample. These could be remaining water, 2-MTHF, catalyst or extracted lipids. Therefore, lignin was purified by re-dissolution in acetone and precipitation in water. The filtered solid was dried thoroughly in a vacuum oven for a minimum of 24 h to ensure that no water remained.

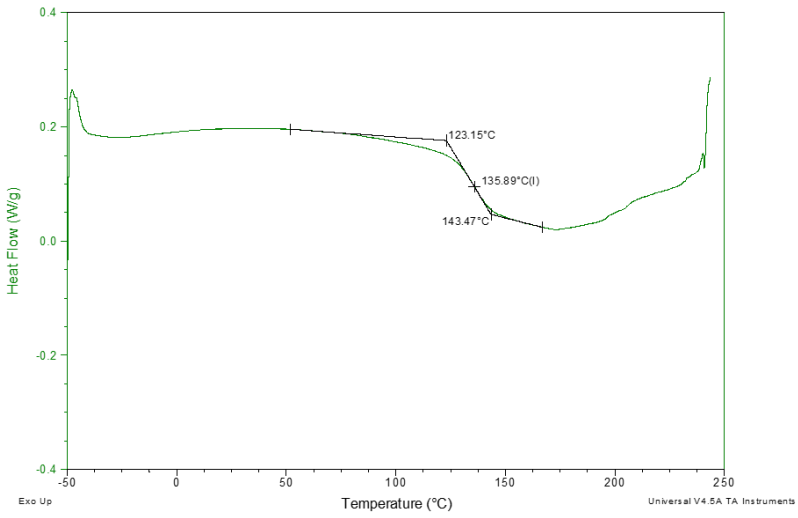

Figure 24: DSC graph of precipitated lignin of YALE27-3.

The purified lignin exhibited a distinct DSC curve. A higher T_g value (128-136 °C) and a clearer onset were detected. There were no observable trends in the measured data, suggesting a correlation between T_g and the S/G ratio or the lignin content of the samples (Table 13).

Table 13: Glass transition temperatures of dried organic extract (raw lignin) and lignin redissolved in acetone and then precipitated in water. Lignin content and S/G ratio of unprocessed poplar samples for comparison.

	Lignin content unprocessed [%]	S/G unprocessed	T_g raw [°C]	T_g precipitated [°C]
ALAA20-1	21.1	1.5	76.2	128.3
ALAA20-1	21.1	1.5	-	135.7
BULF11-4	27.2	2.2	-	126.8
LNZK28-2	21.3	2.7	76.4	133.5
LNZK28-2	21.3	2.7	78.4	-
YALE27-3	21.1	3.8	75.5	136.1

Lignin's unpredictable and inconsistent thermal properties are attributed to structural differences arising from various extraction processes. Choi *et al.* utilized response surface methodology to investigate the structural characteristics of ethanol organosolv lignin and their correlation with thermal properties. The study found that ethanol organosolv lignin with a low molecular weight, high phenolic hydroxyl content, and low aryl-ether linkage content had higher T_g values. These T_g values ranged from 139 °C under mild conditions to 174 °C under harsh conditions.[127] Other groups reported T_g values of 100 °C[128] and 120 °C.[86] A glass transition temperature for OrganoCat lignin had not yet been determined. However, considering the comparable size and structure of OrganoCat and organosolv lignins, the T_g of purified OrganoCat lignin is within a reasonable range. It is important to note that the observed 7.4 °C difference in the T_g of two lignin batches (ALAA20-1) may indicate quality fluctuations within the same sample, which could conceal potential structural correlations.

3.2.5 Conclusions on the impact of intra-species lignin content and structure differences on biomass fractionation

In the experimental setup used to explore the natural genetic variations of poplar in OrganoCat fractionation, no significant correlations ($p > 0.05$) were detected between lignin content, S/G ratio and yields or lignin quality. A notable but non-significant trend was observed, where the solid residue yield showed a negative relationship with the lignin content. As biomass structure and fractionation are complex, this may mean that factors other than the lignin content of poplar dominated the recalcitrance in this process. While the T_g of the poplar OrganoCat lignin was comparable to the values reported for similar organosolv lignin in the literature, no trend was observed between lignin samples with different S/G ratios.

Comparatively, Martinez *et al.* observed minimal variation in lignin and pulp yield across different poplar genotypes, fertilization levels, and OrganoCat process severities, concluding that the process reduces the impact of genetic and nutritional differences.[125] These findings align with the observations in this chapter, suggesting that minor variations in cell wall composition within a species may not significantly influence OrganoCat fractionation outcomes.

However, the literature suggests that lignin content and S/G ratio influence the fractionation yields in other systems. Studies report that higher S/G ratios often improve yields, while low lignin content appears to have an even greater impact on efficiency.[40,116–118]

Current evidence does not rule out the possibility that intra-species lignin content and structural variations affect OrganoCat processing. To gain deeper insight into these dynamics, future studies should expand the sample size and refine process conditions to improve statistical robustness. A promising approach is to use a flow-through variation of the OrganoCat process, which allows for time-resolved fraction collection. This method can elucidate the underlying mechanisms of lignin disintegration and further clarify the structure-function relationship in lignin extraction.

3.3 Flow through OrganoCat variation

Flow-through processing has gained recognition as a viable alternative to batch processing due to its greater efficiency and reduced cost. It has been explored for various alternative biomass fractionation methods.[64,69,71] The flow-through version of the OrganoCat process was proposed by D. Weidener in his thesis, and initial findings were presented.[129]

It was demonstrated that the flow through OrganoCat variation could achieve similar extraction efficiency as batch processing at shorter process times. Initial investigations revealed that a process temperature of 150 °C and a 60-minute reaction time were promising reaction conditions. Under these conditions, the amount of extractives in the organic phase was found to be 25wt% of the initial biomass, exceeding the expected maximum lignin content. Only 10% of the sugars were present in the aqueous phase, leading to the early hypothesis that sugar hydrolysis is less effective during flow-through pretreatment than during batch processing. To further analyze the time-resolved lignin and sugar yields, 12 fractions were collected for 5 min each. The results indicate that lignin and sugars were extracted simultaneously, but sugar extraction appeared to occur more rapidly. The flow-through approach, which allows for short contact times, not only increases the recovery rate of oxalic acid, but also reduces the amount of side products and secondary reactions of the extracted products. Additionally, the formation of furfural was low. Lignin analysis showed slightly higher amounts of β-*O*-4 linkages in most experiments compared to the batch process, while the molecular weight and PDI were lower for the flow-through variation. The results of this study are based solely on singular experiments, and further replications will be required to verify the findings.[129]

This chapter focuses on developing the flow through OrganoCat variation. The goal is to understand the influence of process parameters on the fractionation results and ensure repeatability. After reestablishing the setup at Forschungszentrum Jülich (FZJ), the process parameters were refined using a design of experiments (DOE) approach, and a scale-up was explored. Moreover, by having the ability to collect solvent fractions during the experiment, the OrganoCat process allows for a more detailed examination of biomass fractionation mechanisms. On the other hand, the insight into the stepwise degradation of the cell wall could also be used as an analytical tool for biomass cell wall analysis.

3.3.1 Establishing the reaction

High-Performance Liquid Chromatography (HPLC) equipment was utilized to design the flow reactor (Figure 25). The solvent flow is controlled by two pumps, which can operate at the same or different rates. The biomass is packed loosely in a heated metal tube, with the pressure maintained at 70 bar. Following the reaction, the solvents are cooled and collected, resulting in the presence of lignin in the organic phase and hemicellulose sugars in the aqueous phase. After the completion of the process, the pulp is removed from the reactor, washed, and dried. Oxalic acid was chosen as the catalyst as this process variation does not require a swelling step and, in contrast to FDCA, oxalic acid is soluble in water at room temperature.[52]

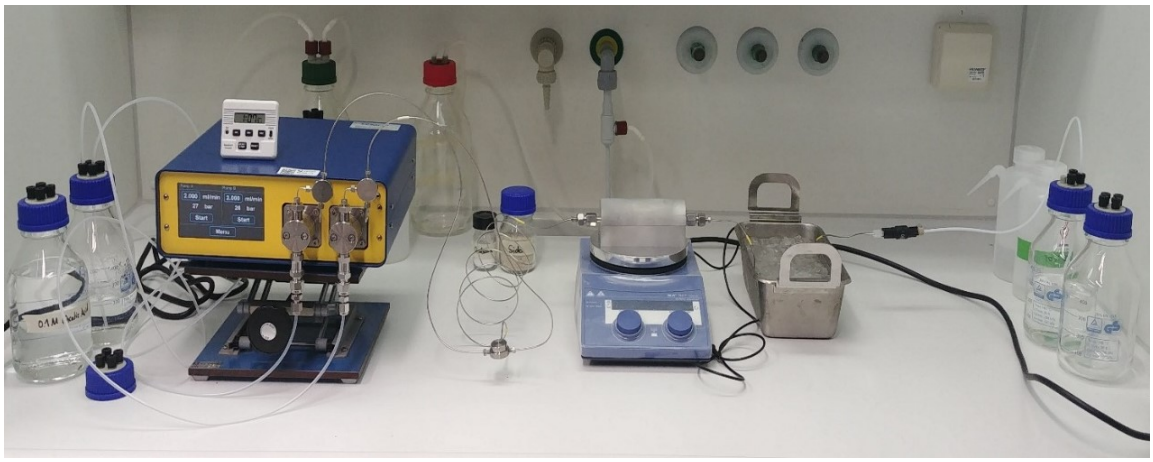

Figure 25: Picture of the flow through OrganoCat setup.

During the reaction, not only lignin but also a substantial amount of oxalic acid was extracted from the aqueous phase into the organic phase. This adds to the gravimetrically determined yield of organic extracts if not removed. Therefore, oxalic acid was removed directly from the yielded organic phase using a 0.2 M $CaCl_2$ solution.

3.3.2 Assessing the flow through process setup

To ensure repeatability of the results, the reaction conditions of 60 min of process time, 160 °C heating temperature and 0.2 mL/min flow per solvent were chosen, and three experiments were conducted (Table 14). The process conditions were chosen to mirror the conditions used in Weidener's work that already showed promising results.[129] The process temperature was chosen slightly higher as the setup showed potential to tolerate higher temperatures.

Table 14: Repetition series of experiments at 160 °C, 60 min, 0.2 mL/min. Average of three experiments, standard derivation given in brackets. *Lignin and pulp yield were determined gravimetrically, given in % of biomass used. The xylose yield was determined using PAHBAH, and the yield of total hemicellulose sugar was determined using ion chromatography of the*

aqueous phase. Lignin characteristics such as β-*O*-4, β-β, and β-5 linkages, as well as the S/G ratio, were determined using HSQC-NMR and linkages given in linkages per 100 S+G units. Lignin linkages are given per 100 S+G units. The previously determined composition of the unprocessed beech wood is given for direct comparison.

Flow through OrgnaoCat		Beech wood composition	
Lignin yield [%]	8.7 (0.8)	Lignin (ABSL) [%]	20.3 (1.8)
Pulp yield [%]	49.8 (1.9)	Cellulose (CrC) [%]	47.1 (3.8)
Xylose yield (PAHBAH) [%]	16.0 (0.6)	Xylose (IC, TFA) [%]	14.4 (2.4)
Sugar yield [%]	23.5 (1)	Hemicellulose sugar (IC, TFA) [%]	18.8 (2.9)
β-*O*-4 [per 100 S+G]	19.5 (1.1)	β-*O*-4 [per 100 S+G]	73.5
β-β [per 100 S+G]	11.4 (0.9)	β-β [per 100 S+G]	10.9
β-5 [per 100 S+G]	4.5 (3.1)	β-5 [per 100 S+G]	5.1
S/G	1.6 (0.1)	S/G	1.5

The experimental results showed good reproducibility. Therefore, a single repetition per reaction condition was chosen for the design of experiments (DOE) approach in the following chapter (3.3.3). Under the selected conditions, 43wt% of the theoretically accessible lignin (lignin yield/ABSL lignin of beech) was extracted. A minor loss of lignin yield may occur during the precipitation of oxalic acid, as some brown, insoluble residue can be observed in the calcium oxalate. Attempts to dissolve these traces in 2-MTHF or acetone were unsuccessful, suggesting that the residue might consist of larger, insoluble lignin molecules. The solid residue was reduced by half, which is close to the expected amount of cellulose (CrC) in beech wood. The xylose yields detected by the PAHBAH analysis matched the xylose yield found in the unprocessed biomass (Table 14). Although the total sugar yield slightly exceeded the expected maximum, this still depicts the initial analysis of the beechwood material.

After comparing the sugar profile of the beech to that of the sugars found in the aqueous phase (Figure 26), it was evident that 27% of the hydrolyzed sugars consisted of glucose. The additional glucose can be attributed not only to hydrolyzed starch, but also to the hydrolyzation of cellulose. The time-resolved analysis in chapter 3.4 showed more evidence for this. Additionally, the proportions of galacturonic acid and galactose increased. A high amount of galacturonic acid, which is usually found in pectin, was extracted. Overall, the hydrolyzed sugar yield not only consists of hemicellulose sugars that are found in the TFA hydrolysis of dAIR biomass, but also includes hydrolyzed starch, pectin, and cellulose.

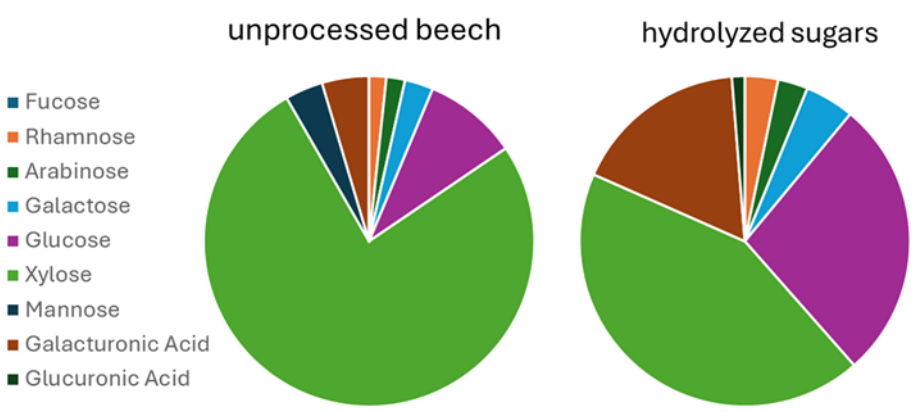

Figure 26: Relative composition of hemicellulose sugars in beech wood (TFA fraction) and hydrolyzed sugars in the aqueous phase after flow through OrganoCat of beech wood at 160 °C for 60 min at 0.2 mL/min.

Upon comparing the fractionation yield with the results achieved earlier by D. Weidener using the same setup[129], it becomes evident that a significantly lower amount of lignin was extracted. In his thesis, 25wt% of the lignin was extracted at a lower process temperature of 150 °C after a process time of 60 min and a flow rate of 0.2 mL/min. Furthermore, experiments conducted at 140 °C yielded 15-17wt% lignin. The discrepancies between the two sets of results may be attributed to the use of a different beechwood sample in Weidener's experiments. However, it is worth noting that the yield of 25wt% lignin is even higher than the expected maximum, which suggests that the organic extract may consist partly of solvent or oxalic acid that has not been removed. The experimental protocol did not include a procedure for oxalic acid removal.

Sugar yields were significantly higher in the repetition experiments than in Weidener's work, which reported yields ranging from 9 to 12 wt%. One possible reason for this increase in sugar yield is the higher process temperature used in the repeated experiments. The hypothesis of Weidener's work that lignin extraction is more effective when using a flow-through approach while sugar extraction is less effective could not be confirmed by these results.[129] Consequently, a more detailed analysis of the flow though process was necessary to understand the influences of the process parameters catalyst, temperature, flow rate and process time on the fractionation yields.

To assess the impact of temperature and catalyst on the flow-through process, each factor was left out, while the other conditions were selected to be at the maximum of the range tested in this work. In the first experiment (**FTB1**), the aqueous phase contained no catalyst,

while the temperature was set at a high level. In the second experiment (**FTB2**), 0.1 M of oxalic acid was added to the aqueous phase. However, no heat was applied during the experiment.

Table 15: Modified Flow-through process experiments omitting a key factor. Yields are given as percentages of the initial biomass.

	Temperature [°C]	Flow rate [mL/min]	Time [min]	Solid residue [wt%]	Lignin yield [wt%]	Sugar yield (IC) [wt%]
FTB1*	180	0.3	90	49.3*	7.5*I	0.6*
FTB2	25	0.3	90	87.4	2.7**	0.1

* no catalyst
** looks dusty, small wood particles visible

The absence of heating resulted in minimal extraction of sugars and lignin (**FTB2**). The dried organic extract corresponded to 2.7% of the initial biomass and exhibited distinct visual characteristics compared to the lignin extracted in other experiments. Its color was light brown, and small particles were discernible, suggesting that small biomass particles had been washed out. The weight of the biomass was reduced by 12.6%, which can be attributed to the lipids, amino acids, other secondary metabolites, and wood dust being extracted.

The experiment **FTB1**, conducted without the oxalic acid catalyst, yielded only a small amount of hydrolyzed sugars, but a substantial amount of lignin, equivalent to 7.5wt%, if the initial plant material was extracted. This result is comparable to that of lignin extracted during previous repetition experiments. The repetition experiments were performed at a lower temperature (160 °C) and for a shorter duration (60 min) than that of the **FTB1** experiment (180 °C, 90 min). The catalyst did not appear to affect the extraction of a portion of lignin. It is possible that a certain amount of easily accessible lignin can be extracted using only an organic solvent and temperature.

HSQC-NMR analysis revealed that lignin extracted in **FTB1** contains 35.6 β-*O*-4 linkages per 100 S+G units. Compared to unprocessed beech wood (73.5 linkages per 100 S+G units), the β-*O*-4 linkage proportion was reduced by approximately 50% in the extract. In the replicate experiment conducted at a lower temperature (160 °C) with oxalic acid, the extracted lignin contained 19.5 β-*O*-4 linkages per 100 S+G units (Table 12), which demonstrates the influence of the catalyst on the cleavage of ether linkages within the lignin.

Through the autoproteolysis of water at 180 °C, a small number of protons were still available for the reactions. Furthermore, the release of acetic acid from the acetyl groups of

hemicellulose during hydrothermal treatment adds more acid catalyst to the process, which can have an impact on lignin and sugar extraction. Tunc *et al.* showed that this autohydrolysis effect has a significant impact on lignocellulose fractionation, reaching a pH of 3-4 while treating hardwood chips at 160 °C with pure water.[130] While the group only observed minimal lignin removal, hemicellulose oligomers were detected under these conditions. Although no singular sugars were detected in **FTB1**, it is possible that sugar oligomers were extracted into the aqueous phase, contributing to the low solid residue observed.

The brief duration for which the solvents are present in the reactor should contribute to reducing the conversion of sugars into furfural. To confirm this hypothesis, the furfural yield was tested at the highest temperature used (180 °C). After 60 min of processing, less than 1 wt% furfural and 5-hydroxymethylfurfural (5-HMF) were produced. This is significantly lower than the yield obtained from the comparable batch experiment (beech, phosphoric acid, 1 h swelling + 3 h reaction, 140 °C), which resulted in 3.9 wt% furfural derivatives. Additionally, increasing the flow rate by a factor of three further reduced the furfural yield by approximately 1/3. This indicates that the time the dissolved sugars are spent in the reactor is directly related to furfural yield.

Table 16: Furfural quantification experiments. Flow through OrganoCat at 180 °C, process time 60 min. Furfural and 5-hydroxymethylfurfural (5-HMF) were quantified by ^{1}H-NMR of the organic phase using mesitylene as internal standard.

flow rate [mL/min]	Sum of furfural and 5-HMF [w% of initial biomass]
0.1	0.96
0.3	0.32

3.3.3 Exploring reaction variables using Design of Experiments (DOE)

In complex processes such as lignocellulose fractionation, various factors can affect the output. Response surface methodology (RSM) can explore the relationship between different process variables and yield and quality parameters as response variables. Design of Experiments (DOE) was used to determine the correlation between these process variables and results to draw valid and impartial conclusions about the dependencies of variables. This technique can be used to optimize a process, product, or system. DOE encompasses several strategies that must be appropriately chosen for the experiment. A full factorial design evaluates all possible combinations of factors and levels, whereas a fractional factorial design can reduce the number of experiments required using statistical methods, but limits the number of factor interactions, that can be explored. A polynomial model is developed to approximate the relationship between variables, which is commonly used to maximize or minimize a response variable of interest.[131]

A Box–Behnken design was chosen to gain insight into the influence of variable reaction coefficients, time, temperature, and solvent flow rate. The design features a quadratic model, where the treatment combinations are the midpoints of edges of the process space and the center (Figure 27).[131] To gain insight into the influence of the reaction conditions on the lignocellulose fractionation in the flow through OrganoCat, a design with three factors and one center point each was chosen. This results in 15 experiments, including the repetition of the central point, to ensure reproducibility of the results.

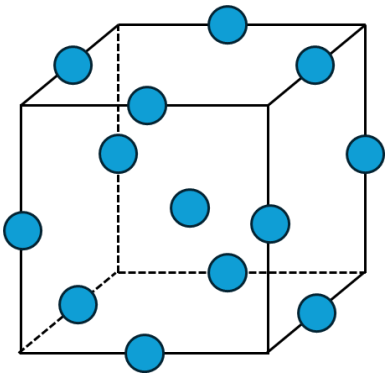

Figure 27: Scheme of the center points used in the Box-Behnken design.

The chosen frame for the optimization is listed in Table 17. For the temperature, 140 °C was chosen as the minimum because this is the temperature at which the batch process is optimal for oxalic acid. In the flow-through process, the contact time is much lower, and the solvent

needs to be heated within the reactor; therefore, it was hypothesized that the flow-through process can handle higher temperatures. A temperature of 180 °C was selected as the maximum process temperature. The risks of higher temperatures include the degradation of oxalic acid to formic acid and CO_2, the conversion of sugars into furfural and 5-HMF, and the β-*O*-4 linkage reduction and recondensation of lignin. It is proposed that these are avoided at short contact times. For the process time, a minimum of 30 min and maximum of 90 min were chosen. The process time was not equal to the classical reaction time in a batch process. While the solid biomass is exposed to solvents for the entire process time, the time the solvent spends in the reactor is determined by the flow rate. The combination of the flow rate and process time determines the loading (catalyst-to-biomass ratio). A lower flow rate implies a higher extraction efficiency because of the higher product concentration. For technical reasons the flow rate can only be adjusted in increments of 0.1 mL/min, therefore flow rates between 0.1 and 0.3 mL/min were chosen. The selected conditions result in biomass loadings from 30 mg/mL (90 min, 0.3 mL/min) to 267 mg/mL (30 min, 0.1 mL/min). This range was chosen to vary around the loading of the batch experiment at 100 mg/mL.

Table 17: Factors chosen for Box Behnken design in design expert.

Factor	Unit	Minimum	Maximum
Temperature	°C	140	180
Time	min	30	90
Flow rate	mL/min	0.1	0.3

Table 18 shows the full set of experiments conducted using the Box Behnken design. As a product of the flow rate and process time, the volume of water and 2-MTHF varied between 3 and 27 mL for each solvent. Depending on the solvent volume and reactor filling, the biomass loading varied between 29 and 267 mg/mL of the aqueous phase. The biomass loading of the batch process compares at 100 mg/mL of aqueous phase.

Table 18: Full set of reaction conditions for the Box Behnken DOE experiments. Solvent volume and biomass loading are given for comparison of the results.

	Temperature [°C]	Time [min]	Flow rate [mL/min]	Solvent volume [mL per phase]	Loading [mg/mL]
FT1	140	30	0.2	6	134
FT2	180	30	0.2	6	134
FT3	140	90	0.2	18	45
FT4	180	90	0.2	18	44
FT5	140	60	0.1	6	115

FT6	180	60	0.1	6	133
FT7	140	60	0.3	18	45
FT8	180	60	0.3	18	42
FT9	160	30	0.1	3	267
FT10	160	90	0.1	9	91
FT11	160	30	0.3	9	90
FT12	160	90	0.3	27	29
FT13	160	60	0.2	12	67
FT14	160	60	0.2	12	67
FT15	160	60	0.2	12	65

Response factors, including sugar yield, lignin content, and solid residue, were evaluated. Furthermore, the extracted lignin was analyzed using HSQC-NMR to gather information about the monomer composition and interunit linkages.

Table 19: Yields of flow through OrganoCat DOE experiments relative to the initial biomass. Xylose yield was determined by PAHBAH using xylose as an internal standard. Total sugar yield was determined from HPAEC-PAD of the aqueous phase. Linkages and S/G ratio analysis are the results of the HSQC-NMR analysis of the yielded lignin.

	Lignin yield [%]	Pulp yield [%]	Xylose yield (PAHBAH) [%]	Sugar yield [IC] [%]	β-*O*-4 [per 100 S+G units]	ß-ß [per 100 S+G units]	ß-5 [per 100 S+G units]	S/G
FT1	3.3	69.2	5.5	9.6	32.4	12.3	7.9	1.1
FT2	9.9	39.4	19.0	33.8	20.7	9.7	8.6	1.5
FT3	8.1	56.5	10.8	12.0	20.0	13.2	2.2	1.5
FT4	14.5	37.4	28.6	45.4	21.5	10.4	9.4	1.5
FT5	3.8	64.9	5.5	5.9	21.4	12.1	2.8	1.7
FT6	8.8	44.3	19.9	30.4	19.7	10.0	2.8	1.6
FT7	5.4	58.4	6.5	12.7	21.3	12.4	2.3	1.4
FT8	12.7	39.5	23.4	30.4	25.3	10.2	9.5	1.6
FT9	4.7	52.8	12.0	23.9	20.0	10.6	2.4	1.5
FT10	7.6	49.3	19.2	24.2	18.5	10.6	2.4	1.6
FT11	5.2	55.3	12.8	16.7	28.6	11.8	2.3	1.6
FT12	11.2	42.7	15.9	27.5	24.2	13.2	2.3	1.5
FT13	7.5	52.3	15.2	24.9	21.9	11.6	2.2	1.5
FT14	9.3	49.7	15.9	20.5	23.3	12.6	2.4	1.7
FT15	9.4	47.5	16.7	25.2	20.6	10.3	8.9	1.6

Lignin yield is reported to be in the range of 3.3 to 14.5wt%, while the solid residue is measured to be between 37 and 69wt% (Table 19).

The sugar yield was measured as the concentration in the aqueous phase and was subsequently calculated based on the theoretical volume of the aqueous phase used in the corresponding experiment. To accurately determine the sugar concentration, two methods

were implemented. One of these methods, using *para*-hydroxybenzoic acid hydrazide (PAHBAH), was employed with xylose (the primary sugar in hemicellulose) as an internal standard. Additionally, all sugars were quantified using ion chromatography (HPAEC-PAD, IC). Although PAHBAH is generally quicker and less equipment intensive, the colorimetric analysis of the reduction reaction tends to underestimate the actual sugar concentration because only pure xylose is used as an internal standard, whereas the aqueous phase produced contains a mixture of sugars. Consequently, ion chromatography is considered a more reliable method, and the data obtained from HPAEC-PAD analysis was utilized for the DOE model. Nevertheless, the results obtained from the PAHBAH assay demonstrate the same trend and should therefore be used to assess sugar extraction efficiency. As shown in Table 19, the measured sugar yields occasionally exceeded the anticipated amount expected from the beech analysis, particularly in experiments **FT2**, **FT4**, **FT6**, and **FT8**. All these experiments were conducted at the highest process temperature of 180 °C, and the sugar composition analyzed by HPAEC-PAD revealed an abundance of glucose. Consequently, as the temperature increased, non-hemicellulose glucose was hydrolyzed. This will be discussed in detail in chapter 3.4.

The reaction conditions and product separation of the batch and flow-through processes are inherently different, which limits their comparability. In the flow-through process, fresh solvents and catalyst are continuously pumped through the stationary biomass phase and exit the reactor to be cooled down after 4-5 minutes, with phase separation occurring shortly thereafter. In the batch variation, however, solvents, catalyst, and extracted products are mixed and heated throughout the entire process duration of 3 h, allowing for more side reactions, continued reaction of the products such as the conversion of sugars into furfural, and increased catalyst degradation. Acknowledging the limitations of comparability between the batch and flow-through processes, Figure 28 provides a general overview of the yields and lignin composition achievable within the flow-through process. The yields and lignin composition of a batch OrganoCat process utilizing oxalic acid and the previously optimized reaction conditions are presented in comparison with the maximum and minimum yields and β-*O*-4 linkage results obtained by screening the process conditions described earlier (Table 19).

The flow through process can achieve similar yields and lignin linkage proportions as the optimized batch OrganoCat process using the same catalyst (0.1 M oxalic acid, 140 °C, 180 min), subject to the process conditions (Figure 28). The flow through process enables higher temperatures and consequently shorter process times. Depending on the time and flow rate, higher solvent volumes are required, resulting in a lower theoretical biomass loading for most reaction conditions. Although the maximum yield for lignin can only be increased by two percent compared to the batch process, the sugar yield was nearly doubled. The higher temperature may contribute to the release of more sugars.

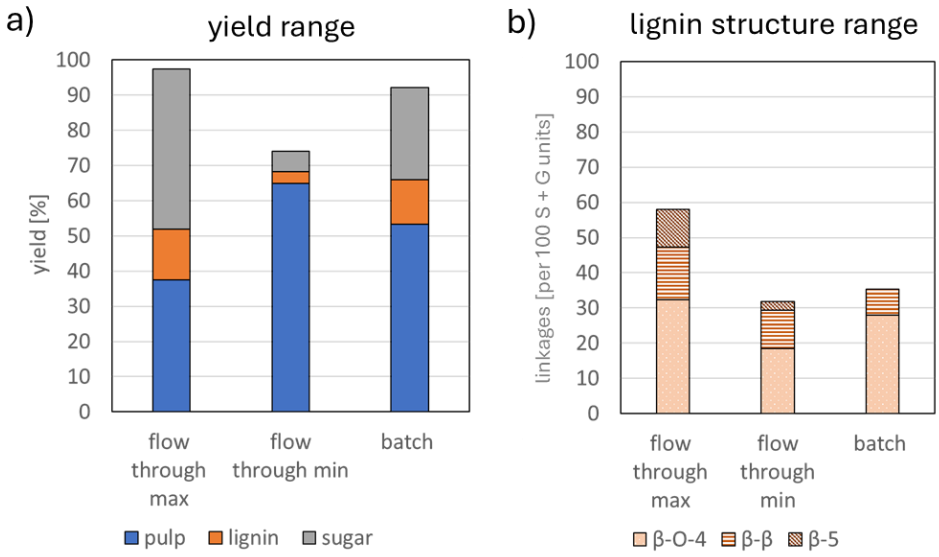

Figure 28: a) Maximum and minimum yields of the flow through process (FT) with beech wood and yields of a comparable batch process with beech wood. Oxalic acid was used as the catalyst for all process variations. Maximum FT yield reaction conditions: 180 °C, 90 min, 0.2 mL/min. Batch reaction conditions: 140 °C, 60 min, 0.1 mL/min. b) FT experiments with highest and lowest resulting β-*O*-4 linkage proportion in extracted lignin. Maximum β-*O*-4 reaction conditions: 140 °C, 30 min, 0.2 mL/min. Minimum β-*O*-4 reaction conditions:180 °C, 60 min, 0.1 mL/min. Batch reaction conditions:140 °C, 3 h.

The proportion of β-*O*-4 linkages achievable through the flow-through process varies between 18 and 32 linkages per 100 S+G units, depending on the reaction conditions, compared to the batch process, which yields 28 linkages per 100 S+G units. The ether linkage proportion in the flow through process often being lower than in the batch process could be caused by the higher temperatures utilized. The removal of solubilized lignin from the reactor is not fast enough to mitigate the cleavage caused by higher temperatures. The proportion of β-β and β-5 linkages measured in the flow-through process is higher than that measured in the batch process, even at low reaction temperatures and short process times.

Based on the data of the Box Behnken design, a response surface model for pulp yield, lignin yield, sugar yield and β-*O*-4 linkages was created using the *design expert* software. Models were selected after comparing the analysis of variance (ANOVA) of possible linear, quadratic and two factor interaction (2FI) models. Desired is a low sequential *p*-value, a high lack-of-fit value and adjusted and predicted R^2 close to 1. Adjusted and predicted R^2 values should differ by less than 0.2. The ANOVA results for the chosen models are listed in Table 20.

Table 20: Statistical parameters from the analysis of variance (ANOVA) for selected models.

response	Model source	Sequential *p*-value	Lack of Fit *p*-value	Adjusted R^2	Predicted R^2
Solid residue	Linear	< 0.0001	0.4640	0.9080	0.8560
Lignin yield	Quadratic	0.0498	0.9474	0.9531	0.9300
Sugar yield	Linear	< 0.0001	0.3021	0.8475	0.7535
β-*O*-4 linkage	2FI, modified	0.0085	0.2385	0.6021	0.1584

The final equations for the selected models are listed in Table 21. The coded equation is not adjusted to the actual units of the factors. High levels of factors are set to +1 by default and low levels to -1. The coded equation is useful for identifying the relative impact of the factors by comparing the factor coefficients.

Table 21: Coded equation (high levels +1, low levels -1) with independent variables A (time), B (temperature), and C (flow rate).

response		Inter-cept	A	B	C	AB	AC	BC	A^2	B^2	C^2
Solid residue	=	50.65	-3.86*	-11.05*	-1.92*	-	-	-	-	-	-
Lignin yield	=	8.71	2.28*	3.17*	1.21*	-0.05	0.81	0.61	-0.14	0.37	-1.40*
Sugar yield	=	22.88	3.13	12.46*	0.37	-	-	-	-	-	-
β-O-4 linkages	=	22.62	-0.98	-2.20*	2.47*	3.29*	-	-	-	-	-

*significant model term ($p < 0.05$)

The most suitable model for solid residue was linear. Figure 29 depicts the two-dimensional representations of the relationships between two factors, with one factor held constant at its central value. The full ANOVA shows that A (time) and B (temperature) are significant model terms. (Appendix 8.6)

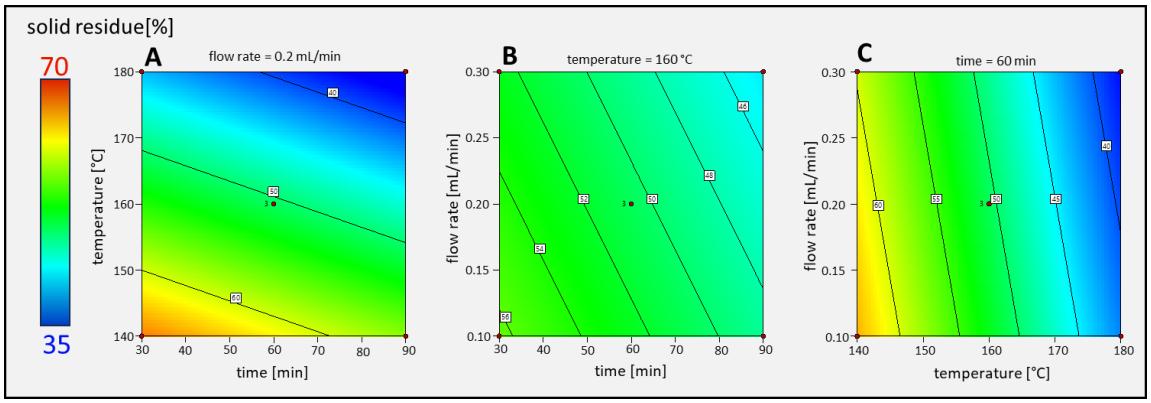

Figure 29: 2D contour models of the RSM for solid residue produced by design expert. The relationship between the two factors is shown in each graph, while the other factor was maintained at a constant level.

The surface model (Figure 29) and the model equation (Table 21) demonstrate that the reaction temperature has a strong negative impact on solid residue. As the reaction temperature increased, more biomass was disintegrated. This is consistent with the general rule that higher temperatures typically result in faster reactions. In contrast, the influences of the process time and flow rate were much less pronounced. However, there is a slight decrease in solid residue with longer process times, which indicates that more biomass is fractioned as the process is prolonged. Although this outcome is anticipated, the trade-offs between the increased yields and the energy and materials required must be carefully weighed. Because the model term C (flow rate) is not significant, all conclusions made from this part of the model have limited validity. A negative correlation existed between the solid residue and flow rate, indicating that higher flow rates resulted in greater biomass degradation. This result was also anticipated because higher flow rates entailed the use of more solvents and catalysts and lower biomass loading.

While the flow rate increases the extraction per time, it exerts a negative effect on the solvent and catalyst volume necessary for achieving the same level of pulp degradation. As the impact of flow rate is relatively minor, these factors must be balanced against the solvent expenditure. An increased solvent flow may also result in enhanced cooling as the solvents enter the reactor at room temperature and undergo heating within the system. Given that the process temperature significantly influences fractionation, preheating of the solvents may enhance the effect of the flow rate.

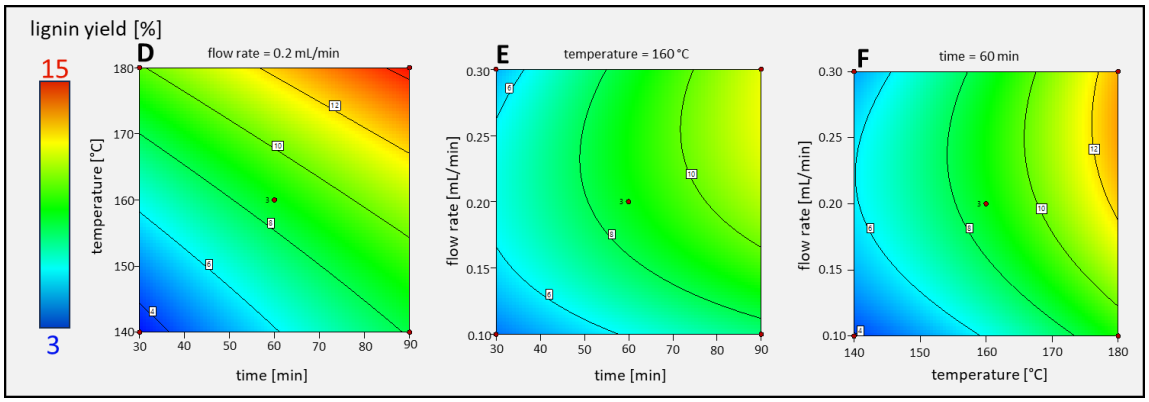

Figure 30: 2D contour models of the RSM for lignin yield produced by design expert. The relationship between the two factors is shown in each graph, while the other factor was maintained at a constant level.

A quadratic model proved to be the most suitable for determining optimal lignin yield. A (time), B (temperature), C (flow rate), and C^2 are the significant model terms. The surface plot illustrated in Figure 30 and the model equation detailed in Table 21 indicate that the process temperature has the greatest positive impact on lignin yield, although its effect is not as distinct as that of the solid residue and sugar yield models. Additionally, the process time had a positive influence on lignin yield. In the studied range, the increase in lignin yield with temperature and process time appeared to be mostly linear, as the model terms for AB, AC, BC, A^2, and B^2 were relatively small and not significant according to the full ANOVA (Appendix 8.6).

Regarding the flow rate, the model terms C and C^2 are significant, indicating that a high flow rate does not necessarily improve the lignin yield, especially under lower temperatures or shorter process times. A medium flow rate of 0.2 mL/min was identified for maximum lignin yields, as the model predicts that further increase of the flow rate to 0.3 mL/min does not increase lignin yields further. Keeping the flow rate as low as possible will also minimize the solvent and catalyst usage.

A linear model demonstrated the highest suitability for showcasing sugar yield. Based on the full ANOVA (Appendix 8.6), only B (temperature) was a significant model term ($p < 0.05$).

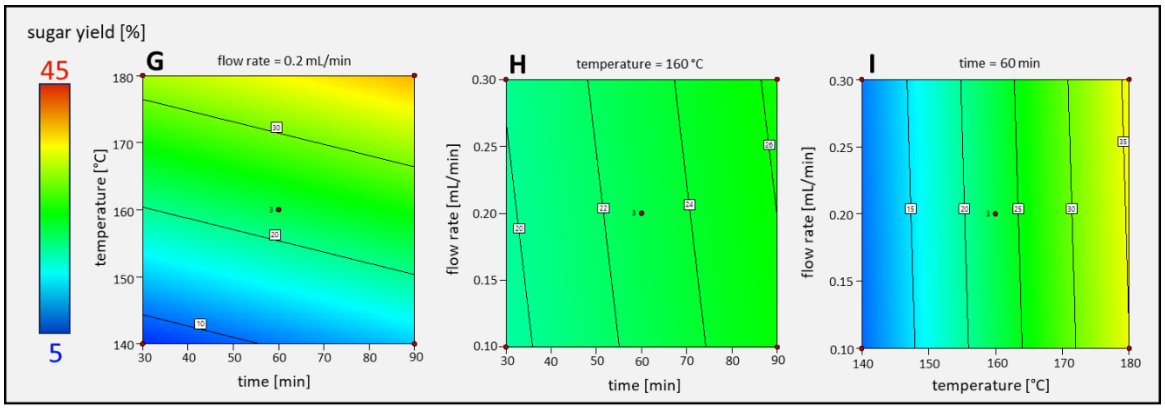

Figure 31: 2D contour models of the RSM for sugar yield produced by design expert. The relationship between the two factors is shown in each graph, while the other factor was maintained *at a constant level.*

The surface plot (Figure 31) and model equation (Table 21) show that the process temperature is the predominant factor affecting the sugar yield, as increasing it from 140 to 180 °C resulted in a threefold increase in the extracted sugars. Assumptions regarding the influence of process time and flow rate are difficult, as the model terms A and C are not significant. Process time exhibited a smaller positive influence on the sugar yield, but the flow rate appeared to have even a negligible impact within the defined parameters. The similarity between the sugar and solid residue models is attributable to the sugars constituting the primary mass components extracted. Overall, sugar extraction was primarily influenced by process temperature, not time. This suggests that most hemicellulose sugars are extracted early in the reaction, and that temperature becomes the limiting factor in determining the amount of sugar hydrolyzed.

From the structural lignin analysis results, only the β-*O*-4 linkages were used for modelling, as the data for the S/G ratio and β-β linkages showed minimal variation. A modified 2FI model was determined to be the best fit for the data, with B (temperature), C (flow rate), and AB as significant model terms. The difference between the predicted R^2 and the adjusted R^2 is greater than 0.2, which may indicate a large block effect or another problem with the model. However, the significant ($p < 0.05$) sequential *p*-value and insignificant ($p > 0.05$) lack-of-fit *p*-value suggest that the model can be used to navigate the design space (Appendix 8.6). Plotting the predicted vs actual values (Figure 32) demonstrates the model's fit with the dataset. Nevertheless, projections made using the model for β-*O*-4 linkages merit caution and may not be entirely accurate.

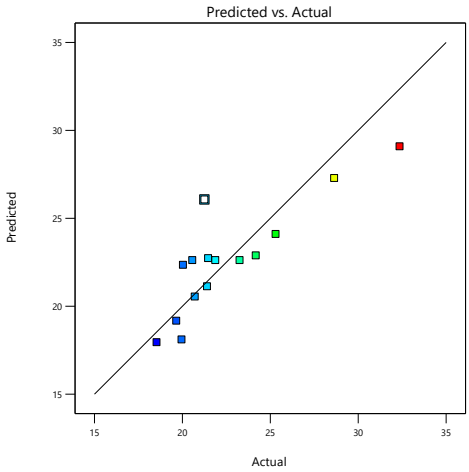

Figure 32:Predicted vs actual plot for the data measured in the BBD for β-*O*-4 linkages and the corresponding model.

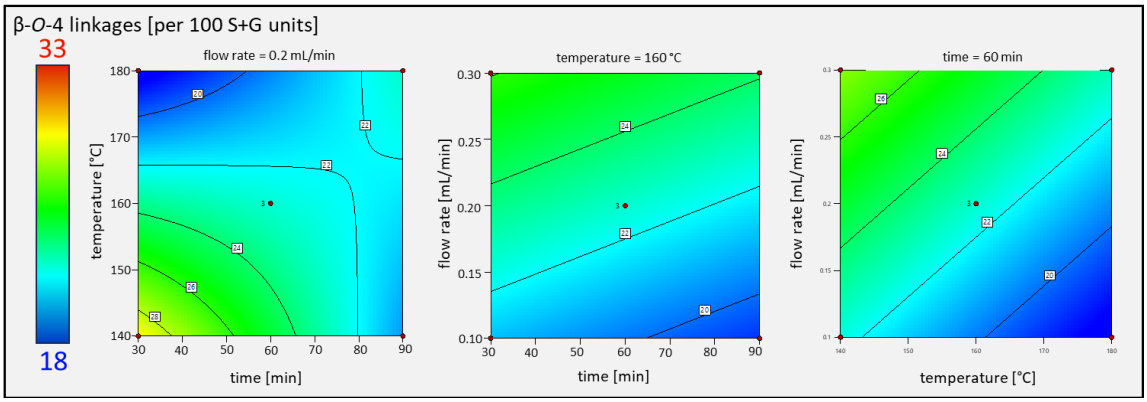

Figure 33: 2D contour models of the RSM for β-O-4 linkages produced by design expert. The relationship between the two factors is shown in each graph, while the other factor was maintained at a constant level.

The surface plot (Figure 33) and the corresponding model equation (Table 21) demonstrate that the maximum proportion of β-*O*-4 linkages can be attained by maintaining a low temperature and brief process duration. Although the dependence on temperature might be linked to the increased energy available to break bonds, the connection between process time and linkage proportion may indicate that lignin with a higher proportion of β-*O*-4 linkages is extracted in the early stages of the process. This phenomenon was most pronounced at 140 °C, but remained observable at 160 °C. At 180 °C, the lignin extracted in the initial stages exhibited a low proportion of β-*O*-4 linkages. However, it is important to note that the overall lignin yield was substantially higher under these conditions. This model indicates that there is a more accessible form of lignin that requires less breakdown to be extracted. Moreover, increasing the temperature and prolonging the processing time resulted in lignin with a lower proportion of ether linkages. A higher flow rate appears to reduce β-*O*-4 linkage cleavage, most likely because the extracted lignin spends less time in the reactor, which reduces reactions after the extraction.

Although factor response modelling only approximates the extraction process, it can still provide valuable insights. Among the factors examined, the reactor temperature had the greatest impact on pulp, lignin, sugar yields, and the proportion of β-*O*-4 linkages in the extracted lignin. As the temperature increased, more lignin and sugars were extracted, resulting in reduced weight of the solid residue. The process time also had a significant influence on the yield, although it was less pronounced than temperature. The impact of process time on lignin yield may be due to the longer extraction time required for lignin than for hemicellulose sugars. In contrast, the solvent flow rate did not influence the extraction efficiency to the same extent as the other two parameters. There is a slight decrease in pulp yield with an increasing flow rate, and for maximal lignin yield, a medium flow rate of 0.2 mL/min appears to be optimal. However, the enhanced cleavage of β-*O*-4 linkages at higher temperatures can be partly mitigated by increasing the solvent flow rate, reducing the time that lignin is exposed to the reaction conditions. This allows for high extraction yields with low lignin degradation, at the cost of a higher solvent-to-biomass ratio.

3.3.4 Upscaling the FT OrganoCat

A reactor tube with a 7.9 times larger volume and a fitting heating mantle were used to process biomass at a larger scale using the flow through concept. It fits 6.7-7.5 times more beechwood. 0.1 M oxalic acid solution was used as the catalyst. The flow rate was set to 1.3 mL/min which is a 6.5-fold increase of 0.2 mL/min, pump and capillary were the same as for the small system. The temperature was set to 160 °C. The desired processing time is 60 min. Thus, the medium reaction conditions of the small-scale experiments were mimicked.

Ensuring the tightness of the reactor, maintaining constant pressure, and preventing clogging posed challenges when scaling up the flow through the OrganoCat process. After 60 min of process time, the setup produced 3.5wt% lignin, 8.7wt% hydrolyzed sugars, and a solid residue reduced to 42.4wt%. (Table 22) Although the reduction of the solid material suggests a high degree of fractionation efficiency, the yields of lignin and sugars were lower than desired. With yields and solid residue not adding up, there might have been a loss of solid residue during the work up.

While making a direct comparison to smaller scale is challenging due to differing setup and process conditions, it is evident that the yields of lignin and sugar are lower. One issue is that

the beginning and end of the reactor are not directly heated because the screws prevent the fitting of the heating mantle. This will have a significant impact on the biomass at the beginning of the process, as the process temperature is not reached in this area. Heat conduction is a general challenge in scaling up, and the larger diameter of the reactor may result in the middle biomass not being reached by the solvent heated to the full process temperature, particularly near the entrance of the reactor.

Therefore, for the following experiment (**FTS2**), the solvents were preheated by passing the entering capillaries through an oil bath heated to 160 °C, resulting in a substantial increase in the lignin yield (Table 22). The amount of solid residue was higher than that in **FTS1**, supporting the hypothesis that some solid residue was lost during the FTS1 workup. In addition, the sugar yield increased by 70%. This experiment was successfully reproducible (**FTS3**).

Table 22: Yields of the flow through OrganoCat scale up with and without solvent preheating. Beech, 0.1 M oxalic acid, 1.3 mL/min, 160 °C.

	FTS1	**FTS2**	**FTS3**
Time [min]	60	60	60
Solvent preheating temperature [°C]	-	160	160
Lignin yield [wt%]	3.5	6.9	6.6
Solid residue [wt%]	42.4	57.1	54.3
Sugar yield [wt%]	5.1	8.7	11.0

Although preheating the solvents has been proven to be effective in scaling up the process, further refinement of the setup is necessary to increase its resilience against clogging, maintain stable pressure, and ensure uniform temperature and solvent flow throughout the reactor.

3.4 Time-resolved lignin and sugar fractions for mechanistic and structural process analysis

Cellulose, lignin, and hemicellulose are closely intertwined in lignocellulosic materials. The efficiency of biomass fractionation processes is influenced by multiple structural factors of lignocellulose, rather than a single determinant like lignin content or β-*O*-4 linkage proportion, as it has been shown in chapter 3.1.[123] Understanding the mechanics of the FT OrganoCat fractionation can not only help to improve the process but may also lead to a deeper understanding of the complex structure of plant cell walls. Several questions remain unresolved: Does the hydrolysis of specific hemicelluloses enhance lignin extractability? And to what extent must lignin ether linkages be disrupted to achieve high lignin solubility?

The FT process provides an opportunity to collect fractions of the liquid phases. Consequently, the time-resolved sugar and lignin yields were measured. This enables the acquisition of insights into the lignocellulose fractionation mechanism of this setup. The following chapter examines the point at which lignin is extracted from the FT OrganoCat process and how this extraction is intertwined with hemicellulose hydrolysis. Additionally, sensitive sugar analysis using HPAEC-PAD provides insight into hemicellulose structure by tracking when and how many specific sugars are released.

To achieve these insights, liquid fractions were collected at 5-minute intervals. The organic and aqueous phases were separated, and the lignin yield was determined gravimetrically from the organic phase, whereas the sugar concentration was determined by HPAEC-PAD of the aqueous phase.

3.4.1 Time resolved yields at different process temperatures

The extraction profiles were obtained at different temperatures. Triplicate experiments were conducted at 140 °C and 160 °C for 90 min, and at 180 °C for 60 min. For the 180 °C experiments conducted for 60-90 min, the average of two experiments was recorded. Figure 34 shows the lignin and sugar yields in each fraction.

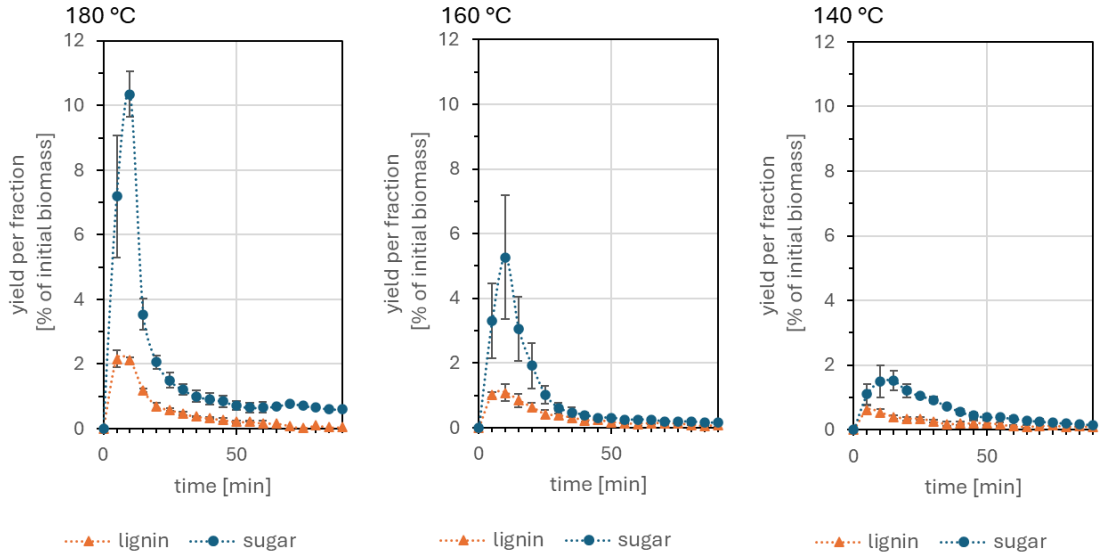

Figure 34: Lignin and sugar yields per fraction of the flow-through process at different temperatures. Samples were collected for 5 min each, and the sugar yield was determined by measuring the sugar concentration in the aqueous phase using ion chromatography. Triplicate experiments were performed for 140 °C and 160 °C 0-90 min and 180 °C 0-60 min, for 180 °C 60-90 min the average of two experiments is shown.

As illustrated in Figure 34, the time-resolved yields demonstrate that both lignin and sugar were extracted at the beginning of the reaction. The extraction of both sugars and lignin was clearly dependent on temperature. In accordance with the results from the DOE, compared to lignin, the sugar yield increase depended more on temperature. This difference was more pronounced in the initial 20 min, during which primary extraction occurred. Fluctuations in the process were observed owing to variations in the temperature and pressure.

The sugars attained their maximum extraction rate at 5-15 min. Sugar hydrolysis accelerated over the first 10 min, and the sugar yield increased from the first to the second (and third at 140 °C) fractions. The reaction temperature exerted a substantial influence on the overall yield of hemicellulose sugars that dissolved in the aqueous phase over time. Not only does the reaction temperature affect the quantity of sugars extracted, but it also determines the rate of extraction, which is most prominent in the first 20 minutes of the process. An increase in temperature from 140 °C to 180 °C nearly tripled sugar yield. At 180 °C, sugar extraction occurred at a nearly constant rate from 20 min until the end of the process, indicating that sugar hydrolysis reached equilibrium. No saturation or complete extraction was observed. This effect is also observable, but less pronounced at lower temperatures. Detailed examination of single sugars will provide information on the underlying mechanisms.

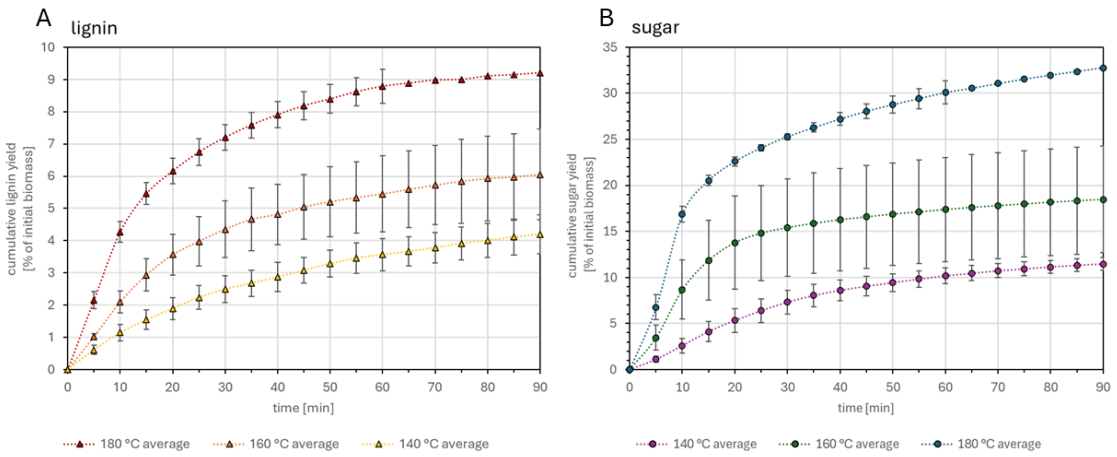

Figure 35: A: Cumulative lignin yield of the flow-through process at different temperatures. B: Cumulative sugar yield during the FT process. Sugar yield was determined by measuring the sugar concentration in the aqueous phase using HPAEC-PAD. Samples were collected for 5 min each. Triplicate experiments were performed for 140 °C and 160 °C 0-90 min and 180 °C 0-60 min, for 180 °C 60-90 min the average of two experiments is shown.

As illustrated in Figure 35, at 160 and 180 °C, the cumulated sugar yield increased sharply within the first 20 min. At 140 °C, the extraction rate was significantly lower. A gradual increase in sugar extraction speed was observed as the temperature increased. However, this trend did not persist at 180 °C, where 69% of the final cumulated sugar yield after 90 min was achieved after the first 20 min. Although a greater quantity of sugars was extracted after 20 min at 180 °C compared to the final sugar yield at lower temperatures, the extraction continued at a much higher linear rate.

A comprehensive analysis of the hemicellulose sugar composition is essential to elucidate the source of increased sugar yield at elevated temperatures. One potential explanation is that specific hemicellulose sugars become accessible and undergo hydrolysis only at high reaction energies. Alternatively, the increased sugar yield may result from the hydrolysis of non-hemicellulose cell wall components such as starch and/or cellulose. The total yield of sugars at 180 °C (32.8wt% of initial biomass) exceeded the amount of hemicellulose sugars measured in the TFA fraction of unprocessed beech (18.8wt% of initial biomass), indicating that the ongoing sugar extraction is derived from non-hemicellulose sugar hydrolysis. The analysis of sugar composition, which will be described in detail later in this chapter, reveals that the later fractions mainly consist of glucose, confirming that cellulose is hydrolyzed during the process.

The system is particularly sensitive to small changes in temperature and pressure at 160 °C. The actual reactor temperature fluctuated within the setup within a range of ±5 °C, resulting

in high standard deviations at 160 °C. In future experiments, an optimized design that prevents such variations should be developed.

The lignin yield depended significantly on the reaction temperature, as discussed in Section 3.3.3. While increasing the process temperature from 140 °C to 160 °C increased the lignin yield by 50% from 4% to 6% of the initial biomass weight, a further increase from 20 °C to 180 °C led to another 50% of yield increase to 9wt% of the initial biomass. The extraction profile changes slightly at different temperatures. Approximately two-thirds of the overall lignin extraction was achieved at the 20-minute mark for both the 160 and 180 °C reactor temperatures (Figure 35). At 140 °C, two-thirds of the final lignin yield was obtained after 40 min. However, as shown more clearly in Figure 34, the difference was primarily evident during the initial 20 min of the process. Afterwards, there was minimal variation in the lignin yield between the fractions from 25 to 90 min. During the first 5-10 minutes, the extraction rate was the highest and almost linear at all temperatures. Thereafter, the extraction rate slows and eventually stagnates, with only a small amount of additional lignin being extracted. The rapid initial release of lignin indicates that a certain portion of lignin is more readily accessible and may not require significant hydrolysis within the biomass to be extracted. In the later stages of the process the cleavage of lignin ether linkages could play a more prominent role. The amount of lignin that could be extracted was largely determined by the extraction temperature, particularly during the initial 20 min. Higher temperatures might be necessary to break specific bonds that retain residual lignin in the pulp, but this could also lead to enhanced degradation of the extracted lignin and sugars.

3.4.2 Compositional Analysis of pulp

To characterize the residual lignin and non-cellulosic polysaccharides in the solid residue, they were analyzed using previously described wet chemical analysis steps. Unlike the extracts, which can be easily separated by taking fractions, pulp analysis requires extraction from the reactor and separate experiments for time-resolved analysis. Therefore, two time points were chosen: the first experiment was stopped after 20 min of process time, at which point, according to earlier kinetics, the main extraction occurred, and the other set was stopped after 90 min. The composition of the solid residue, determined by wet chemical analysis, is shown in Table 19.

Table 23: Solid residue comparison, unprocessed, processed at 160 °C after 20 min and after 90 min. Wet chemical analysis relative to initial biomass.

Process time	Pulp yield [%]	Starch [%]	ASC [%]	Acetyl-ation [%]	Cellulose [%]	Lignin [%]	Hemi-cellulose sugar [%]
0 min	-	16.6 (2.3)	0.8 (0.4)	4.2 (0.6)	47.1 (3.8)	20.3 (1.8)	18.8 (2.9)
20 min	63.2 (2.4)	2.6 (1.1)	0.4 (0.2)	1.4 (0.2)	38.8 (2.1)	16.4 (0.7)	10.9 (0.3)
90 min	50.5 (3.0)	2.1 (0.5)	0.2 (0.1)	0.6 (0.2)	34.1 (3.5)	11.4 (1.3)	7.4 (1.4)

The changes in composition between the raw beech and solid residue after 20 min of processing were greater than those between 20 and 90 min of processing. Although the starch content decreased by 84% within the initial 20 min, only a minimal change was observed during the remainder of the processing time. ASC and acetylation are minor components in beech wood that are essentially reduced at the beginning of the process.

The measured proportion of crystalline cellulose in the solid residue decreased by 18% within the initial 20 min and by 27% after 90 min of processing. This phenomenon could be attributed to the transfer of cellulose from the crystalline to the amorphous form and subsequent hydrolysis. The high sugar yields found for the process consisted of substantial amounts of glucose, confirming this finding. Notably, the reduction in crystalline cellulose occurs at a slower rate between 20 and 90 minutes of process time. As presented in Table 23, cellulosic material is hydrolyzed during the process and extracted into the aqueous phase. In the pulp, the proportion of crystalline cellulose is elevated which desirable as it facilitates further downstream processing of such, for instance in enzymatic hydrolysis.[132]

The lignin content of the solid residue was reduced by 19% of the initial amount within the first 20 min of the process and by 44% after 90 min. Although the extraction rate slowed during the process, the difference was not as large as that for the other components, which confirms the observations made in the lignin yield kinetics. In the extract, 59% of the final lignin yield was obtained within the first 20 min at 160 °C. Notably, more than half of the lignin remained in the solid residue, whereas the time-resolved kinetics showed that lignin extraction was practically negligible in the last 30 min of the process. Therefore, the residual lignin might require harsh extraction conditions. Continuous solvent flow prevents saturation. Therefore, lignin availability appears to be mainly dependent on process temperature instead of process time. This observation agrees with the DOE conducted in the previous chapter (3.3), which also determined temperature to be a major factor in lignin yield in comparison to the process

time or flow rate. Less accessible lignin remained, indicating that there was a temperature-dependent maximum for accessible lignin that could not be exceeded by longer reaction times, a phenomenon that had also been observed in the batch process.[49]

The hemicellulose sugars underwent a reduction of 42% after 20 min of processing and 61% after 90 min. It is noteworthy that approximately two-thirds of the extraction occurred within the initial 20 min, confirming the time-resolved yield (Figure 35). However, not all hemicellulose sugars were removed from the solid residue, even after 90 min of processing, despite the slow kinetics during the final 30 min. This suggests that some sugars are inaccessible, similar to lignin. To gain further insight into the recalcitrant nature of these residual constituents, detailed compositional analysis was conducted.

3.4.3 Time resolved structural analysis of lignin

Further investigation of the differences between the extracted lignins at various temperatures was accomplished by comparing the linkages and monomer compositions in beech wood lignin obtained from experiments conducted at different stages. A minimum of 20 mg of lignin was required for HSQC-NMR analysis. Therefore, samples extracted in the early stage of the experiment (0-20 min) and the later stage (20-90 min) were combined and analyzed. For the extraction at 160 °C, two repetitions were performed (Table 24).

Table 24: Average values for linkage proportion and S/G ratio in lignin extracted within the first 20 min vs. extracted in minute 20-90. All experiments were conducted in triplicates besides 160 °C, which is a duplicate. Standard derivation in brackets.

Temperature [°C]	Process time [min]	ß-*O*-4 [%]	ß-ß [%]	ß-5 [%]	S/G
140	0-20	42.4 (4.1)	14.6 (0.4)	6.5 (0.9)	1.3 (0.1)
	20-90	30.3 (1.6)	14.2 (0.9)	3.0 (0.4)	2.4 (0.1)
160	0-20	34.6	13.2	7.9	1.4
	20-90	26.8	11.3	6.9	2.0
180	0-20	28.4 (0.9)	11.8 (0.7)	5.2 (0.6)	2.1 (0.2)
	20-90	24.0 (0.8)	9.9 (1.0)	5.0 (0.6)	2.0 (0.1)

The structural features of the extracted lignin appeared to vary throughout the process. The lignin obtained at the beginning of the process exhibited a higher proportion of β-*O*-4 linkages than the lignin extracted later. This difference was more pronounced at lower temperatures. It is plausible that the more easily accessible lignin fractions, which are initially extracted, require less cleavage of ether bonds to be separated. As the process progresses, more recalcitrant lignin structures remain, which requires more hydrolysis to be removed from lignocellulose. More ether bond cleavage at higher temperatures can also simply occur without being a prerequisite for extraction. Furthermore, the early extracted lignin fragments may have better solubility in the organic solvent.

A strong increase in the S/G ratio in late lignin at low and mid temperatures was observed, which was not observed at 180 °C. It appears that the more accessible lignin fractions have a lower S monomer content and require less hydrolysis than the more recalcitrant fractions that were extracted later.

At 180 °C, more lignin was extracted within the first 20 min than during the entire process at 140 °C, and approximately the same as after 90 min at 160 °C. Therefore, the early lignin fraction of the 180 °C process may include the more recalcitrant parts observed in the later lignin fractions under milder conditions. For this reason, the difference in β-*O*-4 linkages is less pronounced at higher temperatures and the S/G ratio is the same on average. In the comparison of different plants in chapter 3.1, no clear pattern of preferred monomer linkage extraction was observed. However, the full yield is typically analyzed, and this phenomenon appears to apply only to a very small fraction at the initial stages of the process under mild conditions.

A higher proportion of G units was predominantly found in the vessel secondary walls, whereas the fiber secondary walls contained a greater abundance of S units. This difference is more pronounced in earlywood compared to latewood.[133] Given that vessel cells are responsible for water transport in plants, their lignin might be extracted first during biomass extraction, as they would initially come into contact with solvents and catalysts. Li *et al.* reported a similar observation in organosolv pretreatment of corn stalks. The S/G ratio and proportion of β-O-4 linkages decreased with increasing reaction time. Concurrently, microscopic images revealed that the secondary cell wall degraded initially, followed by access to the lignin-rich compound middle lamella. In corn stover, S units predominate in the secondary cell wall, while G units are prevalent in the central middle lamella, thus elucidating the changes in S/G ratios during the process.[134]

In the context of alkali pulping, literature describes lignin extraction as occurring in three distinct stages: initial, bulk, and final. A softwood lignin model was proposed, dividing it into three fractions with varying arylether bond reactivity. The most reactive fraction (23%) comprised α-*O*-4 and β-*O*-4 bonds in the phenolic phenylpropane units (PPU). The second, bulk fraction (70%) is characterized by β-*O*-4 bonds in non-phenolic PPU, while the recalcitrant third fraction (7%) is dominated by alkylaryletheric bonds in PPU with aliphatic side chains. As substrates for nucleophilic attack in alkaline pulping typically cleave the polymer at the α-position, this position is not available in the third fraction, rendering it resistant to degradation. Subsequently, during oxidative bleaching, this fraction is removed as the reaction centers for electrophilic reactions in lignin are aromatic rings.[135] Although alkali pulping on softwood is very different from the dilute acid OrganoCat treatment on hardwood, different structures within the lignin might influence on how fast they can be extracted them.

The variation in β-β and β-5 linkages remains small, which complicates discerning any potential alterations that may occur during the process. While there appears to be a noticeable distinction between the β-5 linkages at 140 °C in early and late lignin samples, it remains unclear whether this disparity is indeed significant. Further replicates are necessary to substantiate any conclusions. A scale-up of the process would be necessary to produce sufficient lignin to measure fractions at smaller time intervals. This would allow for a more detailed assessment of if and how early lignin is different from late lignin.

3.4.4 Compositional Analysis of extracted sugars

Hemicellulose is an integral component of the cell wall and, in comparison to cellulose, is more readily hydrolysable.[18] Consequently, a substantial quantity of hemicellulose sugars can be found in the aqueous phase following the OrganoCat process. The structure and composition of hemicellulose vary among plant species and are often characteristic of specific groups, with significant differences observed, for example, between hardwoods and grasses. Additionally, other sugar polymers, such as starch and pectin are typically found in plant biomass.

The time-resolved analysis of sugar hydrolysis provided information on the accessibility of certain hemicellulose and the hydrolysis mechanism during the flow through OrganoCat (Figure 36).

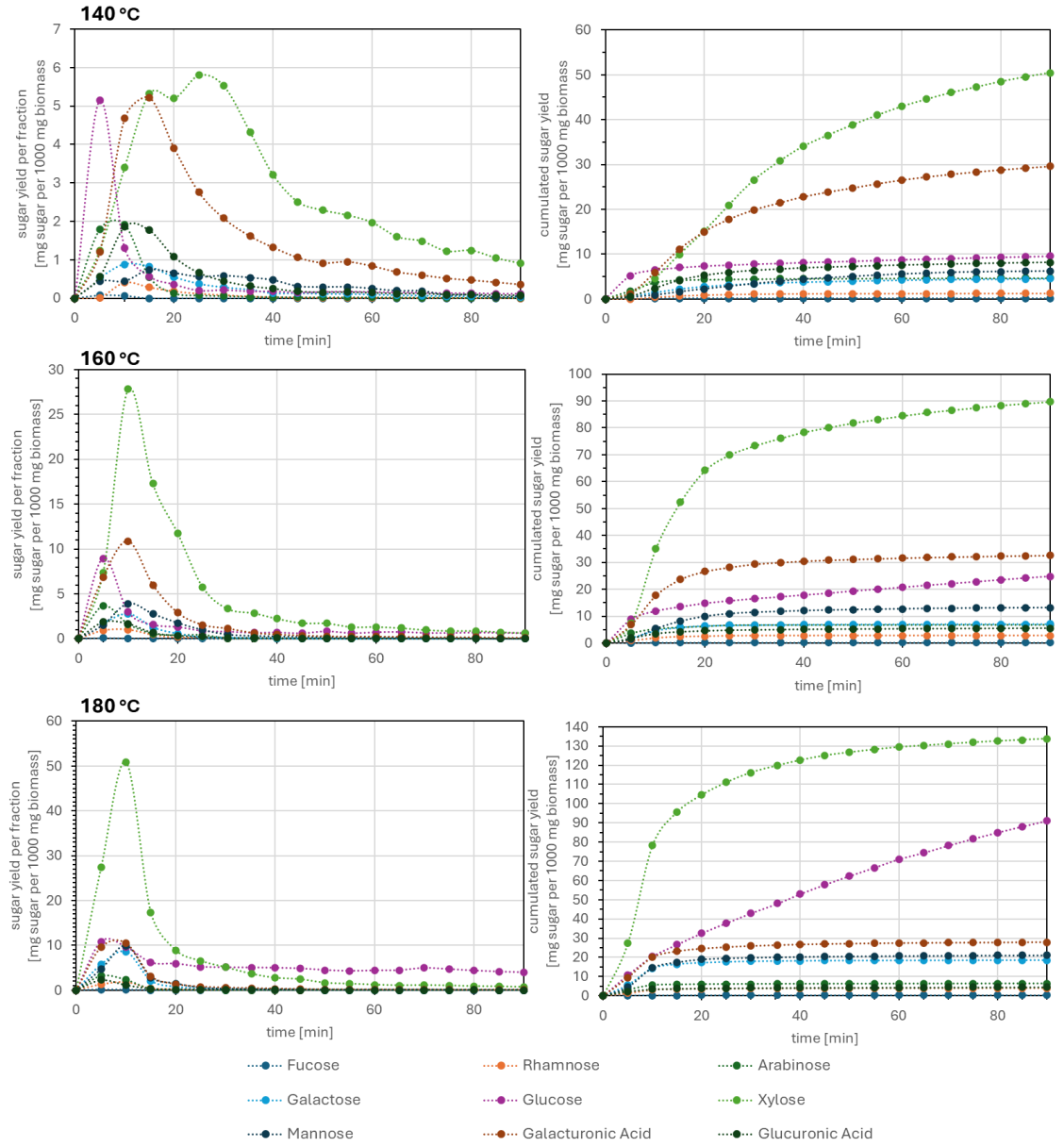

Figure 36: Amount of monosaccharides in aqueous sample of FT OrganoCat processing at 140 °C, 160 °C and 180 °C of beech wood. The samples were collected for 5 min each. Experiments were conducted in triplicates; std. deriv. is not shown for better visibility. The full dataset including standard derivations can be found in Appendix 8.7

Examination of monosaccharides revealed that xylose was the predominant sugar extracted, attributable to the high xylan content in the hemicellulose fraction of beech wood biomass. Nevertheless, the extracted xylose yield remained below the amount of available xylose from beech, indicating that xylose extraction was incomplete at the end of the chosen process time (Table 25).

Table 25: Cumulative yield of sugars after 90 min of the FT OrganoCat taking 5 min fractions. Sugars were quantified from the aqueous phase using HPAEC-PAD. Composition of the sugars in untreated beech for comparison.

T [°C]	Fuc [%]	Rha [%]	Ara [%]	Glc [%]	Glu [%]	Xyl [%]	Man [%]	GlcA [%]	GluA [%]
140	0.01	0.12	0.47	0.45	0.96	5.05	0.62	2.96	0.82
160	0.01	0.28	0.67	0.71	2.48	8.97	1.31	3.26	0.56
180	0.03	0.40	0.63	1.85	9.11	13.37	2.11	2.79	0.45
beech*	0.00	0.38	0.41	0.64	2.10	17.36	0.84	1.05	0.00

*TFA hydrolysis of untreated dAIR, calculated to match % of full biomass

Analysis of the pulp from the FT process at 160 °C (Table 23) showed that 7.6% of the hemicellulose sugars remained in the pulp, of which 47% were xylose. This suggests that even though xylose extraction significantly diminished to trace amounts towards the end of the process time at 160 °C and 180 °C, complete hydrolysis and extraction of xylan did not occur. This phenomenon may be attributed to heterogeneities within the reactor, such as inadequate heating in the initial 2 cm, where the screw was placed. Enhanced reactor design, potentially incorporating an oven or preheated solvents, may facilitate increased sugar extraction. Furthermore, the structure of xylan may influence its hydrolyzability. Xylan can exist in either a three-fold helical screw conformation or a flattened two-fold helical screw ribbon, which adheres to cellulose microfibrils.[21] Hardwoods typically exhibit a higher proportion of twofold xylans compared to threefold xylans.[136] The xylan bound to cellulose microfibrils may be more resistant to hydrolysis and consequently partially remain in the pulp.

Xylose extraction reaches its maximum at the second fraction collected 5-10 minutes into the process at 160 °C and 180 °C. At 140 °C, xylose extraction proceeded more slowly, reaching a maximum at 20-25 minutes. Temperature influences the extraction rate and overall yield of xylose extraction. The delayed onset of xylose extraction may be attributed to the presence of xylose predominantly in the backbone of xylans. The side groups and acetylation found on xylan could initially impede accessibility. After removal, xylose hydrolysis can increase. The correlation between acetylation and sugar release was demonstrated in the acid pretreatment of poplar samples with varying degrees of acetylation.[137] This suggests that the removal of acetate and other side groups is intrinsically linked to sugar hydrolysis.

A high proportion of galacturonic acid was found in the fractionation extract. In the experiments at 140 °C, it constituted approximately one-quarter of the total extract, which is substantially more than the 4.6% anticipated from the analysis of unprocessed beech. The

relative proportion of galacturonic acid decreased with elevated temperatures and a higher total of extracted sugars. However, the absolute yield of galacturonic acid remained consistent at all temperatures, with approximately 30 mg per 1000 mg biomass (Table 23). The additional galacturonic acid may originate from hydrolyzed pectin, which are polysaccharides primarily composed of galacturonic acid.[138] Interestingly, sugars from pectin were not present in these quantities in the analysis of the unprocessed beech wood. They might be removed during the preparational steps of the wet chemical sample analysis (ASC removal and destarching) or not get hydrolyzed using the TFA hydrolyzation protocol.

Galacturonic acid, similar to xylose, exhibits peak extraction at 10 min for 180 °C and 160 °C and at 15-30 minutes for 140 °C. Although the extraction rate decreased, galacturonic acid remained detectable in every fraction throughout the process at all temperatures, suggesting that extraction was not completed after 90 min. This was confirmed by pulp analysis; galacturonic acid remained detectable after 90 min. It has been postulated that pectin influences biomass recalcitrance; however, few studies have evaluated its direct influence. Lionetti *et al*. reported that in genetically modified Arabidopsis, the reduction of homogalacturonan enhanced enzyme saccharification efficiency.[139] The extraction of galacturonic acid throughout the entire process duration may serve as an additional indication that pectin contributes to biomass recalcitrance.

The proportion of glucose increased with increasing process temperature. Overall, the glucose yield exceeded the glucose content found in the unprocessed beech. Glucose can be found in in hardwood hemicellulose in glucomannans, which make up 2-5% of the hemicellulose and xyloglucans, which are mainly found in the primary cell wall.[18] Additional glucose could be released from starch or hydrolyzed cellulose during the fractionation process.

Glucose extraction initially exhibited high rates within the first 5 min at all temperatures, followed by a rapid decrease. The initial glucose may be derived from quickly hydrolyzable starch and accessible xyloglucans from primary cell walls. However, the glucose yield constantly increased with time during the entire processing step. Constant linear glucose extraction was observed, albeit minimally, at 140 °C and more prominently at 160 °C and 180 °C, which differed significantly from the logarithmic extraction pattern of all other sugars.

The constant, temperature-dependent glucose extraction suggests that the availability or accessibility of glucose due to the structural heterogeneity of hemicellulose does not dominate the extraction rate. Rather, the rate-determining step is the hydrolysis mechanism, which is clearly temperature-dependent, while the glucose source is homogenous and not limited within the process time. This evidence supports the hypothesis that cellulose is hydrolyzed given the high amount of available cellulose, which has a homogenous structure.

Mannose is the fourth most prevalent monosaccharide found in the extracts and is present in hemicellulose in the form of glucomannans. Hardwoods typically contain 2-5% glucomannans.[18] While the total yield of mannose is temperature-dependent, its proportion within the extracted sugars remains relatively constant. Mannose extraction peaked in the second fraction at 160 and 180 °C, whereas at 140 °C, extraction was delayed, and the maximum was attained within 10-15 minutes. Mannose extraction was observed in small quantities until the end of the process, despite the absence of mannose detection in the pulp after 20 and 90 min at 160 °C. This observation may be attributed to mannose concentrations falling below the detection limits of the TFA hydrolysis protocol.

Galactose can be found in the hemicellulose in the form of a side group of the mannans and xyloglucan and in pectin.[140,141] The galactose yield exhibited a clear temperature dependence, particularly between 160 °C and 180 °C, where the yield doubled. The proportion in the extract was similar to that in the unprocessed plant but slightly higher at 180 °C (Table 25). At all temperatures, the maximum amount of galactose was observed in the second fraction collected at 5-10 min. At 160 °C and 180 °C, no galactose was detected after 50 min of processing time. At 140 °C, galactose was detectable for up to 80 min. Small amounts of galactose were still detectable in the pulp at 160 °C, suggesting that some galactose was inaccessible.

Arabinose extraction reached its maximum early, occurring in the first fraction at 160 °C and 180 °C and the second fraction at 140 °C. As arabinose is predominantly found as a side group in xylan and pectin, it is consequently more accessible and extracted early.[141] After 35 minutes, arabinose was no longer detectable in the extract, indicating that all available arabinose was extracted in the initial stages.

Glucuronic acid is typically found as side groups in hardwood as O-Acetyl-4-O-Methylglucuronoxylan.[18] Glucuronic acid extraction, therefore, commences early, with the highest concentrations observed in the first 5 min at 160 °C and 180 °C and in the second fraction at 140 °C. Notably, the total yield of glucuronic acid decreased with increasing process temperature, despite the absence of detectable glucuronic acid after 45 min and 50 min at 180 °C and 160 °C, respectively. The high temperature may lead to the thermal degradation of the acid. Glucuronic acid was not detected in the unprocessed beech. Due to the small total amount in the plant, it may have been below the detection limit of the HPAEC-PAD analysis using the TFA hydrolysis protocol.

Rhamnose is present in beech only in minimal quantities, typically at the end motifs of xylan chains.[18] It can also be found in pectin as rhamnogalacturonan.[142] The maximal extraction of rhamnose occurred in the second fraction (5-10 min) at all temperatures, and rhamnose was not detectable in the extract after 35 minutes. This indicates that while rhamnose was not the most readily accessible sugar, it is obtainable very early in the extraction process. The overall rhamnose yield increased with temperature.

Fucose is the least prevalent hemicellulose sugar in beech. Although its yield increased marginally at 180 °C, only minimal quantities were detectable within the initial 10 min of the process.

3.4.5 Detailed examination of sugar extraction within 20 minutes

To investigate the initial sugar extraction more thoroughly, the first 20 min of the experiment at 160 °C was repeated with samples collected at 1-min intervals. The reaction temperature was chosen to represent well balanced extraction results with a high amount of sugar and lignin extracted without the dominance of cellulose hydrolysis. In this detailed examination, the sugar concentrations within each fraction were low, and minor variations in temperature had a significant impact on the resulting concentrations. Three replications of the experiment were conducted to test the reproducibility of the process on a detailed timescale.

Each of these runs exhibited differences due to technical difficulties. In the first experiment, the cumulative yield of xylose was lower than that in the other runs, while more galacturonic acid was extracted. In Figure 37, all runs are presented individually.

Multiple factors may contribute to the inconsistency in the sugar yield within the initial minutes of the process. Despite efforts to maintain consistent process setup and preparation time, variations in biomass density and the necessity to prevent reactor leakages result in differences in the duration of biomass exposure to solvents and catalyst prior to the application of heat and initiation of solvent flow. Moreover, the heating setup utilizing an aluminum block on a heating plate led to temperature fluctuations of ±7 °C, potentially causing variations in reactor heating time. Additional inhomogeneity may arise from the packing and mixing of the biomass. Consequently, to enhance the results, process design improvements are necessary. A potential solution may involve preheating the solvents to mitigate heating effects.

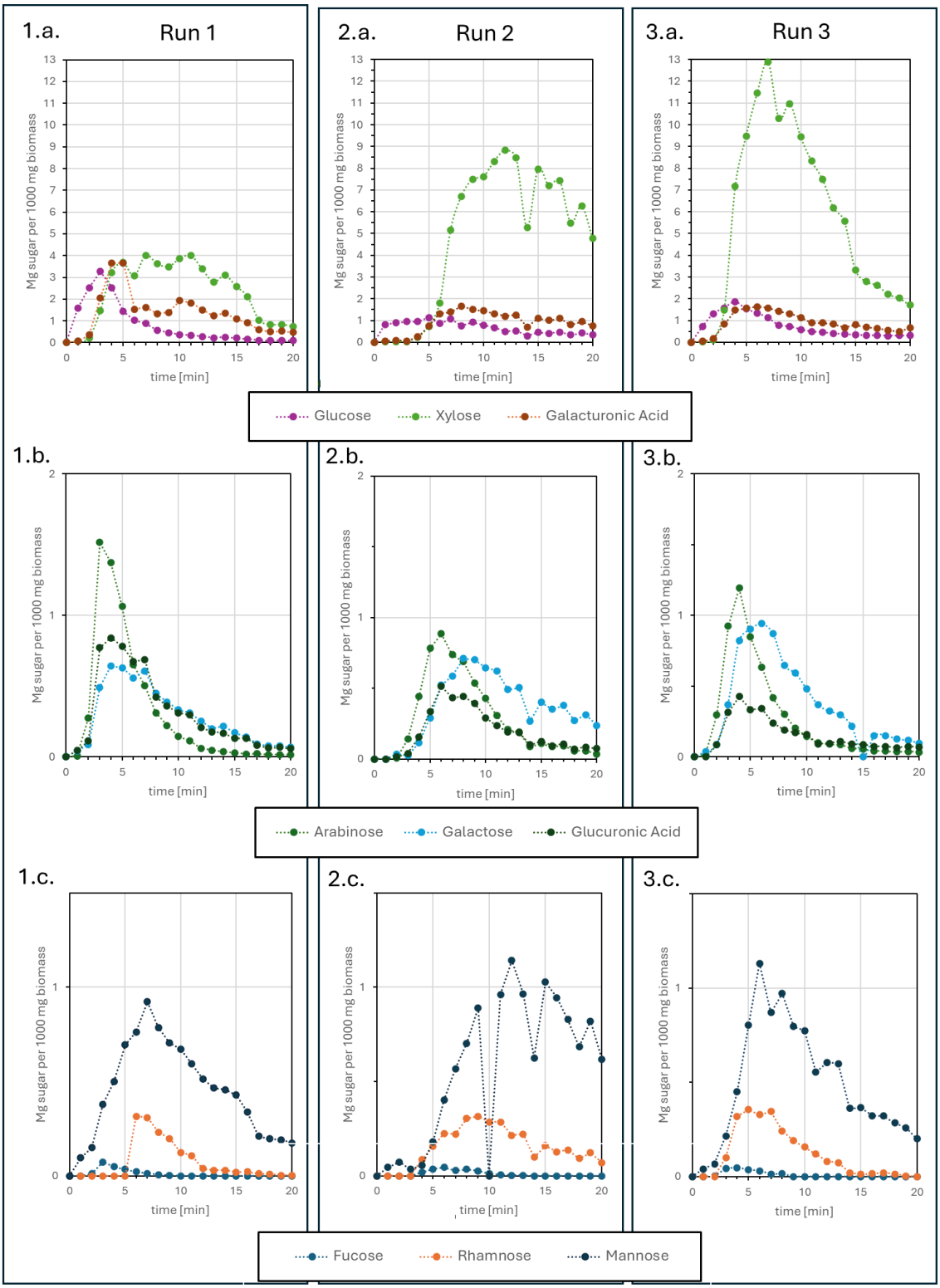

Figure 37: Flow through OrganoCat yield of hydrolyzed sugars per 1 min fraction. The sugar concentrations were analyzed using HPAEC-PAD. Three experiments at 160 °C with a flow rate of 0.2 ml/min were performed and are shown individually. 1.a.-c.) first experiment; 2.a.-c.) second experiment; 3.a.-c.) third experiment. For better visibility sugars were divided into separate graphs by yield. a.) glucose, xylose, galacturonic acid; b) arabinose, galactose, glucuronic acid; c) fucose, rhamnose, mannose.

While the quantity of sugars extracted in each fraction varies between experimental runs, consistent extraction patterns can be observed. Glucose extraction commences initially, with

detectable levels present within the first minute. The reactor was positioned in the heating block upon pump activation, and the biomass was already saturated with solvents. Possibly the reactor did not attain the desired temperature within the first few minutes. Consequently, the glucose extracted within the first minute was accessible at lower temperatures, potentially derived from the hydrolysis of accessible starch reserves. All other sugars were present in significant quantities from fraction 3 or 4 onwards, coinciding with the passage of more heated solvent through the reactor.

Next to glucose, fucose, arabinose, and glucuronic acid attained their maximum extraction early (min 3-6). As these sugars are typically found as polysaccharide side groups, they are initially accessible. Galactose reaches its maximum extraction next, while rhamnose and galacturonic acid reach their maximum later. Xylose and mannose achieved their maximum extraction yields last (min 7-12), which can be attributed not only to their higher content but also to their occurrence as the main chain sugars of xylans and mannans.

3.4.6 Comparing FT extraction patterns of beech and miscanthus

While the flow-through process was established using beech wood, alternative biomass sources can be utilized. The critical factors are particle size and structural stability, as they permit solvent flow and prevent reactor clogging. As miscanthus belongs to the grass family, its detailed lignocellulose composition differs significantly from beech while the proportions of hemicellulose, cellulose and lignin are similar. The lignin exhibits different monomer unit and linkage proportions, and the hemicelluloses comprise different sugar structures.[143] These variations may influence the extractability of the different components. The flow-through process with miscanthus was conducted exclusively at 160 °C. The temperature was chosen as the result for beech because these process parameters represent sufficient extraction over the entire process time without the effect of cellulose hydrolysis dominating the sugar yield, thereby ensuring a good standard for comparison. Extraction yields of lignin and sugars are presented in Figure 38.

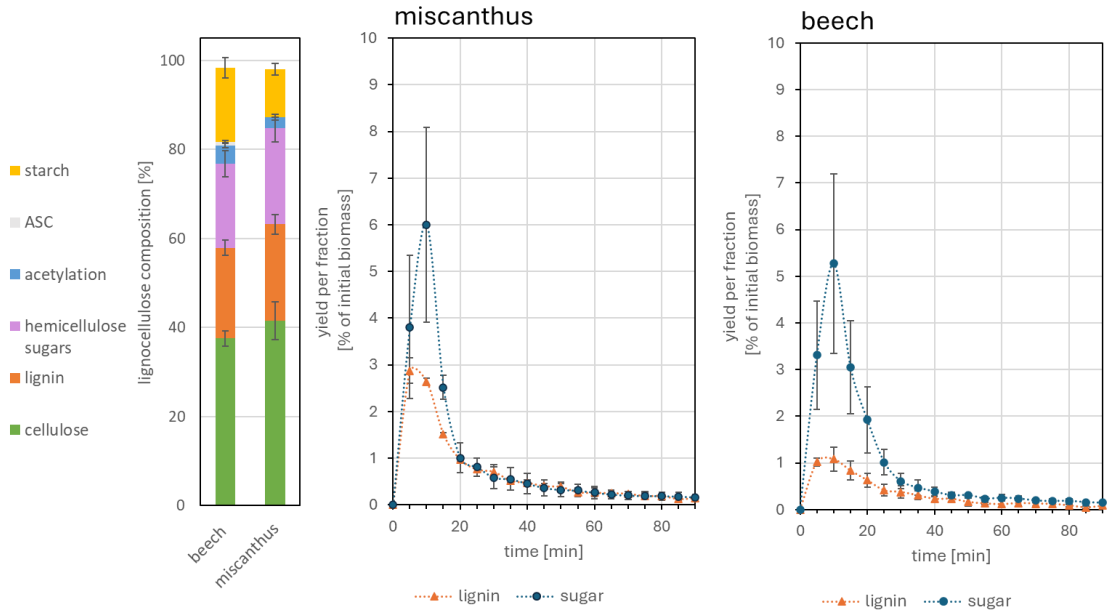

Figure 38: Right: Comparison of beech and miscanthus flow though OrganoCat extraction yields of lignin and sugar per 5 min fraction. The experiments were performed at 160 °C, with a flow rate of 0.2 mL/min. Experiments were conducted in triplicates. Left: Biomass composition determined by wet chemical analysis for comparison.

The sugar extraction process for miscanthus exhibited significant similarities to that of beech, including comparable yields. Similar to beech, the lignin yield reached its maximum within the first 10 min of extraction. However, the total yield was more than double the one derived from beech. This observation suggests that miscanthus lignin is more accessible than beech lignin.

Structural analysis of lignin was conducted using HSQC-NMR, and the results are presented in Table 26, juxtaposed with those of beech.

Table 26: Lignin linkages and monomer units of beech and miscanthus at 160 °C early (0-20 min) and late (20-90 min) in the fractionation, analyzed by HSQC-NMR. Triplicate experiments were performed for miscanthus FT processing, standard derivation in brackets. Duplicate experiments were performed for beech processing, averages are shown. For comparison, the HSQC-NMR results for the unprocessed biomass (0 min) are shown.

biomass	time [min]	ß-*O*-4 [per 100 S + G units]	ß-ß [per 100 S + G units]	ß-5 [per 100 S + G units]	S/G
Miscanthus	0	42.0	4,6	11	0.5
	0-20	31.6 (3.3)	5.6 (0.9)	4.5 (0.5)	0.7 (0.1)
	20-90	33.4 (2.6)	5.3 (0.7)	7.0 (3.3)	0.8 (0.1)
beech	0	71.6	10.8	5.1	1.5
	0-20	34.6	13.2	7.9	1.4
	20-90	26.8	11.3	6.9	2.0

In contrast to beech wood, Miscanthus exhibited no relevant differences in β-*O*-4 linkages or monomer ratios between the two fractions. Given that lignin extraction from Miscanthus also yields higher quantities, this lignin may generally be easier to extract than beech wood lignin.

The native miscanthus lignin exhibits a lower proportion of β-*O*-4 linkages and a higher content of G and H units, suggesting that the structure comprises smaller, perhaps more branched lignin fragments, as G and H units provide more branching points than S units. This characteristic necessitates less hydrolysis for extraction. Moreover, according to the models of hardwood and grass lignocellulose proposed by Kirui *et al*.[136], hardwood lignin is more uniformly integrated into the cellulose and hemicellulose matrix, whereas in grasses, larger lignin agglomerates are present. Consequently, less disentanglement is required to solubilize the lignin in miscanthus.

3.4.7 Comparing hemicellulose hydrolysis of miscanthus and beech

As proposed in chapter 3.4.4, the flow-through mechanism can be utilized to elucidate the structure of hemicellulose. Moreover, as demonstrated in various genotypes of Miscanthus sinensis, the structure of polysaccharides in the cell wall exerts a complex influence on saccharification.[144] Consequently the extracted sugars from flow-through OrganoCat with Miscanthus were compared to the extraction profile of beech wood obtained in previous experiments (Figure 39).

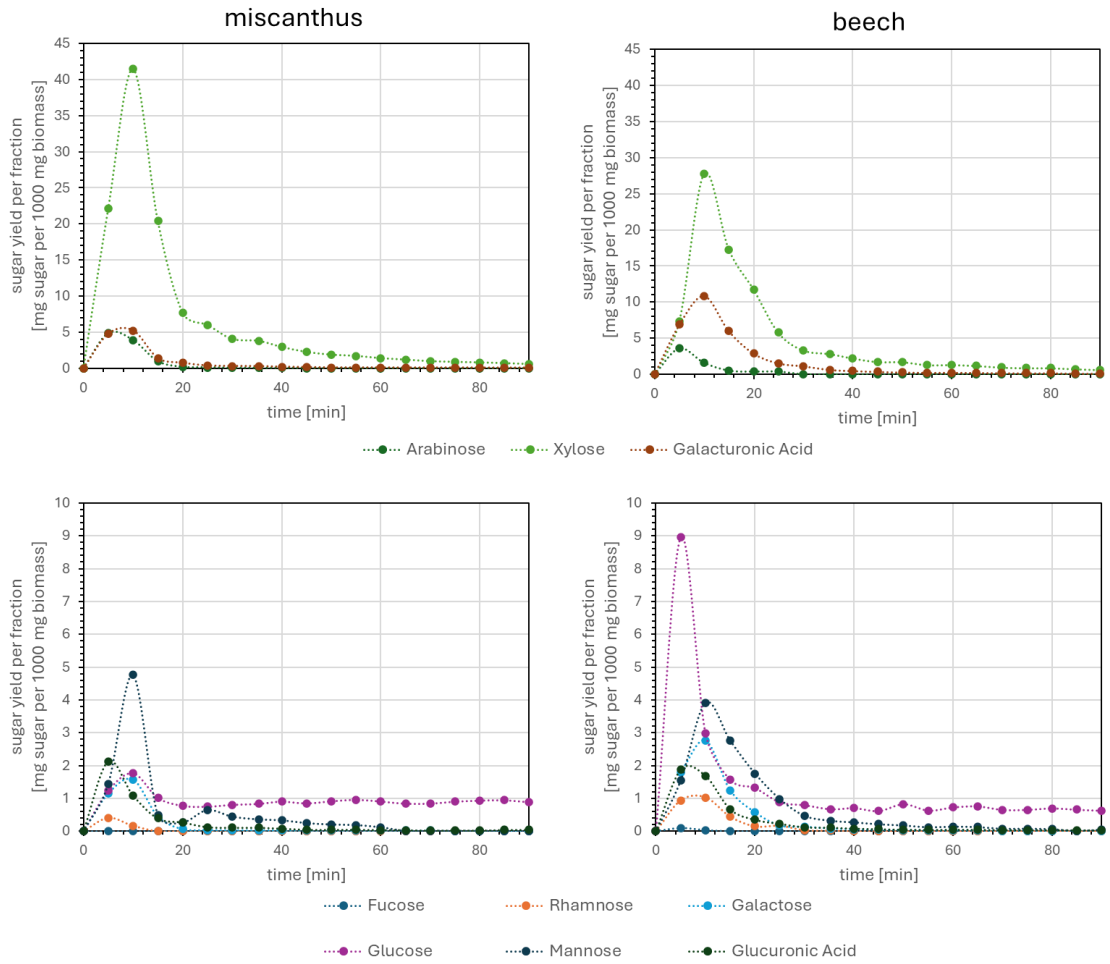

Figure 39: Comparison of sugar extraction from beech and miscanthus using the FT OrganoCat at 160 °C and a solvent flow rate of 0.2 mL/min. Amount of monosaccharides in liquid samples. Samples were collected for 5 min. Experiments conducted in triplicates. The full dataset and standard derivations are shown in Appendix 8.8.

In unprocessed miscanthus, xylose constituted 79% of the hemicellulose sugars, whereas beech hemicellulose comprised 76% xylose. Although the xylose proportions within the two plants were comparable, the structures of the xylans in the two species were different. Miscanthus contains mainly (glucurono)arabinoxylan, whereas in beech, arabinose side chains are less common, and glucuronic acid and acetylation are dominant. [18,145] Miscanthus processing resulted in higher xylose extraction yield. This suggests that the miscanthus xylan structure is more accessible. Xylose extraction increased rapidly within the initial 10 min of the process and subsequently decreased rapidly during the processing of both plant species. Although a greater quantity of xylose is extracted from miscanthus than from beech, the extraction of other sugars is reduced, resulting in equivalent total yields (Table 27). The sugar profile is typical for grasses, which is usually dominated by (glucurono)arabinoxylans with mixed linkage glucans and xyloglucans in the primary cell wall.[146]

Table 27: Comparison of cumulative sugar yield of FT OrganoCat extraction of miscanthus and beech after 90 min at 160 °C, analyzed by HPAEC-PAD. Extraction experiments were performed in triplicates; averages are given with standard derivation in brackets. The sugar composition of unprocessed miscanthus and beech determined by HPAEC-PAD of the TFA hydrolysate is provided for comparison.

	Miscanthus TFA hydrolysate unprocessed [mg/g]	Miscanthus OrganoCat hydrolysate [mg/g of initial biomass]	Beech TFA hydrolysate unprocessed [mg/g]	Beech OrganoCat hydrolysate [mg/g of initial biomass]
Fucose	0	0.0 (0.0)	0	0.1 (0.01)
Rhamnose	0	0.6 (0.8)	4	3 (1)
Arabinose	19	10.4 (0.3)	4	7 (2)
Galactose	11	3.5 (0.8)	6	7 (2)
Glucose	21	17 (8)	21	25 (8)
Xylose	197	121 (38)	174	90 (19)
Mannose	0	10 (5)	8	13 (6)
Galacturonic Acid	3	14 (6)	10	33 (21)
Glucuronic Acid	0.3	5 (1)	0	6 (2)
Total sugars	250	181 (52)	228	183 (55)

Glucose is the second most prevalent sugar in the miscanthus extract. The glucose yield within the initial 20 min was lower; a high quantity of readily accessible glucose present in beech was not observed in miscanthus. Starch reservoirs in miscanthus seem to be smaller and less accessible because of the surrounding cell wall matrix. After the 20-minute mark, consistent glucose extraction was observed, which occurred at the same rate as in beech. This suggests that the cellulose hydrolysis process operates identically for both lignocellulosic materials.

Galacturonic acid was only present in minimal quantities in unprocessed miscanthus; however, it was the third most abundant sugar in the extract. As observed in beech, galacturonic acid can be hydrolyzed from pectin, which make up about 5% of primary and 0.1% of secondary cell walls in grasses.[146]

Arabinose can be detected early in the process, as it is primarily found as a side group of arabinoxylan and glucuronoarabinoxylan, rendering it readily accessible for hydrolysis. Glucuronic acid attains maximum extraction early in the process due to the same phenomenon.

The maximum concentration was observed in the initial fraction, which occurred earlier than that in beech. In miscanthus, rhamnose is not found in xylan end groups but in the form of the pectin rhamnogalacturonan.[147]

Peak concentrations of galactose from galactan and mannose from mannan occurred in the second fraction, as previously observed in beech.

As briefly mentioned before, xylans are present in lignocellulose in either a three-fold conformation or a flat ribbon two-fold helical screw conformation. The flat ribbon two-fold xylans are known to possess the capability to closely align and bind to cellulose microfibrils.[21] Solid state NMR analysis revealed that in grasses, interactions between lignin and xylan were predominantly characterized by non-flattened conformations and lignin units rich in methyl esters (S units), whereas direct lignin-cellulose interactions and interactions between the flat two-fold xylan were infrequent.[148]

Consequently, the group of Kirui *et al.* proposed a model for lignocellulose. In grasses, lignin is found in hydrophobic nanodomains and binds to three-fold xylans via hydrogen bonds. The three-fold xylans are not attached to cellulose directly but are directly connected to the flat two-fold xylan which coats the cellulose microfibrils. In hardwood, the lignin and carbohydrates are more thoroughly integrated than in grass, resulting in the binding of lignin to both three-fold and two-fold xylans.[23]

The loosely bound, hydrophilic lignin agglomerates render the miscanthus lignin more susceptible to extraction with organic solvents. It can be postulated that the screw helix three-fold xylan is more accessible for hydrolysis than the flat ribbon two-fold xylan, which is bound closely to the surface of the cellulose microfibrils. This can explain the higher quantities of lignin and xylose extracted from miscanthus compared to beech. As the lignin-xylan interaction is stronger with lignin rich in methyl units, the dominance of S units instead of G- and H-rich lignin in hardwood strengthens the interaction and makes hardwood lignocellulose more resilient to extraction. The closer interaction of lignin with xylans and the higher proportion of xylans directly coating the cellulose also explain why some of the lignin and xylan are highly resistant to extraction from lignocellulose, and significant quantities can be found in the pulp.

A study comparing the hardwood poplar and the grass switchgrass showed that lignin is the main factor in recalcitrance for poplar, whereas xylan removal is more critical for enzymatic saccharification in switchgrass.[149] This aligns with the results of the OrgnoCat process and fits

into the proposed model, leading to the assumption that the conclusions could be extended to other hardwoods and grasses.

The FT OrganoCat fractionation process revealed the critical role of temperature in lignin and sugar extraction, with elevated temperatures yielding higher quantities, particularly within the first 20 minutes. Glucose dominated sugar extraction, likely due to cellulose hydrolysis, which suggests shorter process times or temperature gradients could minimize cellulose degradation. For hemicellulose, most sugars, except xylose, were extracted within 20 minutes, making targeted adjustments feasible for specific extraction goals.

Lignin extraction occurred rapidly and was largely independent of hemicellulose dissolution. Even without a catalyst, lignin was extracted, highlighting the role of heat and solvent alone, although sugar hydrolysis requires acidic conditions. Plant-specific differences were evident: beech lignin, more integrated with cellulose, exhibited structural variations over time, while miscanthus lignin, with its less interlinked structure, was extracted more rapidly and uniformly.

The efficiency of the OrganoCat process in fractionating lignocellulose, particularly from grasses, underscores its potential for producing lignins with specific structural characteristics. This versatility is crucial for advanced applications like biobased carbon nanofibers, where the structure and solubility of lignin significantly influence electrospinning performance and polymer properties.

3.5 Electrospinning of selected OrganoCat lignin

Lignin holds large potential for biobased materials, including carbon nanofibers.[79,150] The OrganoCat lignin produced in this work retains a portion of its native structure while also exhibiting good solubility in organic solvents, making it a suitable candidate for electrospinning experiments aimed at producing biobased carbon nanofibers. Unlike many lignins, which require the addition of conventional polymers such as polyacrylonitrile (PAN) to achieve uniform fiber formation, the inherent properties of OrganoCat lignin could potentially reduce the need for such additives.[150]

The structural variability of lignin, depending on the plant source and fractionation process, can influence its behavior in electrospinning. To explore this, lignins with different structural features were selected and evaluated to assess the effects of structural variations on spinnability. These electrospinning experiments were conducted in collaboration with the group of S. Renneckar at the University of British Columbia and with the Institute of Energy Technologies – Basics of Electrochemistry (IET-1) at the Forschungszentrum Jülich and will provide valuable insights into optimizing lignin-based nanofiber production.

3.5.1 Electrospinning of poplar OrganoCat lignin

Electrospinning of poplar lignin was conducted within the framework of the research stay at the University of British Columbia. The poplar OrganoCat lignin extracted in the scaled up OrganoCat process (chapter 3.2) was tested using a local electrospinning setup.

In this experiment, a vertical electrospinning setup was employed using the available equipment (Figure 40). 5% polyethylene oxide (PEO) was incorporated, and spinning parameters were selected to replicate previous successful experiments in the same laboratory of S. Renneckar.[151] Under the applied conditions, fiber formation was achieved; however, three-dimensional structures began to develop immediately, preventing fiber collection on the aluminum foil-covered electrode, which prevented further analysis of the spun material.

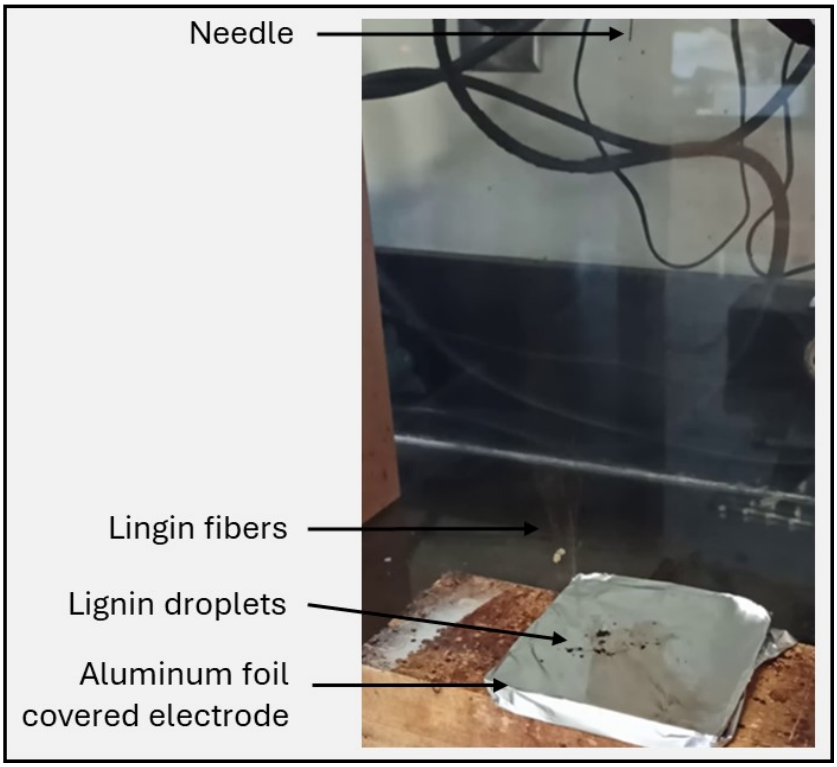

Figure 40: Electrospinning of poplar lignin. A vertical setup was used for electrospinning 50wt% poplar OrganoCat lignin in DMF with the addition of 5 wt% PEO.

The formation of 3D structures during electrospinning has been observed previously, as reported by Sun *et al*..[152] The phenomenon is likely attributed to static charge induced in the fibers during the spinning process. This phenomenon has also been observed under conditions of high relative humidity, wherein the electrostatic attraction between fibers and spinneret is attributed to the presence of a substantial quantity of water molecules.[153]

A comparison using organosolv lignin for electrospinning under similar conditions, executed by V. Selmert of the IET-1, did not reveal any 2D structure formation. This suggests that a component within the extracted OrganoCat lignin was responsible for the charging effect. Potential factors contributing to this phenomenon include residual water that was not removed during drying, salts or acid from the catalyst, or extracted byproducts.

Despite subjecting the lignin to high-vacuum drying for several hours following the removal of 2-MTHF after biomass fractionation and subsequently drying it at 50 °C and 0.001 bar for 24 h prior to dissolution in the spinning solution, it is plausible that an excess of water molecules persisted in the product, which could induce static charges.

To eliminate static charging, the OrganoCat lignin was purified by dissolution in acetone and subsequent precipitation in water. as described in chapter 3.2.4. It was made sure the lignin

was dried thoroughly before dissolution. Subsequently, no spinning conditions have been identified for precipitated lignin thus far that resulted in a stable fiber spinning process using precipitated lignin. Other fractionation methods, such as the established antisolvent precipitation for OrganoCat lignin may lead to better results.[54]

3.5.2 Selection of lignin source for electrospinning

For electrospinning, the polymer solution must have high viscosity, low surface tension, and high conductivity. Highly linear polymers with a high molecular weight not only result in a more viscous solution but also facilitate the formation of a thin fiber that does not break off during the spinning process because of the alignment of long polymer chains. Furthermore, a narrow size distribution aids a more homogeneous alignment of polymer chains. For the carbonization process, the proportion of oxygen and other heteroatoms and functional groups plays a significant role.[154]

Based on the biomass material screening data presented in chapter 3.1, three contrasting OrganoCat lignins were selected for the electrospinning process (Table 28).

Table 28: Lignin structure of selected OrganoCat lignins for electrospinning. S/G monomer ratio and β-*O*-4 linkage proportion determined by HSQC-NMR analysis. Molecular weight M_w and polydispersity index (PDI) were determined using SEC.

biomass	S/G	β-*O*-4 [per 100 S + G units]	M_w [Da]	PDI
eucalyptus	2.6	25.1	3088	4.0
walnut shells	1.8	16.2	3983	4.5
miscanthus	0.7	14.5	4229	4.8

The hardwood eucalyptus exhibited the highest S/G ratio and proportion of β-*O*-4 linkages among all studied plants. Both lignin characteristics are associated with a higher linearity of the polymer; therefore, eucalyptus lignin is potentially well suited for electrospinning. Walnut shell lignin maintains a relatively high S/G ratio but possesses fewer β-*O*-4 linkages. Miscanthus lignin contains slightly fewer β-*O*-4 linkages than walnut shell lignin but demonstrates a very different monomer composition. Not only is the S/G ratio considerably lower, but in addition to more G lignin, miscanthus also contains a substantial amount of H lignin. The reduced methoxylation on the aromatic ring of the monomer increases the likelihood of lignin branching.[111] The molecular weight (M_w) of the OrganoCat lignins is relatively similar. However, eucalyptus lignin exhibited the lowest molecular weight, while

miscanthus demonstrated the highest molecular weight. A high molecular weight is generally considered advantageous for electrospinning with polymers as longer chains allow for more entanglement and therefore higher viscosity of the spinning solution.[154] The polydispersity index (PDI) represents the uniformity of the molecule size. In this context, eucalyptus lignin displays a narrower molecular distribution compared to walnut shell and miscanthus lignin.

3.5.3 Electrospinning of OrganoCat lignin from different biomass sources

The electrospinning of the selected OrganoCat lignin was carried out and optimized by Victor Selmert at the IEK-9 of Forschungszentrum Jülich. A horizontal electrospinning setup was used, as shown in Figure 9. A lignin solution was provided in a syringe and slowly pressed through a metallic needle. An electrical field was applied between the needle and a metallic collector covered with aluminum foil.

Electrospinning of pure lignin nanofibers remains challenging; therefore, several process adaptations have been implemented by S. Selmert. These adaptations encompassed a solvent screening and the evaluation of various lignin concentrations. Additionally, a setup utilizing a coaxial needle was employed as described by Lallave *et al.*.[82] Ultimately, successful electrospinning of OrganoCat lignin was achieved using a coaxial needle and a 55wt% lignin solution in THF. The voltage of the electrical field, flow rate of the lignin solution, and distance between the needle and collector were adjusted for each experiment to provide stable spinning conditions.

Following the adjustment of spinning conditions, walnut shell lignin was successfully spun into fibers. However, after approximately 10 minutes, the spun fibers began to detach from the aluminum foil. Within 30 minutes of initiating the process, three-dimensional structures had formed, nearly reaching the needle, necessitating the termination of the spinning process (Figure 41).

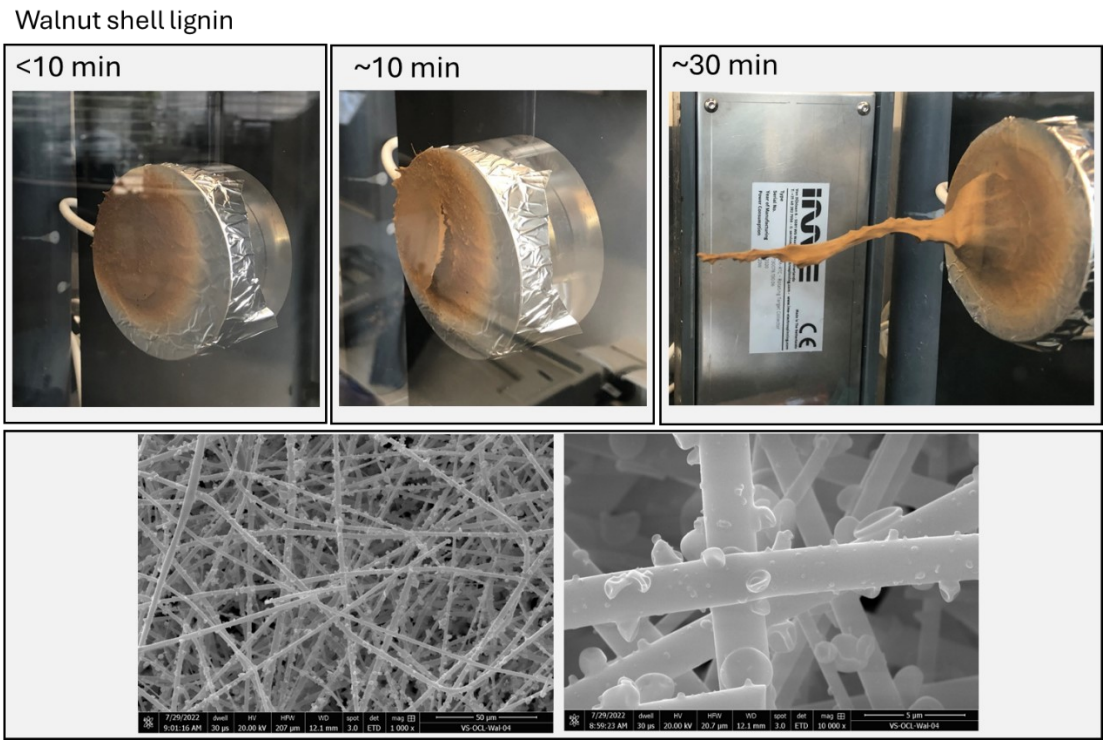

Figure 41: Above: Pictures of the coaxial electrospinning of 55 wt% walnut shell OrganoCat lignin in THF. Voltage: 20 kV; distance: 150 mm; flow rate (lignin):10 µl/min; flow rate (THF):15 µL/min. Below: Scanning electron microscope (SEM) pictures of the fibers.

Scanning electron microscopy (SEM) images revealed that uniform fibers were formed. Droplets of electrospray were visible on the surface of the fibers, indicating that the spinning process was not entirely continuous.

The electrospinning of eucalyptus lignin resulted in the successful formation of fibers. However, three-dimensional structures began to develop immediately, growing from the collector towards the needle. After 20 min, it became necessary to terminate the electrospinning process because the structures approached the needle (Figure 42). Upon closer examination, the SEM images revealed that the eucalyptus lignin fibers exhibited reduced thickness and increased smoothness compared with those derived from walnut shell lignin.

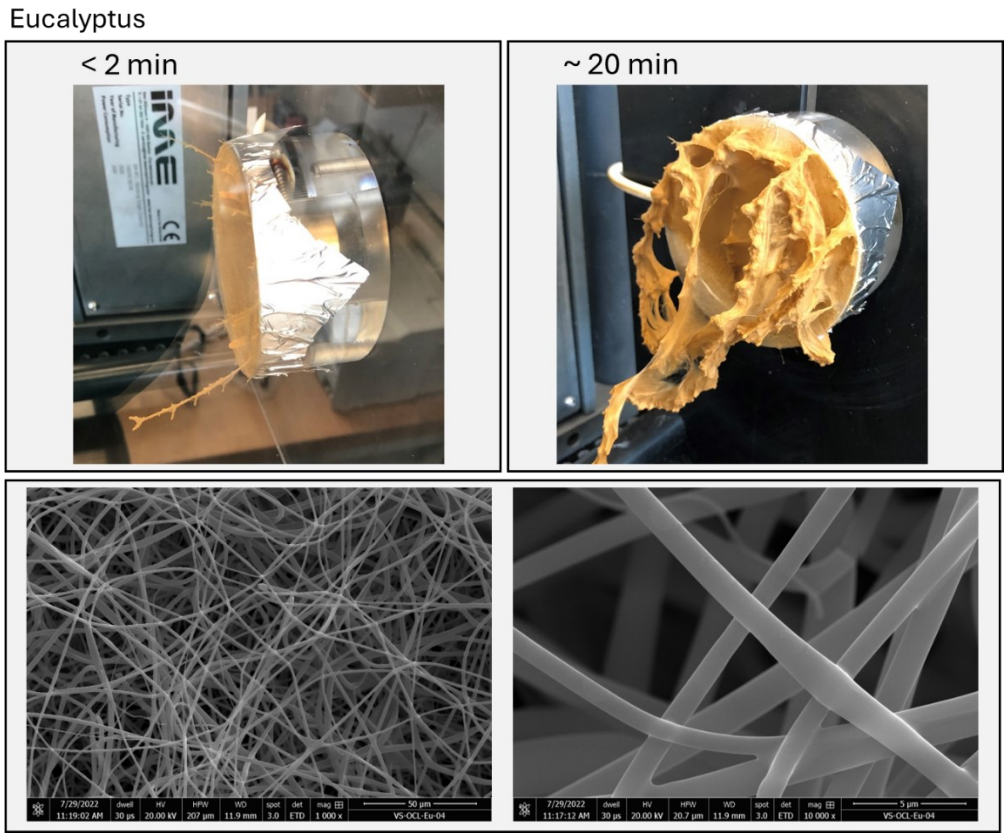

Figure 42: Above: Pictures of the coaxial electrospinning of 55 wt% eucalyptus OrganoCat lignin in THF. Voltage: 25 kV; distance: 205 mm; flow rate (lignin):20 µL/min; flow rate (THF):10 µL/min. Below: Scanning electron microscope (SEM) pictures of the fibers.

Although further process adaptations were made by V. Selmert, in the investigated design space no stable fiber formation could be achieved with miscanthus lignin (Figure 43).

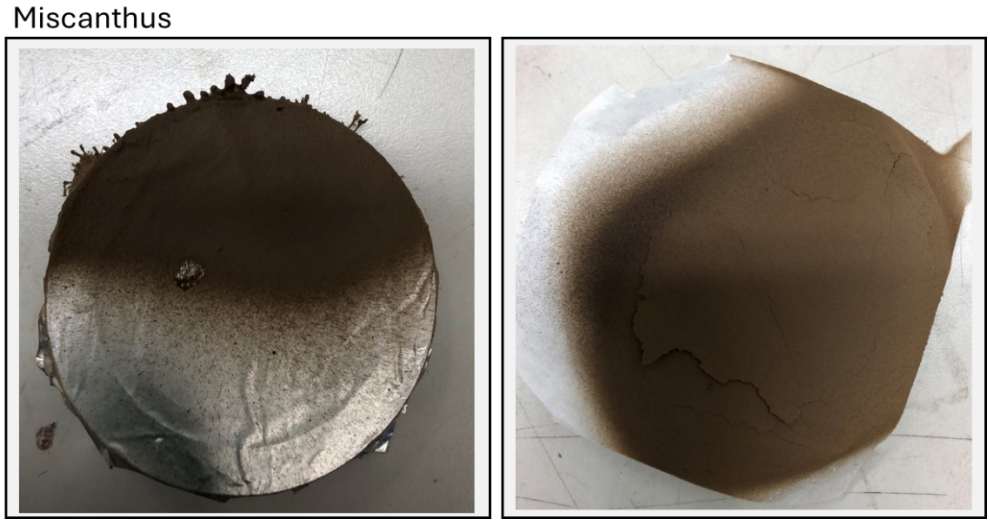

Figure 43: Electrospinning of miscanthus OrganoCat lignin (50 wt% in MTHF). The spinning conditions were set as follows: voltage, 25 kV; distance, 220 mm; flow rate (lignin) 20 µL/min; flow rate (2-MTHF) 5 µL/min. Right: Electrospinning on aluminum foil, left electrospinning on a paper-covered collector.

3.5.4 Conclusions for the electrospinning of OrganoCat lignin

Overall, electrospinning with OrganoCat lignin was demonstrated to be feasible, even without the incorporation of additional polymers which has only been published a few times before.[82,86] Further research is necessary to maintain a stable spinning process; however, it has already become evident that the high S monomer, high β-*O*-4 linkage lignin from eucalyptus yields the most favorable electrospinning results. Although it was also possible to produce fibers with walnut shell lignin, which has a slightly lower S/G ratio and fewer β-*O*-4 linkages, it proved to be considerably challenging to electrospin miscanthus lignin, which is composed of a more heterogeneous monomer structure including significant proportions of S, G, and H units. A high proportion of S units in lignin is associated with a more linear structure as the methoxylation of syringyl results in less linking sites.[155] As walnut shell and miscanthus lignin have a similar proportion of β-*O*-4 linkages (16.2 and 14.5 per 100 S+G units respectively), this lignin characteristic does not appear to be a dominating factor for spinnability. Further investigation, for example, using fractionated lignin of the same material for narrower molecular weight distribution, will have to show if this holds true, as there are multiple structural factors influencing the outcome.

These results were consistent with the findings of previous studies. In the electrospinning of organosolv lignin with PAN, high S hardwood lignin derived from poplar exhibited superior performance in fiber morphology, tensile strength, and other characteristics compared to lignin obtained from softwood (pine) or grass (corn stalk).[87] Similarly, in the electrospinning of Kraft lignin from various sources with cellulose acetate as stabilizing polymer, hardwood lignins (eucalyptus, poplar) demonstrated suitability.[88] The more linear structure of high S lignin, typically found in hardwood, can be identified as the primary factor contributing to favorable outcomes in the electrospinning of lignin.

The relationship between lignin structure and carbon fiber quality was demonstrated through the electrospinning of Kraft and soda lignin in conjunction with PAN. The more linear, high β-*O*-4 soda lignin not only resulted in smoother fiber surfaces but also exhibited higher retention of aromaticity during carbonization. Consequently, carbon fibers derived from soda lignin demonstrated superior mechanical performance compared to those from Kraft lignin.[156] It can be concluded that the selection of biomass source and process conditions influences both the electrospinning process and the mechanical properties of the resultant carbon nanofibers.

Moreover, a higher molecular weight (M_w) does not appear to be a determinant factor for spinnability, as evidenced by the observation that miscanthus OrganoCat lignin exhibited the highest M_w, whereas eucalyptus demonstrated the lowest. Nevertheless, it should be noted that SEC has limitations for determining the molecular weight of lignin as discussed in chapter 3.1.4. The most pertinent consideration here is that SEC separates molecules based on their hydrodynamic radius. As the branching of lignin influences the hydrodynamic radius consequently the retention time and calculated molecular weight changes. This implies that lignin with different S/G ratios cannot be reliably compared using this method. Different molecular weights within lignin structures with similar linearity may still influence the electrospinning process.

The high polydispersity index (PDI) of the OrganoCat lignins (4.0-4.8) indicates that in comparison to a conventional polymer for electrospinning, such as polyacrylonitrile (PAN), the molecular size distribution in lignin is heterogeneous. Fractionation, which has been demonstrated to be effective for OrganoCat lignin using hexane as an antisolvent[54] or CO_2 expansion of the 2-MTHF[157] for precipitation, yields lignin with a narrower molecular weight distribution. A large-scale OrganoCat process is required to produce sufficient lignin to obtain fractions of adequate size for electrospinning. Based on the results of electrospinning experiments with fractionated Kraft lignin, the higher molecular weight fraction should improve crystallization and mechanical performance of lignin carbon fibers.[158]

4 Summary, Conclusion and Outlook

One of the major challenges in biomass valorization concepts is the variability of the lignocellulosic feedstock. Therefore, it is essential to consider the impact of these differences on product yield and quality. This thesis addressed these challenges, particularly the structural variability of lignin, which often limits its applications. The OrganoCat process, an acid-catalyzed biphasic lignocellulose fractionation method, was employed to enhance our understanding of the influence of lignocellulose structure on both the process recalcitrance and the product quality.[50,132] This approach enables the selection of suitable plant material and process conditions for desired product goals and a better understanding of lignocellulose structure.

Comprehensive biomass screening was conducted by comparing ten different plant materials to identify correlations between lignocellulose and lignin structure, product yields, and lignin quality. Plant materials with similar structural properties exhibit similar extraction patterns. For example, sida and walnut shells possess high lignin content and S/G ratios, similar to the hardwoods beech and eucalyptus. This group demonstrated greater recalcitrance towards fractionation, resulting in lower lignin yields, increased β-*O*-4 linkage cleavage, and smaller molecular sizes compared to grasses such as miscanthus, maize, sugarcane bagasse, and szarvasi. Interestingly, these effects appeared to counterbalance each other, leading to no significant differences in lignin yield and β-*O*-4 linkage among all plants. Processing challenges may arise for plants with high contents of alcohol-insoluble residues, as these constituents can also be dissolved into the organic phase and necessitate further purification steps for the lignin.

To gain deeper insight into the direct influence of lignin content and structure on the fractionation process, nine natural genetic variations of poplar were compared using a scaled-up version of the OrganoCat process. Although a trend suggested that higher lignin content in the plant was associated with lower lignin retention in the pulp, these differences need to be confirmed to draw robust conclusions. A larger dataset that incorporates more poplar variations and repetitions is necessary. Here, the implementation of a smaller-scale screenings system could facilitate the processing of a greater number of samples more efficiently.[124,125]

The transition of the OrganoCat process into a semi-continuous flow-through variation opened new possibilities to gain deeper understanding of lignocellulose fractionation. Statistical design of experiments (DOE) was utilized to assess the influence of process parameters (time, flow rate, and temperature) on fractionation yields and the proportion of β-*O*-4 linkages in lignin. The findings revealed that the reaction temperature has the most significant impact on the extraction of lignin and sugars, with sugar yields increasing considerably at elevated temperatures. An optimum solvent flow rate of 0.2 mL/min was identified because higher flow rates did not yield increased extraction. Although the model for ether linkage cleavage in lignin requires refinement through additional measurements, preliminary results indicate that higher temperatures promote β-*O*-4 cleavage. A lower retention time in the reactor, facilitated by higher solvent flow rates, may preserve ether linkages. Initial trials for scaling up the system demonstrated that preheating the solvents is necessary to achieve the desired reaction temperature. Further improvements are needed to stabilize the scaled-up FT process, ensuring its reliability and efficiency.

The FT OrganoCat system also enabled time-resolved insights into lignin and sugar extraction. The investigation revealed that most of the yield was obtained within the first 20 minutes of the process. For beech lignin, a small initial fraction required less depolymerization for extraction than the bulk of lignin extracted later, a pattern that was particularly evident at lower reaction temperatures. A detailed analysis of the sugar extraction timeline indicated that cellulose hydrolysis occurred throughout the process, especially at higher temperatures. Furthermore, the side-chain sugars were extracted slightly earlier than those in the main chains of hemicellulose and pectin. Comparisons of the kinetics between beech and miscanthus confirmed a model for the distribution and interaction of lignin, hemicellulose, and cellulose in cell walls.[136] In grasses such as miscanthus, lignin appears in larger agglomerations and is less interconnected with hemicellulose and cellulose, facilitating easier extraction with reduced depolymerization. Conversely, xylans in hardwoods, such as beech, are often found in a twofold conformation, closely aligned with cellulose microfibrils, rendering them more recalcitrant to hydrolysis. The time-resolved FT OrganoCat process can also be leveraged in future studies to gain further insight into the lignocellulose structures and their disintegration. Improvements could include stabilizing the heating to enhance

repeatability and utilizing the scaled-up version to minimize processing times while still obtaining sufficient lignin for analysis.

The importance of lignin selection was further demonstrated through electrospinning, which valorizes lignin by converting it into carbon nanofibers. A high S/G ratio, associated with a more linear lignin structure, has emerged as a key factor influencing the spinnability of lignin. Eucalyptus lignin yielded the best results, followed by walnut shell lignin, while electrospinning of miscanthus remained challenging. Difficulties arose due to the formation of 3D structures during the electrospinning of OrganoCat lignin, which complicated further analysis. Lignin purification, for instance through antisolvent precipitation, could eliminate molecules that cause charging issues during electrospinning. [54] Moreover, the scale-up of the OrganoCat process could provide a larger quantity of material for further investigation of the electrospinning of OrganoCat lignin. After achieving a stable spinning process, subsequent research could focus on the carbonization of the nanofibers and their further application.

The findings of this thesis contribute to the sustainable utilization of lignocellulosic biomass, highlighting the potential of tailored lignin extraction processes for advanced material applications. By elucidating the structural variability of lignin and its impact on extraction efficiency and product quality, this research offers new approaches for optimizing biorefinery operations. As industries increasingly seek renewable alternatives to fossil-based resources, the insights gained here can guide the selection of appropriate biomass sources and processing techniques, ultimately supporting the transition towards a circular bioeconomy. Future efforts to refine these processes could lead to enhanced yields of high-quality lignin products, thus enabling more sustainable material production and reducing reliance on non-renewable resources.

5 Materials and Experimental procedures

5.1 Chemicals

All chemicals used were obtained from *Sigma-Aldrich Chemie GmbH, Carl Roth GmbH + Co. KG,* and *Fisher Scientific International*. Unless otherwise stated, all chemicals were used without further purification. Enzymes were purchased from *Megazyme Ltd.* Ultrapure water was generated from deionized water using a MicroPure purification system (*Thermo Scientific Barnstead*). Reactions involving compressed gases N_2 and Ar were performed using the high-pressure equipment described in Section 5.3..

5.2 Plant material

Biomass from *Sida hermaphrodita, Silphium perfoliatum, Elymus elongatus* – Szarvasi-1, and *Miscanthus × giganteus* plants originated from a previously conducted field trial.[92] Maize was obtained from a field in Jülich, the full plant including fruits was utilized. Rapeseed straw was harvested from a local field trial. Sugarcane bagasse and eucalyptus wood were kindly provided by EMBRAPA-Brazil. The walnut shells were procured from LEMBERONA GmbH (Austria). Beech wood was purchased as commercial firewood and debarked before being milled. Sida, silphium, szarvasi, miscanthus, rapeseed, and maize were dried for 7 days at 85 °C. Walnut shells, sugarcane bagasse, and beech wood were obtained as dried material.

Plant materials were processed using a hammer mill ($30 s^{-1}$, millM400, *Retsch*, Germany) equipped with a 1 mm sieve. The walnut shells were already ground to a fine powder by the manufacturer prior to use. All materials were employed directly for OrganoCat pretreatment and fractionation. For conducting wet chemical analysis, all materials were further ground to a fine powder using a ball mill M 400 (*Retsch*, Haan, Germany) in a 50 mL metal beaker. The mill was operated at a speed of 30 s^{-1} for a duration of 2 min.

5.3 High pressure laboratory equipment

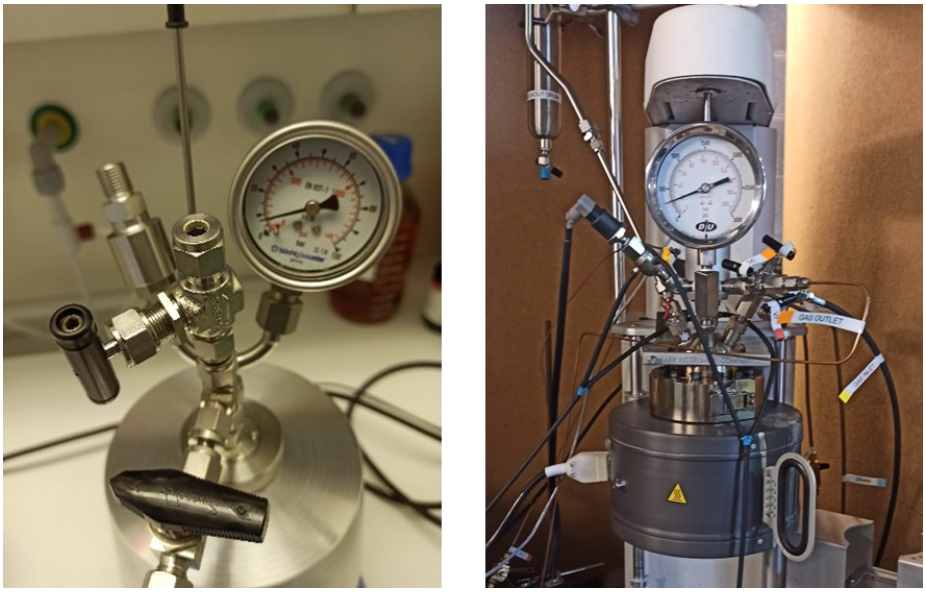

Figure 44: Pictures of the standard 25 mL autoclave used at FZJ (left) and the large 1 L autoclave at UBC (right).

Small scale batch reactor (25 mL)

The pretreatment procedures for lignocellulose were carried out using high-pressure equipment, with temperatures exceeding the boiling points of the solvents used. The batch reactions were executed in a 25 mL Hastelloy autoclave (*Büchi AG*, Switzerland) equipped with a Teflon inlet and a total solvent volume of 1 mL. A manometer was affixed to the autoclave to monitor pressure changes during the reaction. The autoclave was pressurized with 10 bars of argon and heated using a cylindrical aluminum heating block designed for efficient heat transfer on a standard laboratory heating plate. The temperature was regulated through a thermometer positioned within the heating cone, while stirring was accomplished by a magnetic stirring bar situated within the Teflon inlet of the autoclave.

Large scale batch reactor (1 L)

Upscaling reactions was performed at the University of British Columbia within a 1 L autoclave (*Parr Instrument Company*, USA). This autoclave features a mechanical stirring system and a heating mantle for warming, both of which can be controlled digitally. The system also includes a water-cooling mechanism for efficient temperature regulation. The autoclave is equipped with an internal thermometer and a manual manometer for monitoring pressure. Additionally, N_2 gas can be used to apply extra pressure, with digital monitoring available. The

temperature and pressure data for the long heating and cooling phases are recorded digitally by a connected computer.

5.4 Analytical methods

Lignocellulose composition analysis

The composition of raw biomass was determined using a set procedure of wet chemical analysis (Figure 45). All biomass materials were dried until constant weight prior to the analysis. The removal of alcohol-soluble components (ASC) was always carried out first followed by destarching of the sample. Measurement of acetylation, crystalline cellulose, lignin and hemicellulose sugar content were conducted using the dAIR sample.

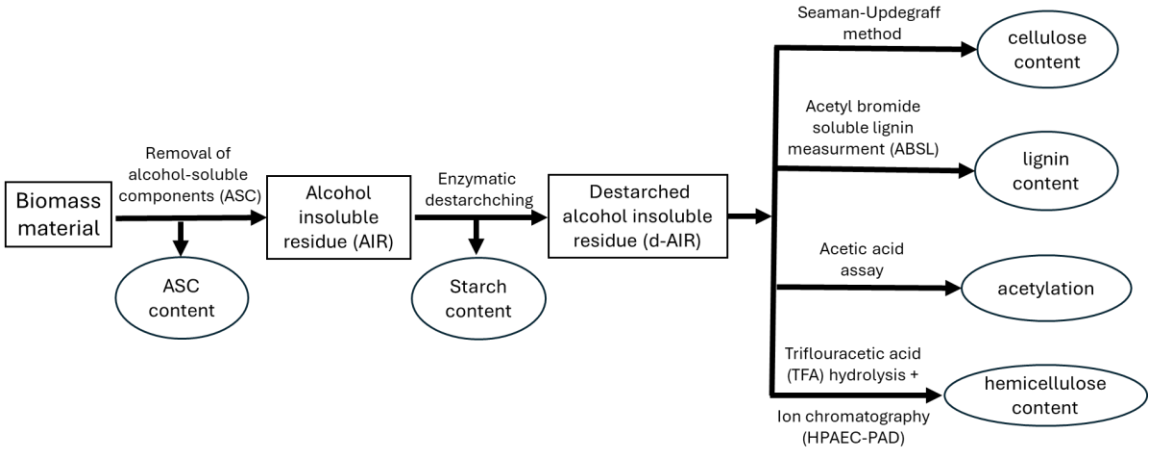

Figure 45: Flow chart of the analytical steps included in the wet chemical analysis.

Removal of alcohol-soluble components (ASC)

100 mg of finely milled biomass were placed inside a 2 mL screw-cap tube. 1 mL of 70% ethanol was added, and the mixture was stirred. After centrifugation (5 min, 14000 rpm, 21 °C), the ethanol was decanted, and 1.3 mL of a chloroform:methanol mixture (v:v, 1:1) were added. The samples were mixed for ten seconds, centrifuged, and the solvent was removed. This process was repeated a minimum of three times or until the solvents were colorless. After the last solvent removal, 1.3 mL of acetone were added, the samples were mixed and centrifuged. The samples were then dried at room temperature until they reached a consistent weight. The resulting alcohol insoluble residue (AIR) was weighed to determine the amount of ASC.

Destarching biomass samples (d-AIR)

The removal of starch from AIR samples was achieved through enzymatic treatment. To initiate the process, 0.75 mL of sodium acetate (NaAc; 10mM, pH5.5) buffer was added to the samples, followed by mixing and shaking for 20 minutes at 80 °C and 1400 rpm. After cooling the samples on ice, 0.75 mL of an enzyme mix containing 0.5 mL amylglucosidase (3260 U/mL) and 03 mL α-amylase(1000 U/mL) in NaAc buffer was added. The samples were mixed for 10 s and then incubated at 37 °C and 400 rpm for 1-7 days. The glucose content of the supernatant was then analyzed. If glucose was detected, additional enzyme mix was added, and incubation was continued. When no glucose was detected, the supernatant was removed, and the sample was heated to 99 °C for 10 min. The sample was then washed with 1 mL of ultrapure water, centrifuged, and decanted. The heating and washing were repeated three times. After this, the sample was washed with acetone and dried at room temperature until it reached a consistent weight. The amount of starch removed was determined by weighing the sample.

Glucose determination

Glucose was determined from the supernatant of enzymatic destarching using a Glucose (Hexokinase) Assay Kit, purchased from *Sigma-Aldrich* and the *BioTek* Synergy 2 UV-VIS spectrometer. The samples were diluted using ultra-pure water to achieve concentrations matching the calibration curve (dilution ratios of 1:20 or 1:50). A mixture was prepared by combining 50 µL of the diluted hydrolysate with 200 µL of glucose assay kit. This mixture was then analysed at 345 nm. The absorbance was continuously monitored until the glucose was fully converted, resulting in a maximum absorbance value.

Once glucose was no longer detectable, the supernatant was extracted, and the samples underwent denaturation at 99 °C for 10 minutes. The sample was then cleaned by adding 1 mL of ultrapure water, followed by centrifugation and decantation, repeating this process three times. Afterwards, acetone was utilized to cleanse the samples, which were then left to air-dry at room temperature overnight.

Measurement of lignocellulose acetylation

The total acetate content of the sample was determined using an acetic acid kit (*KACE-TRM, Megazyme*). Sample preparation was carried out as instructed by the supplier. 2 mg of dAIR biomass was used for each sample. UV-VIS spectrometry was carried out using the *BioTek* Synergy 2 at 340 nm.

Crystalline cellulose determination

Crystalline cellulose content was measured by the Seaman-Updegraff method as described by Foster *et al.*.[98] 2 mg of dAIR biomass were given into a 2 mL screw cap tube and 1 mL Updegraff reagent was added. The mixture was heated to 99 °C and shaken at 900 rpm for 30 min. After cooling, the mixture was centrifuged, and the supernatant was removed. Subsequently the solid was washed once with ultra-pure water and three times with acetone. After removal of the acetone the pellet was left to dry overnight. Then, 175 µL 72% H_2SO_4 were added for Seaman hydrolysis. After 30 min 825 mL H_2O were added. For measurement, the solution was diluted 1:20 and a color reaction was induced by adding 800 mL anthron solution (2 mg/mL). A calibration row was prepared similarly. After reaction for 30 min at 80 °C, light absorption at 625 nm was measured using the *BioTek* Synergy 2 UV-Vis Spectrometer.

TFA hydrolysis of hemicellulose sugars

2 mg of dAIR biomass were mixed with 250 µL 2 M trifluoracetic acid (TFA) and heated at 121 °C for 90 min. After cooling, the sample was centrifuged at 14000 rpm for 5 min. 100 µL of the supernatant were taken off and evaporated. The dried sugars were then diluted in 400 µL ultra-pure water and quantified using ion chromatography (HPAEC-PAD, IC).

High-performance anion exchange chromatography with pulsed amperometric detection (HPAEC-PAD, IC) - Monosaccharide analysis

The composition of monosaccharides and hydrolysates was examined using high-performance anion exchange chromatography with pulsed amperometric detection (HPAEC-PAD, IC). The analysis employed a CarboPac PA20 column (Dionex) with a flow rate of 0.5 mL min^{-1}. Prior to each analysis, the column underwent equilibration with 2 mM NaOH for 10 minutes. Sugar elution began with 2 mM NaOH for 18 min, followed by 550 mM NaOH for 10 min. The column was then cleaned with 800 mM NaOH for 10 min. Monosaccharide quantities were

standardized against an internal reference (2-deoxy-D-glucose) and measured using calibration curves specific to each monosaccharide.

Lignin quantification

Acetyl bromide soluble lignin (ABSL)

The lignin content of biomass was measured using the acetyl bromide method (ABSL) as described by Foster *et al.*.[98] 100 µL of 25% acetyl bromide solution were added to 1 mg of dAIR biomass. For calibration, Kraft lignin purchased at *Sigma-Aldrich* was solved in 25% acetyl bromide solution and treated the same way as the sample. Sample and calibration solution were heated at 50 °C for 2 h and shaken at 300 rpm for 1 h at 50 °C. After cooldown, 400 µL 2 M NaOH and 70 µL 0.5 M hydroxylammonium chloride solution were added and mixed for 10 s. Then 1.43 mL acetic acid were added and mixed for 10 s. The absorption at 280 nm was measured using the *Biotek* Synergy 2 UV/Vis Spectrometer.

Klason lignin (KL)

The lignin content of poplar pulp was measured using the Klason lignin (KL) method. The method was modified from the TAPPI protocol (T222 om-02, Acid-insoluble lignin in wood and pulp). Wood samples were ground to 40-mesh using a Wiley Mill. Samples (~0.150 g) were subjected to acetone extraction by placing them in filter-paper pockets within a Soxhlet apparatus. Extraction was performed with 150 mL acetone at boiling temperature for 8 h. Post extraction, samples were dried at 105 °C. Approximately 0.2 g of the dried sample was placed into serum bottles, and 3 mL of 72% H_2SO_4 was added. Samples were macerated for 2 h at room temperature, followed by dilution with 112 mL deionized water. Sugar controls were prepared to estimate decomposition losses. Samples and controls were autoclaved at 121 °C for 1 h. Hydrolysates were vacuum-filtered through pre-weighed sintered-glass crucibles. The retentate was washed with deionized water, dried at 105 °C, and weighed to determine the acid-insoluble lignin. The filtrates were used for sugar analysis by HPLC and acid-soluble lignin determination via spectrophotometry at 205 nm.

For HPLC, samples and sugar standards (arabinose, rhamnose, galactose, glucose, xylose, mannose) were prepared, and chromatograms obtained under specified conditions (flow rate: 0.8 mL min^{-1}, column: Dionex PA1). Post-column detection was performed via pulsed amperometry using a gold electrode.

Pyrolysis-Gas Chromatography-Mass Spectrometry (Py-GC-MS) Analysis

A Curie point pyrolizer (*Pilodist*) connected to a GC-MS system, comprising a gas chromatograph 7890 and a single quadrupole mass spectrometer 5975C TAD inert XL MSD (*Agilent*), was utilized for lignin sample pyrolysis. Powdered biomass or pulp samples (1–2 mg) were placed in custom-made tubes (0.9 cm length, 1.8 mm inner diameter) constructed from ferromagnetic metal foils (nickel-iron alloy, 0.9 x 0.67 cm, Japan Analytical Industry, TC = 590 °C). The metal tube was closed by pressing with flat pliers, inserted into a glass liner, and positioned in the pyrolizer. Pyrolysis occurred in the glass liner at 590 °C for 10 s. An Optima-5-HT column (60 m x 0.25 mm i.d., 0.25 µm film thickness, *Macherey-Nagel*) was used to separate lignin pyrolysis products. Helium served as the carrier gas with a constant flow of 1.0 ml/min. The GC oven temperature was programmed to increase from 80 °C to 340 °C (held for 20 min) at 5 °C/min. The injector was maintained at 280 °C, and all pyrolysis was conducted in split mode (1:10). The mass spectrometer operated in electron impact (EI, 70 eV) mode, scanning from m/z 30 – 650. The GC interface and ion chamber temperatures were set at 280 °C and 250 °C, respectively. A custom-made C8 – C24 alkane mixture solution was analyzed to improve peak assignment in the pyrolysis chromatograms by calculating Kovat's indices. Data analysis was performed using MassHunter 4.2 software (*Agilent*). Pyrolysis product identification was achieved by comparing mass spectra with those in *NIST* and *Wiley* mass spectral libraries, referencing compounds reported in the literature,[159] and using Kovat's indices.

PAHBAH (4-hydroxybenzoic acid hydrazide) - Quantification of reducing end sugars

The PAHBAH method outlined by Lever[160] was used to measure reducing end sugars in an aqueous hydrolysate. For lignocellulose subjected to phosphoric acid pretreatment, the hydrolysate underwent a 200-fold dilution.

The PAHBAH reagent was created by combining two distinct solutions, labeled A and B. To produce Solution A, 2 mL of 3-hydroxybenzo hydrazide solution (0.25 g/mL, v/v) was mixed with 0.5% HCl. Solution B was prepared by first dissolving 12.45 g of trisodium citrate in 200 mL of water, then adding 20 g of NaOH to 200 mL of water. Subsequently, 1.10 g of $CaCl_2$ was introduced, and the mixture was diluted to a total volume of 1000 mL using water. Both solutions were shielded from light exposure by wrapping them in aluminum foil and were

stored at a temperature of 4 °C. For each set of measurements, a fresh batch of PAHBAH reagent was prepared.

A calibration series was generated using glucose solution (5 mg/mL). 50 µL of sample or calibration dilutions were mixed with 100 µL of PAHBAH reagent and left to react for 10 min at 100 °C and 300 rpm. All the samples were diluted with 850 µL of ultrapure water. The solution was analyzed using a *Biotek* Synergy 2 UV/Vis Spectrometer at 410 nm wavelength.

Nuclear magnetic resonance spectroscopy (NMR) -Furfural and 5-hydroxymethylfurfural

Furfural was quantified from the 2-MTHF phase of the OrganoCat fractionation using ^{1}H-NMR. measurements were conducted on *Bruker* AVANCE 600 MHz NMR spectrometer. 20 µL of sample were dissolved in 0.5 mL of DMSO-d_6. The corresponding aldehyde proton signals of furfural (9.56 ppm, 1H) and 5-hydroxymethylfurfural (9.67 ppm, 1H) were integrated and quantified using mesitylene as internal standard.

^{1}H-^{13}C heteronuclear single quantum correlation nuclear magnetic resonance (^{1}H-^{13}C-HSQC-NMR) spectrometric analysis of biomass and lignin

Both extracted lignin and full biomass were analyzed by ^{1}H-^{13}C heteronuclear single quantum correlation nuclear magnetic resonance (^{1}H-^{13}C-HSQC-NMR). The biomass was prepared according to the protocol of Cheng *et al*.[94] using the following optimized conditions. The plant material (1 g) was ground by a *Retsch* PM 100 planetary ball mill utilizing a 50 mL zirconium dioxide (ZrO_2) vessel containing ZrO_2 ball bearings (10 mm x 10) spinning at 600 rpm with alternating grinding (5 min) and interval breaks (5 min) in a total time of 7 h. 25 mg of biomass were then suspended in 0.75 mL deuterated dimethyl sulfoxide DMSO-d_6 and 10 µL [Emim]OAc were added. The mixture was stirred for 2 h at 60 °C until the biomass dissolved.

For the measurement of extracted lignin, 25-50 mg of the sample were dissolved in 0.75 mL DMSO-d_6.

^{1}H-^{13}C-HSQC NMR measurements were taken on a Bruker AVANCE 600 MHz NMR spectrometer with a Bruker standard pulse sequence “hsqcetgpsisp.2”. The measurement was conducted with a spectral width of 16 ppm in F2 (^{1}H) dimension with 2048 data points (TD1) and 240 ppm in F1 (^{13}C) dimension with 256 data points (TD2), a scan number (SN) of 128, interscan delay (D1) of 1 s, and an acquisition time of 10 h. The chemical shift was referenced

to the solvent DMSO signal ($\delta(^{1}H)$ = 2.500 ppm; $\delta(^{13}C)$ = 39.52 ppm). The signals of monomer units and linkages were integrated and referenced to the lignocellulose structures according to literature.[94] The sum of aromatic units was calculated using the following formula:

$$\Sigma(\text{arom.}) = (S_{2,6} / 2 + G_2) + (H_{2,6} / 2)$$

The percentage of each unit was calculated as

$$S = (S_{2,6}/ 2) / \Sigma(\text{arom.}) * 100\%$$

$$G = (G_2/ \Sigma(\text{arom.}) * 100\%$$

$$H = (H_{2,6} / 2) / \Sigma(\text{arom.}) * 100\%$$

Linkages are given as linkage per 100 monomer units. Due to overlapping peaks, β-*O*-4 is calculated using only the α proton signal. β-β and β-5 linkages are calculated using all signals of the corresponding linkage. Linkages were calculated according to the following formulas:

$$\beta\text{-}O\text{-}4 \text{ linkages} = \alpha\ \beta\text{-}O\text{-}4 / \Sigma(\text{arom.}) * 100\%$$

$$\beta\text{-}\beta \text{ linkages} = (\alpha\ \beta\text{-}\beta + \beta\ \beta\text{-}\beta + \gamma\ \beta\text{-}\beta) / \Sigma(\text{arom.}) * 100\%$$

$$\beta\text{-}5 \text{ linkages} = (\alpha\ \beta\text{-}5 + \beta\ \beta\text{-}5 + \gamma\ \beta\text{-}5) / \Sigma(\text{arom.}) * 100\%$$

Size exclusion chromatography for the determination of molecular weights

Size exclusion chromatography (SEC) was utilized to investigate the molecular size distribution of lignin samples. The analysis was conducted using an *Agilent* Series 1200 SEC instrument equipped with a RID detector (Optilab Rex 837, *Wyatt Technology*) and a SEC column system. This system consisted of a precolumn PSS PolarSil (8 × 50 mm, 5 µm particle size) followed by three PSS PolarSil Linear S columns (8 × 300 mm, 5 µm particle size) arranged in series. The SEC measurements employed N,N-dimethylformamide containing 0.1 M lithium chloride as the eluent, with the column temperature set at 45 °C and a flow rate of 1 mL min^{-1}. Lignin samples were prepared at a concentration of 30 g L^{-1} in the eluent, and 10 µL was injected for analysis. The system was calibrated using the PSS ReadyCal-Kit Poly(styrene) standard, which

covered a molecular weight range from 266 to 66,000 Da, using the same eluent as the lignin samples. The SEC data was processed using PSS WinGPC software.

5.5 Biomass pretreatment

Phosphoric acid (PA) OrganoCat treatment

In the initial swelling phase, 500 mg of plant biomass was combined with 250 µL of 85% phosphoric acid and 250 µL of ultrapure water. This mixture was heated for 1 h at 80 °C in a sealed 25 mL high-pressure reactor, which was subsequently cooled and opened. The fractionation stage involved adding 4.5 mL of ultrapure water and 5 mL of 2-MTHF to the reactor contents. To minimize 2-MTHF evaporation, 10 bar of Argon pressure was applied to the closed stainless-steel high-pressure reactor equipped with a Teflon inlet. The mixture was then stirred continuously while being heated at 140 °C for 3 h. Following cooling and depressurization, the liquid phase was separated via brief centrifugation at 1880 x g for 2 minutes, and the organic phase was extracted using a pipette. Lignin was obtained by evaporating the 2-MTHF and drying completely in an exicator at room temperature for three days. Lignin yield was measured gravimetrically. The aqueous phase underwent filtration to remove the cellulose-enriched pulp. Sugar concentration and composition in the aqueous phase were analyzed using high-performance anion-exchange chromatography with pulsed amperometric detection (HPAEC-PAD). The pulp was dried at 80 °C for 48 h, and biomass mass loss was determined gravimetrically. All lignocellulose fractionation procedures were conducted at least in triplicate.

Phosphoric acid (PA) OrganoCat pretreatment in 1 L reactor

For the scaled-up OrganoCat process with Phosphoric acid (PA) as catalyst, the procedure was modified to omit the swelling step. 20 g of poplar biomass were introduced into a 1 L Parr reactor along with 200 mL 2-MTHF, 190 mL H_2O, and 10 mL 85% phosphoric acid. The reactor was sealed, and the stirring rate was set at 200 rpm. Subsequently, 10 bar of N_2 pressure were applied. The heating process was initiated, and upon reaching 140 °C, the reaction was maintained under stirring conditions for 3 h. Following this period, the heating was discontinued, and the internal cooling system was activated. After 20 minutes of cooling, the stirring was terminated. Once the reaction mixture attained room temperature, the reactor was unsealed. The solid pulp was subsequently isolated by filtration and washed with water

3-4 times. It was then dried at 80 °C for 24 h, and the yield was determined gravimetrically. The liquid phases were separated, and the aqueous phase was subjected to three extractions with 30 mL 2-MTHF to recover residual lignin. The organic phases were combined, and the solvent was removed by evaporation. The lignin was dried under vacuum for 5 h, and the yield was determined gravimetrically.

Processing lignocellulose in the flow through (FT) reactor

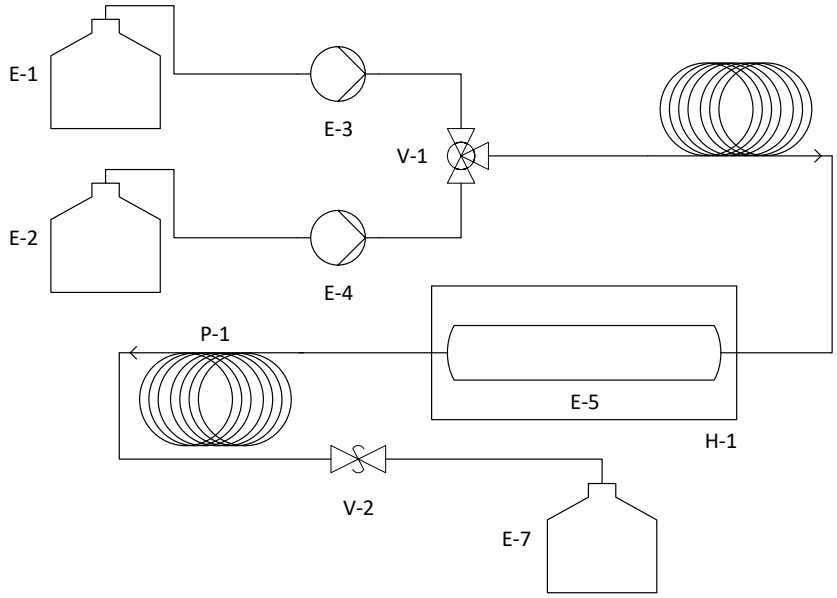

E-1, E-2	solvent bottle 1 and 2
E-3, E-4	pump heads of dosage pump
V-1	t transition piece
E-5	flow through reactor/HPLC-column
H-1	heating block with thermometer sleeve
V-2	high pressure valve (1000 psi / 69 bar)
E-7	collection bottle

The flow through (FT) biomass fractionation system was constructed using a stainless-steel tube reactor with dimensions of 4.6 mm inner diameter and 15 cm length. The reactor was situated within an aluminum heating block (H-1) on a heating plate, with temperature regulation achieved via a thermometer in the block linked to the heating plate. To prevent particle escape, 2 µm pore size stainless-steel frits were positioned at both reactor ends. Solvent bottles (E-1 and E-2) contained 0.1 M aqueous oxalic acid solution and 2-MTHF, which were concurrently transported by a high-pressure dosing pump (C09-20.2-200 DK-VA, *Fink Chem + Tec GmbH*) featuring two independently controlled pulp heads (E-3, E-4) capable of generating up to 200 bar pressure. The solvents were conveyed through 1/16" stainless steel tubing and combined in a T-valve (V-1) connected to the reactor (E-5). Upon exiting the reactor, the solvents passed through a 1/16" stainless steel capillary (P-1) immersed in an ice bath for rapid cooling. The capillary was linked to a backpressure valve (V-2) that maintained a constant reactor pressure of 70 bar, minimizing solvent evaporation when operating above its boiling point. The solvents were ultimately collected in a glass bottle (E-7).

The reactor was loaded with 750-800 mg of beech wood, applying gentle pressure. After connecting the reactor to the solvent supply and positioning it vertically, solvents were simultaneously pumped through until they exited. The reactor was then linked to P-1, and the pump was briefly activated to achieve a final pressure of 70 bar. Following a leak check, the reactor was inserted into the preheated heating block (H-1). Both solvents were immediately pumped at equal rates. Upon reaching the desired process duration, pumping ceased, and the reactor was cooled in an ice bath. The solid pulp was extracted from the tube and rinsed in a filter with 3 × 30 mL of water. A pipette was used to separate the liquid phases. The organic phase underwent oxalic acid removal via precipitation using an equal volume of 0.2 M $CaCl_2$. A rotary evaporator was used to remove the organic phase, the lignin was then vacuum-dried for 24 h. Lignin yields were determined by gravimetric analysis. HPAEC-PAD was utilized to analyze the sugar concentration and composition in the aqueous phase.

Scale up of the FT process

The experimental setup for the larger FT variation was analogous to the previously described configuration. The reactor was substituted with a larger stainless-steel tube measuring 1 cm in inner diameter and 25 cm in length. The reactor was filled with 5.3-6 g of milled biomass. To prevent particle escape, 2 µm pore size stainless-steel frits were positioned at both reactor ends. Following the connection of the reactor to the pump and solvent bottles, the pump was initiated and operated until solvent emerged from the reactor. The pump was subsequently halted, and the capillary leading through the ice bath (P-1) was connected. The pump was restarted, and the system was inspected for leakages upon reaching the desired pressure of 70 bar. Subsequently, the reactor was placed into a suitable aluminum heating block, and the pump was activated. Solvents were collected in E-7. Following the reaction, the pulp and solvents were processed as previously described. Optional preheating of the solvents was achieved by directing the stainless-steel capillaries through an oil bath heated to the process temperature prior to entering the reactor.

5.6 Statistical analysis

Statistical analyses were conducted using *SPSS, IBM Statistics,* v25.0 (2017). For the Pearson correlation analysis and plotting of the graph in Figure 19, *RStudio, Posit Software,* v2023.03.0 was used.

Delignification

The extent of lignin removal from the solid residue was determined as delignification, measured using the ABSL technique.

$$delignification = \left(1 - \frac{AcBr\ lignin\ in\ pulp\ \cdot pulp\ yield}{AcBr\ lignin\ in\ unprocessed\ plant}\right)\%$$

Correlation analysis

Pearson

Pearson correlation coefficients (P) were calculated (with significance value $p < 0.05$) to examine associations between various parameters of unprocessed and extracted biomass and structural features of lignin. The assumption of normality was made as 10 replicated existed for each parameter.

Spearman correlation

Spearman correlation coefficients (ρ) were calculated ($p < 0.05$) for examining the relationships of lignin content and S/G units of unprocessed poplar and extraction yields of poplar fractionation. The assumption of normality was not made as the number of replicates was low.

Principal component analysis (PCA)

A principal component analysis was conducted using all obtained biochemical parameters of the wet chemical analysis of unprocessed biomass and structural parameters of native lignin, normalized data was used. PC1 and PC2 were determined to be sufficient for analysis as they explained 81.6% of variance.

Non-parametric variance analysis: Kurskal wallis test

To determine if there were significant differences in extract yields and lignin characteristics, non-parametric variance analysis was employed using the Kruskal Wallis test ($p < 0.05$).

Design of experiments (DOE)

A 3k factorial Box Behnken design (BBD) was implemented using *Design-Expert* software version 13.0 (*STAT-EASE Inc*.) to assess the effects of three primary independent variables: temperature, process time, and solvent flow rate on solid residue, lignin yield, sugar yield, and β-*O*-4 linkages. The three variables were assigned low (-1), central (0), and high levels. The study comprised 15 experiments, including three replications of the central point to estimate experimental error. The response factors measured were solid residue, lignin yield, and sugar yield (all expressed as wt% of initial biomass), along with β-*O*-4 linkage proportion (per 100 S+G units). To illustrate the interaction between two variables while keeping the third at its midpoint (0), contour graphs were utilized.

6 References

[1] S. Darda, T. Papalas, A. Zabaniotou, Journal of Cleaner Production 2019, 208, 575.

[2] a) P. G. Levi, J. M. Cullen, *Environmental science & technology* **2018**, *52*, 1725; b) IEA - International Energy Agency, *2023*.

[3] European Commission: Directorate-General for Research and Innovation, *A sustainable bioeconomy for Europe – Strengthening the connection between economy, society and the environment – Updated bioeconomy strategy*, Publications Office, **2018**.

[4] M. Antar, D. Lyu, M. Nazari, A. Shah, X. Zhou, D. L. Smith, *Renewable and Sustainable Energy Reviews* **2021**, *139*, 110691.

[5] J. A. Okolie, A. Mukherjee, S. Nanda, A. K. Dalai, J. A. Kozinski, *Intl J of Energy Research* **2021**, *45*, 14145.

[6] F. H. Isikgor, C. R. Becer, *Polym. Chem.* **2015**, *6*, 4497.

[7] M. Margarida Martins, F. Carvalheiro, F. Gírio, *Biomass Conv. Bioref.* **2024**, *14*, 3183.

[8] J. Zhu, L. Chen, C. Cai, *ChemSusChem* **2021**, *14*, 3031.

[9] S. Shrestha, S. Goswami, D. Banerjee, V. Garcia, E. Zhou, C. N. Olmsted, E. L.-W. Majumder, D. Kumar, D. Awasthi, A. Mukhopadhyay et al., *ChemSusChem* **2024**, e202301460.

[10] D. S. Bajwa, G. Pourhashem, A. H. Ullah, S. G. Bajwa, *Industrial Crops and Products* **2019**, *139*, 111526.

[11] a) A. Liszka, R. Wightman, D. Latowski, M. Bourdon, K. B. R. M. Krogh, M. Pietrzykowski, J. J. Lyczakowski, *Frontiers in Plant Science* **2023**, *14*, 1283093; b) J. Y. Zhu, X. Pan, *Renewable and Sustainable Energy Reviews* **2022**, *164*, 112583.

[12] N. Sorek, T. H. Yeats, H. Szemenyei, H. Youngs, C. R. Somerville, *BioScience* **2014**, *64*, 192.

[13] C. Somerville, H. Youngs, C. Taylor, S. C. Davis, S. P. Long, *Science (New York, N.Y.)* **2010**, *329*, 790.

[14] H. Chen in *Biotechnology of lignocellulose*. *Theory and practice* (Ed.: H. Chen), Springer, Dordrecht, **2014**, pp. 25–71.

[15] L. H. Thomas, V. T. Forsyth, A. Martel, I. Grillo, C. M. Altaner, M. C. Jarvis, *Cellulose* **2014**, *21*, 3887.

[16] A. Thygesen, J. Oddershede, H. Lilholt, A. B. Thomsen, K. Ståhl, *Cellulose* **2005**, *12*, 563.

[17] P. E. Marriott, L. D. Gómez, S. J. McQueen-Mason, *The New phytologist* **2016**, *209*, 1366.

[18] J. Rao, Z. Lv, G. Chen, F. Peng, *Progress in Polymer Science* **2023**, *140*, 101675.

[19] R. A. Dixon, J. Barros, *Open biology* **2019**, *9*, 190215.

[20] R.-C. Sun, *ChemSusChem* **2020**, *13*, 4385.

[21] T. J. Simmons, J. C. Mortimer, O. D. Bernardinelli, A.-C. Pöppler, S. P. Brown, E. R. deAzevedo, R. Dupree, P. Dupree, *Nat Commun* **2016**, *7*, 13902.

[22] J. Wang, E. Minami, H. Kawamoto, *J Wood Sci* **2020**, *66*.

[23] A. Kirui, W. Zhao, F. Deligey, H. Yang, X. Kang, F. Mentink-Vigier, T. Wang, *Nature communications* **2022**, *13*, 538.

[24] H. Nishimura, A. Kamiya, T. Nagata, M. Katahira, T. Watanabe, *Scientific reports* **2018**, *8*, 6538.

[25] a) G. Henriksson, M. Lawoko, M. E. E. Martin, G. Gellerstedt, *Holzforschung* **2007**, *61*, 668; b) D. Tarasov, M. Leitch, P. Fatehi, *Biotechnology for biofuels* **2018**, *11*, 269.

[26] a) Y. Pu, F. Hu, F. Huang, B. H. Davison, A. J. Ragauskas, *Biotechnology for biofuels* **2013**, *6*, 15; b) R. B. Melati, F. L. Shimizu, G. Oliveira, F. C. Pagnocca, W. de Souza, C. Sant'Anna, M. Brienzo, *Bioenerg. Res.* **2019**, *12*, 1.

[27]M. E. Bruins, J. P. Sanders, *Biofuels, Bioprod. Bioref.* **2012**, *6*, 135.
[28]a) S. Nanda, R. Azargohar, A. K. Dalai, J. A. Kozinski, *Renewable and Sustainable Energy Reviews* **2015**, *50*, 925; b) S. N. Naik, V. V. Goud, P. K. Rout, A. K. Dalai, *Renewable and Sustainable Energy Reviews* **2010**, *14*, 578.
[29]a) L. D. Quinn, K. C. Straker, J. Guo, S. Kim, S. Thapa, G. Kling, D. K. Lee, T. B. Voigt, *Bioenerg. Res.* **2015**, *8*, 1081; b) P. Yadav, P. Priyanka, D. Kumar, A. Yadav, K. Yadav in *Springer eBooks Energy*, *Vol. 10* (Eds.: A. A. Rastegari, A. N. Yadav, A. Gupta), Springer, Cham, **2019**, pp. 315–335.
[30]D. Tilman, J. Hill, C. Lehman, *Science (New York, N.Y.)* **2006**, *314*, 1598.
[31]C. Nitsos, U. Rova, P. Christakopoulos, *Energies* **2018**, *11*, 50.
[32]L. Penín, M. López, V. Santos, J. L. Alonso, J. C. Parajó, *Bioresource technology* **2020**, *311*, 123528.
[33]M. Budzinski, R. Nitzsche, *Bioresource technology* **2016**, *216*, 613.
[34]V. Larnaudie, M. D. Ferrari, C. Lareo, *Renewable and Sustainable Energy Reviews* **2022**, *158*, 112115.
[35]L. Cumplido-Marin, A. R. Graves, P. J. Burgess, C. Morhart, P. Paris, N. D. Jablonowski, G. Facciotto, M. Bury, R. Martens, M. Nahm, *Agronomy* **2020**, *10*, 928.
[36]A. T. Ubando, C. B. Felix, W.-H. Chen, *Bioresource technology* **2020**, *299*, 122585.
[37]C. S. G. P. Queirós, S. Cardoso, A. Lourenço, J. Ferreira, I. Miranda, M. J. V. Lourenço, H. Pereira, *Biomass Conv. Bioref.* **2020**, *10*, 175.
[38]H.-M. Wang, Y.-C. Sun, B. Wang, D. Sun, Q. Shi, L. Zheng, S.-F. Wang, S.-J. Liu, R.-R. Xia, R.-C. Sun, *ACS Sustainable Chem. Eng.* **2019**, *7*, 13886.
[39]S. Zhou, T. Runge, S. D. Karlen, J. Ralph, E. Gonzales-Vigil, S. D. Mansfield, *ChemSusChem* **2017**, *10*, 3565.
[40]S. D. Mansfield, K.-Y. Kang, C. Chapple, *New Phytologist* **2012**, *194*, 91.
[41]E. M. Anderson, M. L. Stone, R. Katahira, M. Reed, W. Muchero, K. J. Ramirez, G. T. Beckham, Y. Román-Leshkov, *Nature communications* **2019**, *10*, 2033.
[42]P. Azadi, O. R. Inderwildi, R. Farnood, D. A. King, *Renewable and Sustainable Energy Reviews* **2013**, *21*, 506.
[43]B. Saake, R. Lehnen in *Ullmann's encyclopedia of industrial chemistry*, Wiley, Chichester, **2010**, pp. 21–36.
[44]Z. Strassberger, S. Tanase, G. Rothenberg, *RSC Adv* **2014**, *4*, 25310.
[45]a) S. I. Mussatto, G. Dragone, G. J. Rocha, I. C. Roberto, *Carbohydrate Polymers* **2006**, *64*, 22; b) P. Mousavioun, W. Doherty, *Industrial Crops and Products* **2010**, *31*, 52.
[46]S. C. Rabelo, P. Y. S. Nakasu, E. Scopel, M. F. Araújo, L. H. Cardoso, A. C. Da Costa, *Bioresource technology* **2023**, *369*, 128331.
[47]E. K. Pye, J. H. Lora, *Tappi Journal* **1991**, *74*, 113.
[48]T. vom Stein, P. M. Grande, H. Kayser, F. Sibilla, W. Leitner, P. Domínguez de María, *Green Chem.* **2011**, *13*, 1772.
[49]D. Weidener, H. Klose, W. Leitner, U. Schurr, B. Usadel, P. Domínguez de María, P. M. Grande, *ChemSusChem* **2018**, *11*, 2051.
[50]D. Weidener, W. Leitner, P. Domínguez de María, H. Klose, P. M. Grande, *ChemSusChem* **2021**, *14*, 909.
[51]J. Viell, A. Harwardt, J. Seiler, W. Marquardt, *Bioresource technology* **2013**, *150*, 89.
[52]P. M. Grande, J. Viell, N. Theyssen, W. Marquardt, P. Domínguez de María, W. Leitner, *Green Chem.* **2015**, *17*, 3533.

[53]T. M. Wood, K. Bhat in *Methods in Enzymology : Biomass Part A: Cellulose and Hemicellulose*, Academic Press, **1988**, pp. 87–112.
[54]A. Holtz, D. Weidener, W. Leitner, H. Klose, P. M. Grande, A. Jupke, *Separation and Purification Technology* **2020**, *236*, 116295.
[55]T. Damm, P. M. Grande, N. D. Jablonowski, B. Thiele, U. Disko, U. Mann, U. Schurr, W. Leitner, B. Usadel, P. Domínguez de María et al., *Bioresource technology* **2017**, *244*, 889.
[56]D. Weidener, M. Dama, S. K. Dietrich, B. Ohrem, M. Pauly, W. Leitner, P. Domínguez de María, P. M. Grande, H. Klose, *Biotechnol Biofuels* **2020**, *13*.
[57]E. Cooreman, T. Vangeel, K. van Aelst, J. van Aelst, J. Lauwaert, J. W. Thybaut, S. van den Bosch, B. F. Sels, *Ind. Eng. Chem. Res.* **2020**, *59*, 17035.
[58]a) O. Y. Abdelaziz, C. P. Hulteberg, *ChemSusChem* **2020**, *13*, 4382; b) I. Kumaniaev, E. Subbotina, J. Sävmarker, M. Larhed, M. V. Galkin, J. S. M. Samec, *Green Chem.* **2017**, *19*, 5767.
[59]a) O. Bobleter, *Progress in Polymer Science* **1994**, *19*, 797; b) O. Bobleter, G. Bonn, R. Concin, *Institute of Radiochemistry University of Innsbruck, Innsbruck* **1980**, *3*; c) G. Bonn, R. Concin, O. Bobleter, *Wood Sci. Technol.* **1983**, *17*, 195.
[60]S. Bhagia, H. Li, X. Gao, R. Kumar, C. E. Wyman, *Biotechnology for biofuels* **2016**, *9*, 245.
[61]S. Machmudah, W. Wahyudiono, H. Kanda, M. Sasaki, M. Goto, *Eng. J.* **2015**, *19*, 25.
[62]a) E. M. Anderson, M. L. Stone, M. J. Hülsey, G. T. Beckham, Y. Román-Leshkov, *ACS Sustainable Chem. Eng.* **2018**, *6*, 7951; b) E. M. Anderson, M. L. Stone, R. Katahira, M. Reed, G. T. Beckham, Y. Román-Leshkov, *Joule* **2017**, *1*, 613.
[63]D. G. Brandner, J. S. Kruger, N. E. Thornburg, G. G. Facas, J. K. Kenny, R. J. Dreiling, A. R. C. Morais, T. Renders, N. S. Cleveland, R. M. Happs et al., *Green Chem.* **2021**.
[64]J. H. Jang, D. G. Brandner, R. J. Dreiling, A. J. Ringsby, J. R. Bussard, L. M. Stanley, R. M. Happs, A. S. Kovvali, J. I. Cutler, T. Renders et al., *Joule* **2022**, *6*, 1859.
[65]A. Kramarenko, D. Etit, G. Laudadio, F. N. D'Angelo, *ChemSusChem* **2021**, *14*, 3838.
[66]a) H. Zhou, L. Tan, Y. Fu, H. Zhang, N. Liu, M. Qin, Z. Wang, *ChemSusChem* **2019**, *12*, 1213; b) H. Zhou, J. Y. Xu, Y. Fu, H. Zhang, Z. Yuan, M. Qin, Z. Wang, *Green Chem.* **2019**, *21*, 4625; c) J. Xu, Z. Shao, Y. Li, L. Dai, Z. Wang, C. Si, *Industrial Crops and Products* **2021**, *164*, 113350.
[67]H. Zhou, Q. Liu, X. Zhong, Y. Chu, Z. Wang, Y. Wang, *Industrial Crops and Products* **2021**, *173*, 114124.
[68]Z. Wang, S. Qiu, K. Hirth, J. Cheng, J. Wen, N. Li, Y. Fang, X. Pan, J. Y. Zhu, *ACS Sustainable Chem. Eng.* **2019**, *7*, 10808.
[69]C. Cai, N. Li, H. Liu, J. Zhang, J. Y. Zhu, F. Wang, *Chemical Engineering Journal* **2023**, *453*, 139730.
[70]a) D. S. Zijlstra, C. W. Lahive, C. A. Analbers, M. B. Figueirêdo, Z. Wang, C. S. Lancefield, P. J. Deuss, *ACS Sustainable Chem. Eng.* **2020**, *8*, 5119; b) D. S. Zijlstra, C. A. Analbers, J. de Korte, E. Wilbers, P. J. Deuss, *Polymers* **2019**, *11*, 1913.
[71]A. T. Smit, M. Hoek, P. A. Bonouvrie, A. van Zomeren, L. A. Riddell, P. C. A. Bruijnincx, *ACS Sustainable Chem. Eng.* **2024**.
[72]A. Rahimi, A. Ulbrich, J. J. Coon, S. S. Stahl, *Nature* **2014**, *515*, 249.
[73]A. J. Ragauskas.
[74]T. Aro, P. Fatehi, *ChemSusChem* **2017**, *10*, 1861.
[75]G. J. Giardino, H. Wang, J. Niu, D. Wang, *Chemical Physics Reviews* **2024**, *5*.

[76]a) W. Schutyser, T. Renders, S. van den Bosch, S.-F. Koelewijn, G. T. Beckham, B. F. Sels, *Chemical Society reviews* **2018**, *47*, 852; b) H. Wang, M. Tucker, Y. Ji, *Journal of Applied Chemistry* **2013**, *2013*, 1.
[77]A. Boarino, H.-A. Klok, *Biomacromolecules* **2023**, *24*, 1065.
[78]O. Yu, K. H. Kim, *Applied Sciences* **2020**, *10*, 4626.
[79]X. Wu, J. Jiang, C. Wang, J. Liu, Y. Pu, A. Ragauskas, S. Li, B. Yang, *Biofuels, Bioprod. Bioref.* **2020**.
[80]D. A. Baker, T. G. Rials, *J. Appl. Polym. Sci.* **2013**, *130*, 713.
[81]W. Fang, S. Yang, X.-L. Wang, T.-Q. Yuan, R.-C. Sun, *Green Chem.* **2017**, *19*, 1794.
[82]M. Lallave, J. Bedia, R. Ruiz-Rosas, J. Rodríguez-Mirasol, T. Cordero, J. C. Otero, M. Marquez, A. Barrero, I. G. Loscertales, *Adv. Mater.* **2007**, *19*, 4292.
[83]I. Dallmeyer, F. Ko, J. F. Kadla, *Ind. Eng. Chem. Res.* **2014**, *53*, 2697.
[84]W. E. Tenhaeff, O. Rios, K. More, M. A. McGuire, *Adv. Funct. Mater.* **2014**, *24*, 86.
[85]Q. Cao, Y. Zhang, J. Chen, M. Zhu, C. Yang, H. Guo, Y. Song, Y. Li, J. Zhou, *Industrial Crops and Products* **2020**, *148*, 112181.
[86]M. Parot, D. Rodrigue, T. Stevanovic, *ACS Sustainable Chem. Eng.* **2023**, *11*, 607.
[87]B. Du, H. Zhu, L. Chai, J. Cheng, X. Wang, X. Chen, J. Zhou, R.-C. Sun, *Industrial Crops and Products* **2021**, *170*, 113745.
[88]L. García-Fuentevilla, J. F. Rubio-Valle, R. Martín-Sampedro, C. Valencia, M. E. Eugenio, D. Ibarra, *International journal of biological macromolecules* **2022**, *214*, 554.
[89]J. Yang, Y. C. Ching, C. H. Chuah, *Polymers* **2019**, *11*.
[90]a) N. D. Jablonowski, M. Pauly, M. Dama, *Frontiers in Plant Science* **2021**, *12*, 767254; b) N. Brosse, A. Dufour, X. Meng, Q. Sun, A. Ragauskas, *Biofuels, Bioprod. Bioref.* **2012**, *6*, 580.
[91]Siwek, Włodarczyk, Możdżer, Bury, Kitczak, *Applied Sciences* **2019**, *9*, 4016.
[92]N. D. Jablonowski, T. Kollmann, M. Nabel, T. Damm, H. Klose, M. Müller, M. Bläsing, S. Seebold, S. Krafft, I. Kuperjans et al., *GCB Bioenergy* **2017**, *9*, 202.
[93]a) M. Choudhary, A. Singh, M. Gupta, S. Rakshit, *Biofuels, Bioprod. Bioref.* **2020**, *14*, 402; b) B. M. Tofacina, *Cellulose Chem. Technol.* **2019**, *53*, 837.
[94]K. Cheng, H. Sorek, H. Zimmermann, D. E. Wemmer, M. Pauly, *Analytical chemistry* **2013**, *85*, 3213.
[95]Y.-H. P. Zhang, J. Cui, L. R. Lynd, L. R. Kuang, *Biomacromolecules* **2006**, *7*, 644.
[96]P. Klímek, P. Meinlschmidt, R. Wimmer, B. Plinke, A. Schirp, *Industrial Crops and Products* **2016**, *92*, 157.
[97]J. Rumpf, X. T. Do, R. Burger, Y. B. Monakhova, M. Schulze, *Biomacromolecules* **2020**, *21*, 1929.
[98]C. E. Foster, T. M. Martin, M. Pauly, *JoVE* **2010**.
[99]Z. Gong, L. Shuai, *Trends in Chemistry* **2023**, *5*, 163.
[100] J. Ralph, C. Lapierre, W. Boerjan, *Current opinion in biotechnology* **2019**, *56*, 240.
[101] a) H. Kim, D. Padmakshan, Y. Li, J. Rencoret, R. D. Hatfield, J. Ralph, *Biomacromolecules* **2017**, *18*, 4184; b) T. Zhang, S. Zhang, W. Lan, F. Yue, *Journal of Renewable Materials* **2023**, *11*, 555.
[102] J. V. Vermaas, M. F. Crowley, G. T. Beckham, *ACS Sustainable Chem. Eng.* **2020**, *8*, 17839.
[103] D. Vural, J. C. Smith, L. Petridis, *Green Chem.* **2020**, *22*, 4331.
[104] H. Kawamoto, *J Wood Sci* **2017**, *63*, 117.

[105] H. Kawamoto, T. Watanabe, S. Saka, *Journal of Analytical and Applied Pyrolysis* **2015**, *113*, 630.
[106] M. Akazawa, Y. Kojima, Y. Kato, *Journal of Analytical and Applied Pyrolysis* **2016**, *118*, 164.
[107] S. Kim, S. C. Chmely, M. R. Nimlos, Y. J. Bomble, T. D. Foust, R. S. Paton, G. T. Beckham, *J. Phys. Chem. Lett.* **2011**, *2*, 2846.
[108] E. Bartolomei, Y. Le Brech, A. Dufour, V. Carre, F. Aubriet, E. Terrell, M. Garcia-Perez, P. Arnoux, *ChemSusChem* **2020**, *13*, 4633.
[109] G. van Meer, D. R. Voelker, G. W. Feigenson, *Nat Rev Mol Cell Biol* **2008**, *9*, 112.
[110] G. Kowalska, U. Pankiewicz, R. Kowalski, *Agriculture* **2020**, *10*, 132.
[111] R. Vanholme, B. Demedts, K. Morreel, J. Ralph, W. Boerjan, *Plant Physiol.* **2010**, *153*, 895.
[112] M. Nar, H. R. Rizvi, R. A. Dixon, F. Chen, A. Kovalcik, N. D'Souza, *Carbon* **2016**, *103*, 372.
[113] B. M. Upton, A. M. Kasko, *Chemical reviews* **2016**, *116*, 2275.
[114] A. D. McKown, J. Klápště, R. D. Guy, A. Geraldes, I. Porth, J. Hannemann, M. Friedmann, W. Muchero, G. A. Tuskan, J. Ehlting et al., *New Phytologist* **2014**, *203*, 535.
[115] L. Rosso, S. Cantamessa, S. Bergante, C. Biselli, A. Fricano, P. M. Chiarabaglio, M. Gennaro, G. Nervo, F. Secchi, A. Carra, *Life* **2023**, *13*, 533.
[116] Y. Zhang, T. Culhaoglu, B. Pollet, C. Melin, D. Denoue, Y. Barrière, S. Baumberger, V. Méchin, *Journal of agricultural and food chemistry* **2011**, *59*, 10129.
[117] M. H. Studer, J. D. DeMartini, M. F. Davis, R. W. Sykes, B. Davison, M. Keller, G. A. Tuskan, C. E. Wyman, *Proceedings of the National Academy of Sciences of the United States of America* **2011**, *108*, 6300.
[118] X. Li, E. Ximenes, Y. Kim, M. Slininger, R. Meilan, M. Ladisch, C. Chapple, *Biotechnology for biofuels* **2010**, *3*, 27.
[119] A. M. Johnson, H. Kim, J. Ralph, S. D. Mansfield, *Biotechnology for biofuels* **2017**, *10*, 48.
[120] I. Porth, J. Klápště, O. Skyba, B. S. K. Lai, A. Geraldes, W. Muchero, G. A. Tuskan, C. J. Douglas, Y. A. El-Kassaby, S. D. Mansfield, *The New phytologist* **2013**, *197*, 777.
[121] A. R. Robinson, S. D. Mansfield, *The Plant journal : for cell and molecular biology* **2009**, *58*, 706.
[122] D. Weidener, A. Holtz, H. Klose, A. Jupke, W. Leitner, P. M. Grande, *Molecules* **2020**, *25*, 3330.
[123] M. Li, Y. Pu, A. J. Ragauskas, *Frontiers in chemistry* **2016**, *4*, 45.
[124] J. Martinez Diaz, P. M. Grande, H. Klose, *Front. Chem. Eng.* **2023**, *5*.
[125] J. Martinez Diaz, P. M. Grande, H. Klose, *Industrial Crops and Products* **2024**, *222*, 119820.
[126] K. Wang, H. Yang, X. Yao, F. Xu, R.-C. Sun, *Bioresource technology* **2012**, *116*, 99.
[127] J.-H. Choi, S.-M. Cho, J.-C. Kim, S.-W. Park, Y.-M. Cho, B. Koo, H. W. Kwak, I.-G. Choi, *ACS omega* **2021**, *6*, 1534.
[128] M. Culebras, M. J. Sanchis, A. Beaucamp, M. Carsí, B. K. Kandola, A. R. Horrocks, G. Panzetti, C. Birkinshaw, M. N. Collins, *Green Chem.* **2018**, *20*, 4461.
[129] Dennis Weidener, RWTH Aachen, Aachen, **2021**.
[130] Mehmet Sefik Tunc, Juben Chheda, Evert van der Heide, Jerry Morris, Adriaan van Heiningen, *Holzforschung* **2014**, *68*, 401.
[131] X. Zhou, Q. Li, C. Hong, *J. Phys.: Conf. Ser.* **2021**, *2009*, 12042.

[132] L. Schoofs, D. Weidener, U. Schurr, H. Klose, P. M. Grande, *Journal of visualized experiments : JoVE* **2021**.
[133] K. Takabe, S. Miyauchi, R. Tsunoda, K. Fukazawa, *IAWA J* **1992**, *13*, 105.
[134] X. Li, Y. Xia, X. Hu, Q. Liu, W. Li, L. Yan, L. Ma, *Industrial Crops and Products* **2023**, *201*, 116896.
[135] a) E. I. Evstigneyev, S. M. Shevchenko, *Wood Sci Technol* **2019**, *53*, 7; b) E. I. Evstigneyev, A. V. Kalugina, A. Y. Ivanov, A. V. Vasilyev, *Journal of Wood Chemistry and Technology* **2017**, *37*, 294.
[136] A. Kirui, W. Zhao, F. Deligey, H. Yang, X. Kang, F. Mentink-Vigier, T. Wang, *Nat Commun* **2022**, *13*, 538.
[137] A. M. Johnson, H. Kim, J. Ralph, S. D. Mansfield, *Biotechnology for biofuels* **2017**, *10*, 48.
[138] S. Willför, A. Sundberg, A. Pranovich, B. Holmbom, *Wood Sci Technol* **2005**, *39*, 601.
[139] V. Lionetti, F. Francocci, S. Ferrari, C. Volpi, D. Bellincampi, R. Galletti, R. D'Ovidio, G. de Lorenzo, F. Cervone, *Proc. Natl. Acad. Sci. U.S.A.* **2010**, *107*, 616.
[140] Jerrold Everett Winandy, *WFS* **2017**, *49*, 2.
[141] D. Mohnen, *Current Opinion in Plant Biology* **2008**, *11*, 266.
[142] J. S. Kim, G. Daniel, *Trees* **2018**, *32*, 393.
[143] J. Schäfer, M. Sattler, Y. Iqbal, I. Lewandowski, M. Bunzel, *GCB Bioenergy* **2019**, *11*, 191.
[144] A. P. de Souza, C. L. Alvim Kamei, A. F. Torres, S. Pattathil, M. G. Hahn, L. M. Trindade, M. S. Buckeridge, *Journal of experimental botany* **2015**, *66*, 4351.
[145] R. M. F. Da Costa, S. Pattathil, U. Avci, S. J. Lee, S. P. Hazen, A. Winters, M. G. Hahn, M. Bosch, *New Phytologist* **2017**, *213*, 1710.
[146] J. Vogel, *Current Opinion in Plant Biology* **2008**, *11*, 301.
[147] K. H. Caffall, D. Mohnen, *Carbohydrate Research* **2009**, *344*, 1879.
[148] X. Kang, A. Kirui, M. C. Dickwella Widanage, F. Mentink-Vigier, D. J. Cosgrove, T. Wang, *Nat Commun* **2019**, *10*, 1.
[149] J. D. DeMartini, S. Pattathil, J. S. Miller, H. Li, M. G. Hahn, C. E. Wyman, *Energy Environ. Sci.* **2013**, *6*, 898.
[150] E. Svinterikos, I. Zuburtikudis, M. Al-Marzouqi, *ACS Sustainable Chem. Eng.* **2020**, *8*, 13868.
[151] M. Cho, L. Ji, L.-Y. Liu, A. M. Johnson, S. Potter, S. D. Mansfield, S. Renneckar, *Industrial Crops and Products* **2020**, *155*, 112833.
[152] B. Sun, Y.-Z. Long, F. Yu, M.-M. Li, H.-D. Zhang, W.-J. Li, T.-X. Xu, *Nanoscale* **2012**, *4*, 2134.
[153] a) B. Bessaire, M. Mathieu, V. Salles, T. Yeghoyan, C. Celle, J.-P. Simonato, A. Brioude, *ACS applied materials & interfaces* **2017**, *9*, 950; b) A. Laforgue, L. Robitaille, A. Mokrini, A. Ajji, *Macromol. Mater. Eng.* **2007**, *292*, 1229.
[154] J. Xue, T. Wu, Y. Dai, Y. Xia, *Chemical reviews* **2019**, *119*, 5298.
[155] T. Kishimoto, W. Chiba, K. Saito, K. Fukushima, Y. Uraki, M. Ubukata, *Journal of agricultural and food chemistry* **2010**, *58*, 895.
[156] R. Zhang, Q. Du, L. Wang, Z. Zheng, L. Guo, X. Zhang, X. Yang, H. Yu, *Green Chem.* **2019**, *21*, 4981.
[157] D. Weidener, H. Klose, W. Graf von Westarp, A. Jupke, W. Leitner, P. Domínguez de María, P. M. Grande, *Green Chem.* **2021**, *23*, 6330.
[158] Q. Li, S. Xie, W. K. Serem, M. T. Naik, L. Liu, J. S. Yuan, *Green Chem.* **2017**, *19*, 1628.

[159] R. D. Hatfield, H.-J. G. Jung, J. Ralph, D. R. Buxton, P. J. Weimer, *J. Sci. Food Agric.* **1994**, *65*, 51.

[160] a) M. Lever, *Analytical Biochemistry* **1972**, *47*, 273; b) M. Lever, *Analytical Biochemistry* **1977**, *81*, 21.

7 List of Figures and Tabels

Figure index

FIGURE 1: SCHEMATIC DEPICTION OF THE STRUCTURE OF LIGNOCELLULOSE AS FOUND IN THE PLANT CELL WALL WITH EXAMPLES OF THE MOLECULAR STRUCTURES OF ITS COMPONENTS..... 3
FIGURE 2: EXAMPLE STRUCTURES OF THE MOST COMMON HEMICELLULOSE STRUCTURES FOUND IN HARDWOODS AND *GRAMINEAE* (GRASS) CELL WALLS..... 5
FIGURE 3: CHEMICAL STRUCTURE OF THE THREE MAIN SUBUNITS OF LIGNIN: CONFERYL ALCOHOL, SYNAPYL ALCOHOL, AND *P*-COUMARYL ALCOHOL..... 5
FIGURE 4: EXAMPLE STRUCTURE OF A SMALL LIGNIN MOLECULE WITH THE THREE MOST COMMONLY FOUND LINKAGES. THE LINKAGES ARE B-ARYL ETHER (B-*O*-4), PHENYLCOUMARAN (B-5), AND RESINOL (B-B)..... 7
FIGURE 5: MODEL OF CELLULOSE, HEMICELLULOSE, AND LIGNIN INTERACTIONS IN HARDWOODS AND GRASSES. ADAPTED FROM KIRUI *ET AL.*.[23]..... 8
FIGURE 6: SCHEMATIC DEPICTION OF THE ORGANOCAT PROCESS. OXALIC ACID,[48] 2-5-FURANDYCARBOXYLIC ACID,[49] AND PHOSPHORIC ACID[50] HAVE BEEN ESTABLISHED AS ORGANIC CATALYSTS. 2-METHYLTETRAHYDROFURAN (2-MTHF) IS USED AS ORGANIC SOLVENT..... 12
FIGURE 7: RECALCITRANCE FACTORS OF LIGNIN PROPERTIES ON BIOMASS CELL WALL FRACTIONATION, ADAPTED FROM RAGAUSKAS *ET AL.*.[73] 17
FIGURE 8: SCHEMATIC HIERARCHY OF LIGNIN APPLICATIONS FROM LOW TO HIGH VALUES. ADAPTED FROM MARGARIDA MARTINS *ET AL.*.[7]..... 18
FIGURE 9: SCHEMATIC OF BASIC ELECTROSPINNING SETUP..... 20
FIGURE 10: PRINCIPAL COMPONENT ANALYSIS (PCA) OF NORMALIZED UNPROCESSED BIOMASS DATA. INCLUDED DATA: ALCOHOL SOLUBLE COMPONENTS, STARCH, CRYSTALLINE CELLULOSE, ABSL LIGNIN, HEMICELLULOSE SUGAR CONTENT, AND ACETYLATION. 27
FIGURE 11: FRACTIONATION YIELDS AFTER PA ORGANOCAT PROCESSING. THE SOLID RESIDUE AND LIGNIN CONTENT WERE DETERMINED GRAVIMETRICALLY AFTER DRYING. THE HYDROLYZED SUGAR CONCENTRATION WAS MEASURED USING HPAEC-PAD AND EXTRAPOLATED TO THE TOTAL YIELD. FURFURAL CONCENTRATION WAS MEASURED IN ^{1}H-NMR AND SIMILARLY CALCULATED TO REPRESENT THE TOTAL YIELD. ALL YIELDS ARE GIVEN IN WT% OF THE UNPROCESSED BIOMASS. 29
FIGURE 12: WET CHEMICAL ANALYSIS RESULTS OF SOLID RESIDUE IN COMPARISON WITH THE COMPOSITIONAL ANALYSIS OF THE UNPROCESSED MATERIAL. THE PULP RESULTS WERE ADJUSTED TO THE CORRESPONDING YIELDS FOR DIRECT COMPARISON. 31
FIGURE 13: PARTIAL 2D HSQC-NMR SPECTRA OF WHOLE CELL WALL (A AND D), PULP (B AND E), AND LIGNIN AFTER ORGANOCAT EXTRACTION (C AND F) OF MAIZE. THE TOP THREE SPECTRA: RELEVANT LIGNIN ALIPHATIC REGION (Δ_H = 4.0 – 5.5 PPM, Δ_C = 65 – 90 PPM). THE BOTTOM THREE SPECTRA: LIGNIN AROMATIC REGION (Δ_H = 6.0 – 8.0 PPM, Δ_C = 100 - 140 PPM).. 33
FIGURE 14: A: MONOMER COMPOSITION [%] DETERMINED BY HSQC-NMR ANALYSIS OF UNPROCESSED MAIZE, MAIZE PULP, AND EXTRACTED MAIZE LIGNIN. B: PROPORTIONS OF B-*O*-4, B-B, AND B-5 LINKAGES PER 100 S + G UNITS DETERMINED BY HSQC-NMR ANALYSIS OF UNPROCESSED MAIZE, MAIZE PULP, AND EXTRACTED MAIZE LIGNIN..... 34
FIGURE 15: HEATMAP OF THE RELATIVE PROPORTIONS OF PY-GC-MS COMPONENTS IN UNTREATED BIOMASS AND EXTRACTED LIGNIN. THE FULL DATASET CAN BE FOUND IN APPENDIX 8.4..... 37
FIGURE 16: SEC CHROMATOGRAM OF PA ORGANOCAT BEECH LIGNIN, A: DRIED ORGANIC EXTRACT, B: AFTER RE-SOLVING WITH ACETONE AND PRECIPITATION IN WATER..... 41
FIGURE 17: SEC CHROMATOGRAM OF PA ORGANOCAT MAIZE LIGNIN, THREE TECHNICAL REPLICATES. 41
FIGURE 18: SEC CHROMATOGRAMS OF PA ORGANOCAT LIGNIN FROM EUCALYPTUS, WALNUT SHELLS, SIDA, SZARVASI, MISCANTHUS, BAGASSE, SILPHIUM, AND RAPESEED. 41
FIGURE 19: A: SCHEMATIC REPRESENTATION OF PEARSON CORRELATION BETWEEN DELIGNIFICATION AND LIGNIN CHARACTERISTICS BEFORE AND AFTER PROCESSING MEASURED BY HSQC-NMR. THE FULL DATASET CAN BE FOUND IN APPENDIX 8.5. B: ABOVE: GRAPHICAL REPRESENTATION OF THE CORRELATION BETWEEN B-*O*-4 LINKAGES OF EXTRACTED LIGNIN AND DELIGNIFICATION. BELOW: GRAPHICAL REPRESENTATION OF THE CORRELATION BETWEEN B-B LINKAGES AND MOLECULAR WEIGHT M_N. 43
FIGURE 20: COMPARISON OF SOLID RESIDUE AND LIGNIN CONTENT OF UNPROCESSED BIOMASS. AVERAGE DATA POINTS WERE USED FOR SPEARMAN CORRELATION WHEN REPETITIONS WERE PRESENT. 51
FIGURE 21: COMPARISON OF THE RESIDUAL LIGNIN CONTENT IN PULP TO THE LIGNIN CONTENT AND S/G RATIO OF UNPROCESSED POPLAR SAMPLES, UTILIZING AVERAGE DATA POINTS WERE USED FOR SPEARMAN CORRELATION WHEN REPETITIONS WERE PRESENT. 52
FIGURE 22: HSQC-NMR SPECTRA OF LIGNIN EXTRACTED FROM ALAA20-1. THE LIGNIN WAS REDISSOLVED IN ACETONE AND PRECIPITATED IN WATER TO REMOVE IMPURITIES PRIOR TO THE MEASUREMENT. 53

Figure 23: DSC graph of lignin of YALE27-3, dried organic extract..... 55
Figure 25: DSC graph of precipitated lignin of YALE27-3..... 55
Figure 26: Picture of the flow through OrganoCat setup. 59
Figure 27: Relative composition of hemicellulose sugars in beech wood (TFA fraction) and hydrolyzed sugars in the aqueous phase after flow through OrganoCat of beech wood at 160 °C for 60 min at 0.2 mL/min.... 61
Figure 28: Scheme of the center points used in the box Behnken design. 64
Figure 29: a) Maximum and minimum yields of the flow through process (FT) with beech wood and yields of a comparable batch process with beech wood. Oxalic acid was used as the catalyst for all process variations. Maximum FT yield reaction conditions: 180 °C, 90 min, 0.2 mL/min. Batch reaction conditions: 140 °C, 60 min, 0.1 mL/min. b) FT experiments with highest and lowest resulting b-*O*-4 linkage proportion in extracted lignin. Maximum b-*O*-4 reaction conditions: 140 °C, 30 min, 0.2 mL/min. Minimum b-O-4 reaction conditions:180 °C, 60 min, 0.1 mL/min. Batch reaction conditions:140 °C, 3 h..... 68
Figure 30: 2D contour models of the RSM for solid residue produced by design expert. The relationship between the two factors is shown in each graph, while the other factor was maintained at a constant level. 70
Figure 31: 2D contour models of the RSM for lignin yield produced by design expert. The relationship between the two factors is shown in each graph, while the other factor was maintained at a constant level. 71
Figure 32: 2D contour models of the RSM for sugar yield produced by design expert. The relationship between the two factors is shown in each graph, while the other factor was maintained *at a constant level.* 72
Figure 33:Predicted vs actual plot for the data measured in the BBD for b-*O*-4 linkages and the corresponding model. 73
Figure 34: 2D contour models of the RSM for b-O-4 linkages produced by design expert. The relationship between the two factors is shown in each graph, while the other factor was maintained at a constant level. . 73
Figure 35: Lignin and sugar yields per fraction of the flow-through process at different temperatures. Samples were collected for 5 min each, and the sugar yield was determined by measuring the sugar concentration in the aqueous phase using ion chromatography. Triplicate experiments were performed for 140 °C and 160 °C 0-90 min and 180 °C 0-60 min, for 180 °C 60-90 min the average of two experiments is shown..... 77
Figure 36: A: Cumulative lignin yield of the flow-through process at different temperatures. B: Cumulative sugar yield during the FT process. Sugar yield was determined by measuring the sugar concentration in the aqueous phase using HPAEC-PAD. Samples were collected for 5 min each. Triplicate experiments were performed for 140 °C and 160 °C 0-90 min and 180 °C 0-60 min, for 180 °C 60-90 min the average of two experiments is shown. 78
Figure 37: Amount of monosaccharides in aqueous sample of FT OrganoCat processing at 140 °C, 160 °C and 180 °C of beech wood. The samples were collected for 5 min each. Experiments were conducted in triplicates; std. deriv. is not shown for better visibility. The full dataset including standard derivations can be found in Appendix 8.7..... 85
Figure 38: Flow through OrganoCat yield of hydrolyzed sugars per 1 min fraction. The sugar concentrations were analyzed using HPAEC-PAD. Three experiments at 160 °C with a flow rate of 0.2 ml/min were performed and are shown individually. 1.a.-c.) first experiment; 2.a.-c.) second experiment; 3.a.-c.) third experiment. For better visibility sugars were divided into separate graphs by yield. a.) glucose, xylose, galacturonic acid; b) arabinose, galactose, glucuronic acid; c) fucose, rhamnose, mannose. 91
Figure 39: Right: Comparison of beech and miscanthus flow though OrganoCat extraction yields of lignin and sugar per 5 min fraction. The experiments were performed at 160 °C, with a flow rate of 0.2 mL/min. Experiments were conducted in triplicates. Left: Biomass composition determined by wet chemical analysis for comparison. 93
Figure 40: Comparison of sugar extraction from beech and miscanthus using the FT OrganoCat at 160 °C and a solvent flow rate of 0.2 mL/min. Amount of monosaccharides in liquid samples. Samples were collected for 5 min. Experiments conducted in triplicates. The full dataset and standard derivations are shown in Appendix 8.8..... 95
Figure 41: Electrospinning of poplar lignin. A vertical setup was used for electrospinning 50wt% poplar OrganoCat lignin in DMF with the addition of 5 wt% PEO. 100
Figure 42: Above: Pictures of the coaxial electrospinning of 55 wt% walnut shell OrganoCat lignin in THF. Voltage: 20 kV; distance: 150 mm; flow rate (lignin):10 µL/min; flow rate (THF):15 µL/min. Below: Scanning electron microscope (SEM) pictures of the fibers. 103
Figure 43: Above: Pictures of the coaxial electrospinning of 55 wt% eucalyptus OrganoCat lignin in THF. Voltage: 25 kV; distance: 205 mm; flow rate (lignin):20 µL/min; flow rate (THF):10 µL/min. Below: Scanning electron microscope (SEM) pictures of the fibers. 104

Figure 44: Electrospinning of miscanthus OrganoCat lignin (50 wt% in MTHF). The spinning conditions were set as follows: voltage, 25 kV; distance, 220 mm; flow rate (lignin) 20 µL/min; flow rate (2-MTHF) 5 µL/min. Right: Electrospinning on aluminum foil, left electrospinning on a paper-covered collector. 104
Figure 45: Pictures of the standard 25 mL autoclave used at FZJ (left) and the large 1 L autoclave at UBC (right). 111
Figure 46: Flow chart of the analytical steps included in the wet chemical analysis. 112

Table index

Table 1: Overview of plant biomass materials used for inter-species comparisons. 24
Table 2: Composition of selected plant biomass determined by wet chemical analysis. Lignin content, acetylation, crystalline cellulose, and hemicellulose sugar were determined after extraction of the alcohol soluble components and destarching. Results of those measurements are calculated to represent the percentage of full biomass weight. All experiments were conducted in triplicates, standard derivation is given in brackets. Data is sorted by lignin content. 25
Table 3: Composition of hemicellulose sugars after TFA hydrolysis determined by high-performance anion exchange chromatography with pulsed amperometric detection (HPAEC-PAD). Sorted by xylose yield. Values are expressed as a percentage of total biomass weight. 26
Table 4: HSQC-NMR analysis of lignin in unprocessed biomass 26
Table 5: Monomer unit composition [%] (Syringyl S, guaiacyl G, *p*-hydroxyphenyl H) for the ten selected plant species determined by HSQC-NMR. Measurements of the extracted lignin were conducted for a minimum of three technical repetitions, and the averages are shown with standard deviations in brackets. 34
Table 6: Monomer unit composition [%] (Syringyl, Guaiacyl, *p*-hydroxyphenyl) for the ten selected plant species determined by Py-GC-Ms. 36
Table 7: S/G ratios of lignin in unprocessed material and in extracted lignin. Comparison of the HSQC-NMR and Py-GC-MS results. 36
Table 8: Proportion of ether (b-*O*-4), resinol (b-b,) and phenylcoumaran (b-5) linkage proportion in unprocessed biomass and extracted lignin, per 100 S+G units measured by HSQC-NMR- For the extracted lignin, three technical replicates were measured. Averages are given with standard derivation in brackets. 39
Table 9: SEC chromatography data for weight average (M_w) and number average (M_n) molecular mass of extracted lignin and polydispersity index (PDI). 42
Table 10: Selection of nine poplar accessions characterized by contrasting chemotypic properties, specifically focusing on total lignin content (including soluble and Klason lignin (insoluble), KL) and the S/G ratio was determined by thioacidolysis.[121] The data, originally obtained by Porth *et al.* and previously published[120], provides the foundation for the selection process. 48
Table 11: Fractionation yields after upscaled PA OrganoCat without swelling using selected poplar samples. Solid residue and lignin yield were determined gravimetrically after drying, residue (insoluble) lignin in pulp was determined using the Klason method. Delignification was calculated using the quotient of lignin in the biomass and pulp yield-corrected residue of lignin in the pulp 50
Table 12: S/G ratios of unprocessed samples determined by thioacyoilysis; b-*O*-4, b-b, b-5 linkages of extracted lignin; H, G, and S units of extracted lignin; S/G of extracted lignin, all determined by HSQC-NMR. Ppt = samples precipitated for cleanup. 54
Table 13: Glass transition temperatures of dried organic extract (raw lignin) and lignin redissolved in acetone and then precipitated in water. Lignin content and S/G ratio of unprocessed poplar samples for comparison. 56
Table 14: Repetition series of experiments at 160 °C, 60 min, 0.2 mL/min. Average of three experiments, standard derivation given in brackets. *Lignin and pulp yield were determined gravimetrically, given in % of biomass used. The xylose yield was determined using PAHBAH, and the yield of total hemicellulose sugar was determined using ion chromatography of the aqueous phase. Lignin characteristics such as* b-*O*-4, b-b, and b-5 linkages, as well as the S/G ratio, were determined using HSQC-NMR and linkages given in linkages per 100 S+G units. Lignin linkages are given per 100 S+G units. The previously determined composition of the unprocessed beech wood is given for direct comparison. 59
Table 15: Modified Flow-through process experiments omitting a key factor. Yields are given as percentages of the initial biomass. 62
Table 16: Furfural quantification experiments. Flow through OrganoCat at 180 °C, process time 60 min. Furfural and 5-hydroxymethylfurfural (5-HMF) were quantified by ^{1}H-NMR of the organic phase using mesitylene as internal standard. 63
Table 17: Factors chosen for Box Behnken design in design expert. 65
Table 18: Full set of reaction conditions for the Box Behnken DOE experiments. Solvent volume and biomass loading are given for comparison of the results. 65
Table 19: Yields of flow through OrganoCat DOE experiments relative to the initial biomass. Xylose yield was determined by PAHBAH using xylose as an internal standard. Total sugar yield was determined from HPAEC-PAD of the aqueous phase. Linkages and S/G ratio analysis are the results of the HSQC-NMR analysis of the yielded lignin. 66
Table 20: Statistical parameters from the analysis of variance (ANOVA) for selected models. 69

TABLE 21: CODED EQUATION (HIGH LEVELS +1, LOW LEVELS -1) WITH INDEPENDENT VARIABLES A (TIME), B (TEMPERATURE), AND C (FLOW RATE). 69
TABLE 22: YIELDS OF THE FLOW THROUGH ORGANOCAT SCALE UP WITH AND WITHOUT SOLVENT PREHEATING. BEECH, 0.1 M OXALIC ACID, 1.3 ML/MIN, 160 °C. 75
TABLE 23: SOLID RESIDUE COMPARISON, UNPROCESSED, PROCESSED AT 160 °C AFTER 20 MIN AND AFTER 90 MIN. WET CHEMICAL ANALYSIS RELATIVE TO INITIAL BIOMASS 80
TABLE 24: AVERAGE VALUES FOR LINKAGE PROPORTION AND S/G RATIO IN LIGNIN EXTRACTED WITHIN THE FIRST 20 MIN VS. EXTRACTED IN MINUTE 20-90. ALL EXPERIMENTS WERE CONDUCTED IN TRIPLICATES BESIDES 160 °C, WHICH IS A DUPLICATE. STANDARD DERIVATION IN BRACKETS. 82
TABLE 25: CUMULATIVE YIELD OF SUGARS AFTER 90 MIN OF THE FT ORGANOCAT TAKING 5 MIN FRACTIONS. SUGARS WERE QUANTIFIED FROM THE AQUEOUS PHASE USING HPAEC-PAD. COMPOSITION OF THE SUGARS IN UNTREATED BEECH FOR COMPARISON. 86
TABLE 26: LIGNIN LINKAGES AND MONOMER UNITS OF BEECH AND MISCANTHUS AT 160 °C EARLY (0-20 MIN) AND LATE (20-90 MIN) IN THE FRACTIONATION, ANALYZED BY HSQC-NMR. TRIPLICATE EXPERIMENTS WERE PERFORMED FOR MISCANTHUS FT PROCESSING, STANDARD DERIVATION IN BRACKETS. DUPLICATE EXPERIMENTS WERE PERFORMED FOR BEECH PROCESSING, AVERAGES ARE SHOWN. FOR COMPARISON, THE HSQC-NMR RESULTS FOR THE UNPROCESSED BIOMASS (0 MIN) ARE SHOWN. 93
TABLE 27: COMPARISON OF CUMULATIVE SUGAR YIELD OF FT ORGANOCAT EXTRACTION OF MISCANTHUS AND BEECH AFTER 90 MIN AT 160 °C, ANALYZED BY HPAEC-PAD. EXTRACTION EXPERIMENTS WERE PERFORMED IN TRIPLICATES; AVERAGES ARE GIVEN WITH STANDARD DERIVATION IN BRACKETS. THE SUGAR COMPOSITION OF UNPROCESSED MISCANTHUS AND BEECH DETERMINED BY HPAEC-PAD OF THE TFA HYDROLYSATE IS PROVIDED FOR COMPARISON. 96
TABLE 28: LIGNIN STRUCTURE OF SELECTED ORGANOCAT LIGNINS FOR ELECTROSPINNING. S/G MONOMER RATIO AND B-*O*-4 LINKAGE PROPORTION DETERMINED BY HSQC-NMR ANALYSIS. MOLECULAR WEIGHT M_w AND POLYDISPERSITY INDEX (PDI) WERE DETERMINED USING SEC. 101

8 Appendix

8.1 Principal component analysis

Rotated component Matrix

Rotated Component Matrix[a]

	Component		
	1	2	3
alc soluble untreated biomass	-,867	-,324	-,344
starch untreated biomass	-,966		
crystalline cellulose untreated biomass	,902	,130	,165
AcBr lignin untreated biomass	,956	,220	
IC total sugar untreated biomass	,727	-,557	
acetic acid untreated biomas	,682	,666	
S/G ratio HSQC-NMR untreated biomass		,893	-,296
beta-O-4 linkage proportion untreated biomass	,178	,953	,195
beta-beta proportion untreated biomass		,971	,152
beta-5 proportion untreated biomass	,124		,985

Extraction Method: Principal Component Analysis.
Rotation Method: Varimax with Kaiser Normalization.

a. Rotation converged in 4 iterations.

Dendrogram for cluster identification

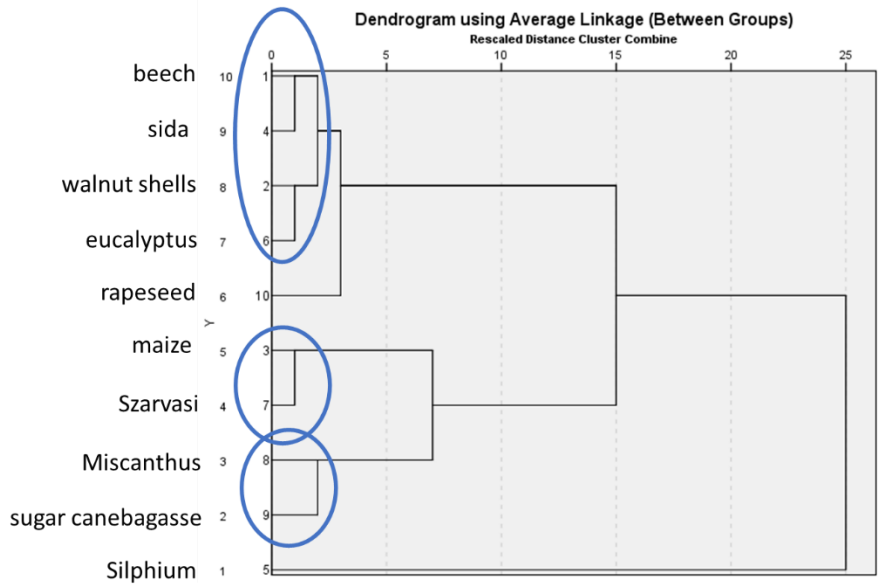

8.2 Sugar composition, biomass material screening

Unprocessed material, TFA hydrolysis with HPAEC-PAC

[wt% of untreated biomass], average of three technical replicates

	Fuc	Rha	Ara	Glc	Glu	Xyl	Man	GlcA	GluA
beech	0.0	0.4	0.4	0.6	2.1	17.4	0.8	1.0	0.0
eucalyptus	0.0	0.2	0.1	0.3	2.6	10.2	0.5	0.8	0.0
walnut shells	0.0	0.2	0.2	0.4	0.4	13.6	0.0	0.7	0.0
sida	0.1	0.4	0.4	0.5	1.4	12.5	0.8	1.5	0.1
silphium	0.1	0.5	1.7	1.7	1.1	9.0	1.0	3.2	0.3
szarvazi	0.0	0.0	2.4	0.3	0.9	19.5	0.9	0.2	0.1
miscanthus	0.0	0.0	1.9	1.1	2.1	19.7	0.0	0.3	0.0
sugar cane bagasse	0.0	0.0	1.8	0.3	2.3	20.0	0.0	0.3	0.0
rapeseed	0.1	0.3	0.5	0.5	0.5	10.0	0.6	0.9	0.2
maize	0.0	0.0	3.2	0.7	2.6	21.0	1.1	0.3	0.2

OrganoCat processing, HPAEC-PAD of aqueous phase

[wt% of untreated biomass], average of three technical replicates

	Rha	Ara	Glc	Glu	Xyl	Man	GlcA	GluA
beech	0.4	1.4	1.4	5.8	20.7	1.1	0.0	0.0
eucalyptus	0.3	0.5	1.8	2.8	9.4	0.4	0.0	0.0
walnut shells	0.6	1.4	2.7	5.5	22.6	0.0	0.0	0.0
sida	1.1	1.6	1.5	6.0	12.8	1.6	0.0	0.0
silphium	0.5	2.3	2.9	6.6	3.6	1.1	0.0	0.0
szarvasi	0.0	1.6	0.5	6.0	15.1	0.0	0.0	0.1
miscanthus	0.0	1.1	0.3	2.0	16.2	0.0	0.0	0.1
sugar cane bagasse	0.0	1.4	0.6	4.1	15.8	0.0	0.0	0.1
rapeseed	0.5	0.8	2.7	3.6	20.5	0.0	0.5	0.3
maize	3.0	0.8	1.4	49.7	13.1	0.5	0.1	0.1

8.3 Additional HSQC-NMR Spectra

Silphium – aliphatic area

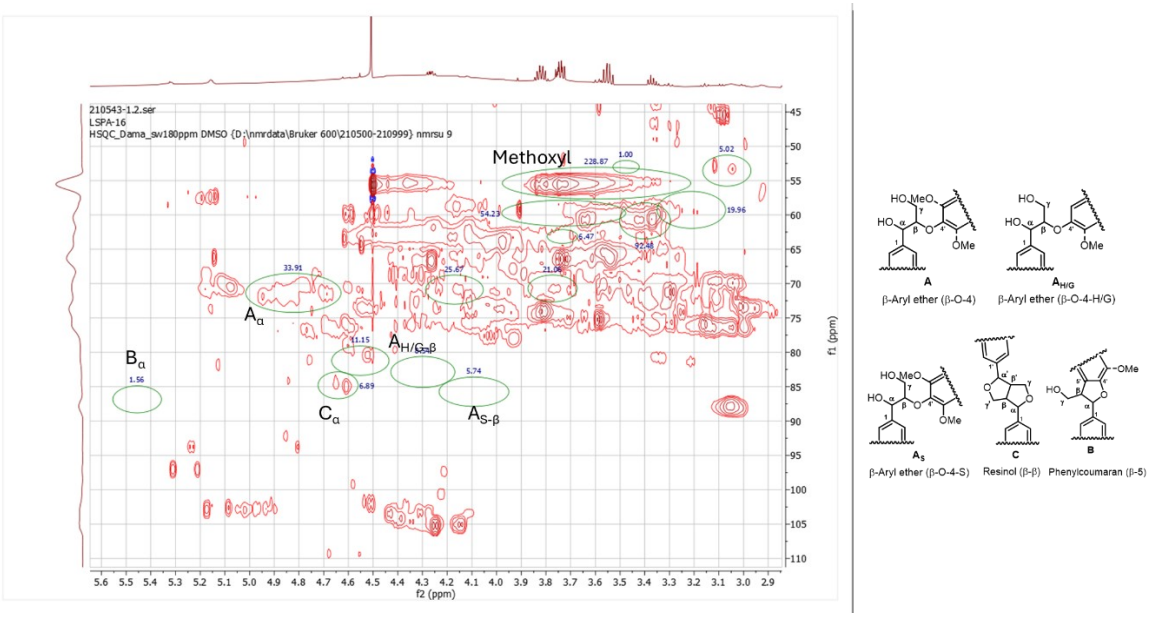

Silphium – aromatic area

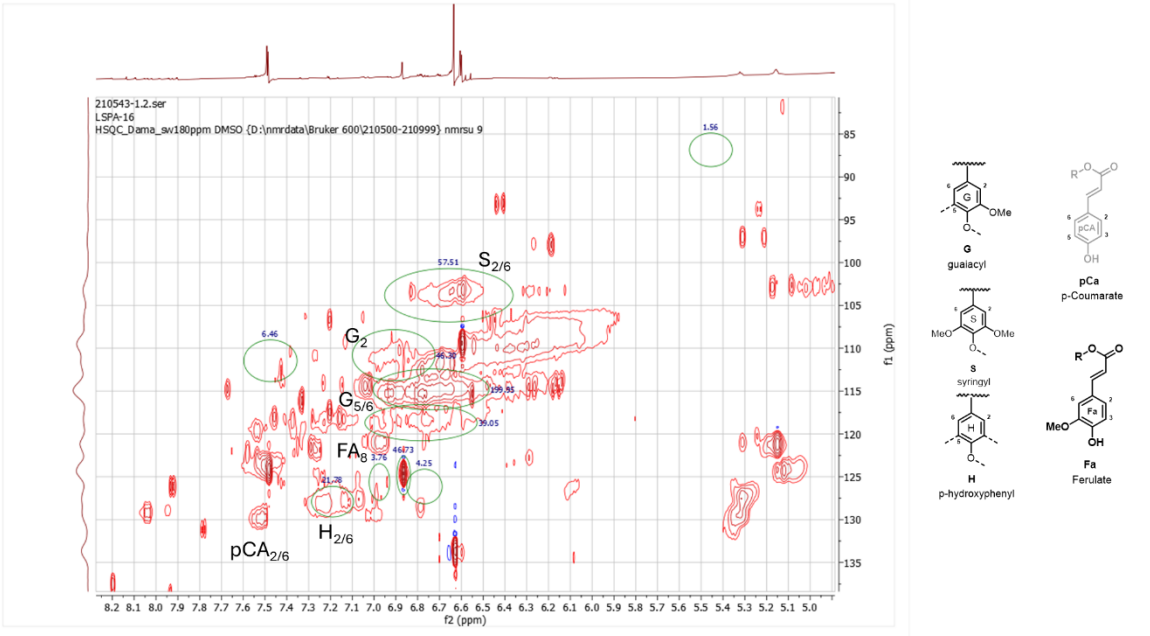

8.4 Py-GC-MS

Untreated biomass

Relative quantity of components measured in Py-GC-MS of native biomass.

Compound		beech [%]	walnut shells [%]	Sida [%]	Szarvasi [%]	Miscanthus [%]	Eucalyptus [%]	Bagasse [%]	Rapeseed [%]	Silphium [%]	Maize [%]
Guaiacol	G	5.7	6.7	10.6	10.0	9.1	4.7	5.7	9.6	6.5	8.1
4-Methylguaiacol	G	4.5	5.3	3.5	4.8	4.4	5.1	4.5	4.6	1.8	2.9
3-Methoxycatechol	G	3.0	3.4	2.4	2.1	2.2	3.9	3.1	2.1	0.9	2.1
4-Ethylguaiacol	G	2.2	2.1	2.5	3.6	2.7	2.3	2.6	2.2	2.1	2.6
4-Vinylguaiacol	G	7.0	6.7	12.1	22.5	13.7	6.4	11.4	11.7	8.7	18.6
Eugenol	G	1.1	1.5	0.8	0.7	0.9	1.2	0.5	1.2	0.5	0.3
4-Propylguaiacol	G	0.6	0.7	0.6	0.5	0.5	0.6	0.4	0.6	0.3	0.3
Vanillin	G	2.4	3.9	1.9	2.2	2.9	2.4	2.4	3.1	0.8	2.4
(Z)-Isoeugenol	G	0.7	1.0	0.7	0.5	0.6	0.8	0.3	0.8	0.4	0.3
(E)-Isoeugenol	G	4.9	5.3	4.3	3.4	3.6	4.7	2.2	5.6	2.3	1.6
Acetovanillone	G	1.6	2.3	1.1	0.8	1.0	1.5	0.9	1.8	0.6	0.5
Guaiacylacetone	G	1.5	1.9	2.1	1.9	1.8	1.4	1.2	2.0	1.0	0.9
(E)-Coniferyl_aldehyde	G	0.2	1.2	0.6	0.1	0.6	0.1	0.3	1.5	0.0	0.1
(E)-Ferulic_acid_methylester	G	0.0	0.1	0.0	0.3	0.3	0.0	0.3	0.1	0.0	0.2
Phenol	H	0.5	2.3	2.2	2.8	3.3	0.5	3.2	1.5	14.5	4.2
o-Cresol	H	0.2	0.5	0.8	0.5	0.8	0.2	0.3	0.5	1.8	0.7
m/p-Cresol	H	0.3	1.5	1.2	1.4	1.7	0.4	1.7	1.0	4.1	1.7
Xylenol	H	0.2	0.7	0.9	1.5	2.2	0.2	3.0	0.5	3.4	2.2
Catechol	H	3.7	3.5	5.2	6.8	5.1	3.7	4.0	3.0	16.0	6.5
4-Vinylphenol	H	0.1	0.9	2.9	13.1	18.1	0.1	25.0	0.4	10.9	23.8
Syringol	S	10.5	9.8	10.3	5.8	7.3	10.6	7.1	9.7	5.5	6.8
4-Methylsyringol	S	5.1	4.6	2.4	1.6	2.0	5.3	3.2	3.0	1.2	1.3
4-Ethylsyringol	S	3.6	3.2	2.9	1.3	1.2	3.8	1.8	2.2	1.9	0.8
4-Vinylsyringol	S	13.1	8.0	13.7	4.8	4.6	12.1	3.1	13.2	7.4	3.7
4-Allylsyringol	S	2.6	2.1	1.1	0.5	0.8	3.3	0.9	1.4	0.6	0.4
(Z)-4-Propenylsyringol	S	1.7	1.5	0.8	0.3	0.6	2.0	0.6	1.0	0.6	0.4
Syringaldehyde	S	4.0	4.3	2.0	0.5	1.3	3.3	1.2	3.6	0.6	0.6
(E)-4-Propenylsyringol	S	9.7	6.6	5.1	2.3	3.3	9.9	4.1	6.3	3.2	2.7
Acetosyringon	S	4.0	4.1	1.6	2.0	1.5	4.2	2.1	2.6	0.9	1.9
Syringyl_acetone	S	3.7	2.8	3.0	1.0	1.4	3.3	1.9	2.6	1.5	0.9
Propiosyringon	S	1.8	1.6	0.5	0.3	0.6	1.7	0.9	0.7	0.3	0.4

Organic extract

Relative quantity of components measured in Py-GC-MS of extracted lignin.

Compound		beech [%]	walnut [%]	sida [%]	szarvasi [%]	miscanthus [%]	eucalyptus [%]	sugar cane bagasse [%]	rapeseed [%]	silphium [%]	maize [%]
Guaiacol	G	13.1	18.5	18.4	20.3	15.8	14.3	10.3	15.0	6.6	14.9
4-Methylguaiacol	G	2.9	2.3	2.1	2.8	2.5	1.6	2.0	3.8	1.3	1.1
3-Methoxycatechol	G	7.2	7.2	5.6	1.7	3.2	7.7	3.0	5.7	1.3	1.2
4-Ethylguaiacol	G	2.6	1.8	3.2	6.8	5.3	1.7	4.8	2.7	4.3	5.5
4-Vinylguaiacol	G	1.5	0.5	2.2	7.1	4.9	0.9	4.5	3.2	3.8	8.0
Eugenol	G	0.7	0.3	0.6	0.1	0.5	0.5	0.2	0.5	0.4	0.1
4-Propylguaiacol	G	0.4	0.3	0.5	0.2	0.3	0.2	0.1	0.2	0.1	0.1
Vanillin	G	0.3	0.5	0.4	1.3	0.7	0.6	0.8	1.7	0.5	2.0
(Z)-Isoeugenol	G	0.2	0.1	0.2	0.1	0.1	0.1	0.1	0.2	0.0	0.0
(E)-Isoeugenol	G	0.7	0.4	0.7	0.3	0.5	0.4	0.2	0.8	0.3	0.2
Acetovanillone	G	1.6	1.4	1.5	1.6	1.6	1.3	1.4	1.8	0.6	1.1
Guaiacylacetone	G	8.4	9.4	10.0	5.3	5.6	7.9	3.3	11.4	3.9	2.9
(E)-Coniferyl_aldehyde	G	0.0	0.0	0.0	0.0	0.0	0.0	0.0	0.0	0.0	0.0
(E)-Ferulic_acid_methylester	G	0.0	0.0	0.1	0.1	0.2	0.0	0.1	0.0	0.0	0.1
Phenol	H	1.7	7.6	7.5	16.0	13.5	0.8	17.8	3.2	27.9	21.8
o-Cresol	H	0.5	0.6	0.4	2.2	0.9	0.1	1.2	0.5	1.3	1.3
m/p-Cresol	H	1.2	2.7	1.1	5.2	1.9	1.4	2.9	1.2	5.4	4.0
Xylenol	H	0.4	0.5	3.6	6.1	8.7	0.1	11.1	0.8	8.2	8.2
Catechol	H	3.5	4.6	3.8	6.2	3.9	2.2	2.7	4.4	9.2	3.3
4-Vinylphenol	H	0.1	0.1	2.5	3.2	8.3	0.1	9.9	0.3	8.3	10.1
Syringol	S	15.9	19.0	12.8	4.9	7.2	21.1	6.9	11.2	3.8	4.8
4-Methylsyringol	S	2.6	1.7	1.2	0.4	0.8	2.3	1.1	2.2	0.7	0.2
4-Ethylsyringol	S	2.4	3.0	1.3	0.6	0.7	2.0	0.9	1.6	0.9	0.4
4-Vinylsyringol	S	0.6	0.2	0.3	0.3	0.2	0.1	0.5	2.1	0.9	0.4
4-Allylsyringol	S	1.0	0.3	0.5	0.0	0.2	0.8	0.2	0.6	0.1	0.0
(Z)-4-Propenylsyringol	S	0.2	0.1	0.1	0.0	0.1	0.1	0.1	0.2	0.1	0.0
Syringaldehyde	S	0.1	0.1	0.0	0.1	0.0	0.3	0.4	0.5	0.0	0.1
(E)-4-Propenylsyringol	S	0.9	0.2	0.5	0.1	0.2	0.5	0.3	0.7	0.3	0.1
Acetosyringon	S	4.7	1.9	2.1	0.9	1.3	4.4	1.3	2.5	0.5	0.6
Syringyl_acetone	S	16.1	11.7	13.5	4.7	7.7	17.4	8.3	15.2	6.9	4.9
Propiosyringon	S	8.7	3.0	3.5	1.3	3.2	9.2	3.7	5.7	2.2	2.6

Pearson correlation coefficients for Py-GC-MS components which change >5% during processing, lignin content in untreated biomass and pulp and delignification.

	Guaiacol	4-Vinyl-guaiacol	Phenol	Catechol	4-Vinyl-phenol	Syringol
Guaiacol	1.000					
4-Vinylguaiacol	0.866*	1.000				
Phenol	-0.079	0.085	1.000			
Catechol	-0.364	-0.315	0.852*	1.000		
4-Vinylphenol	0.203	0.574	0.229	-0.210	1.000	
Syringol	-0.342	-0.626	-0.603	-0.336	-0.503	1.000
4-Methylsyringol	-0.437	-0.591	-0.587	-0.269	-0.493	0.889*
4-Vinylsyringol	-0.287	-0.668	-0.424	0.030	-0.827*	0.723
(E)-4-Propenylsyringol	-0.484	-0.671	-0.680	-0.266	-0.704*	0.650
Syringyl acetone	-0.165	-0.316	-0.298	-0.056	-0.537	-0.012
ABSL lignin in pulp	-0.218	-0.500	-0.721*	-0.397	-0.466	0.857*
ABSL lignin in biomass	-0.117	-0.248	-0.799*	-0.654	-0.142	0.670
delignification	-0.027	-0.032	-0.722*	-0.726*	0.106	0.430

*significant ($p < 0.05$)

	4-Methyl-syringol	4-Vinyl-syringol	(E)-4-Propenylsyringol	Syringyl acetone	ABSL lignin in pulp	ABSL lignin in biomass	Delignification
Guaiacol							
4-Vinylguaiacol							
Phenol							
Catechol							
4-Vinylphenol							
Syringol							
4-Methylsyringol	1.000						
4-Vinylsyringol	0.579	1.000					
(E)-4-Propenyl-syringol	0.706*	0.707	1.000				
Syringyl acetone	-0.082	0.425	0.628	1.000			
ABSL lignin in pulp	0.844*	0.685	0.666	0.040	1.000		
ABSL lignin in biomass	0.711*	0.325	0.543	0.023	0.860	1.000	
delignification	0.502	0.020	0.368	0.007	0.621	0.934	1.000

*significant ($p < 0.05$)

8.5 Correlations between lignin parameters

Pearson coefficient data for selected lignin parameters.

	Solid residue	delignification	S/G raw	β-*O*-4 raw	β-β raw	Lignin in pulp	Lignin yield
Solid residue	1.000	-0.398	0.344	0.094	0.416	0.814*	-0.244
delignification		1.000	-0.620	-0.419	-0.826*	-0.217	0.261
S/G raw			1.000	0.666*	0.790*	0.231	-0.144
β-*O*-4 raw				1.000	0.709*	-0.081	-0.283
β-β raw					1.000	0.205	-0.379
Lignin in pulp						1.000	-0.200
Lignin yield							1.000

*significant ($p < 0.05$)

	Sugar yield	S/G extracted	β-*O*-4 extracted	β-β extracted	M_w	M_n	PDI
Solid residue	-0.464	0.696*	-0.838*	-0.071	-0.069	0.065	-0.049
delignification	0.048	-0.586	0.840*	-0.791*	0.746*	0.404	-0.046
S/G raw	-0.184	0.799*	-0.289	0.552	-0.508	-0.144	-0.245
β-*O*-4 raw	-0.466	0.469	0.100	0.773*	-0.683*	-0.520	0.214
β-β raw	-0.355	0.710*	-0.465	0.766	-0.738*	-0.571	0.177
Lignin in pulp	0.014	0.567	-0.841*	-0.386	0.366	0.411	-0.114
Lignin yield	0.024	-0.118	0.278	-0.107	0.166	0.526	-0.785*
Sugar yield	1.000	-0.249	0.050	-0.410	0.543	0.459	-0.045
S/G extracted		1.000	-0.634*	0.387	-0.385	-0.029	-0.123
β-*O*-4 extracted			1.000	0.119	-0.063	-0.116	0.000
β-β extracted				1.000	-0.954*	-0.750*	0.240
M_w					1.000	0.809*	-0.265
M_n						1.000	-0.696*
PDI							1.000

*significant ($p < 0.05$)

8.6 Full ANOVA for DOE

Solid residue

Source	Sum of Squares	df	Mean Square	F-value	*p*-value	
Model	1125.28	3	375.09	47.07	< 0.0001	significant
A-Time	118.89	1	118.89	14.92	0.0026	
B-Temperature	976.82	1	976.82	122.58	< 0.0001	
C-flow rate	29.57	1	29.57	3.71	0.0803	
Residual	87.66	11	7.97			
Lack of Fit	76.31	9	8.48	1.49	0.4640	not significant
Pure Error	11.34	2	5.67			
Cor Total	1212.93	14				

Lignin yield

Source	Sum of Squares	df	Mean Square	F-value	*p*-value	
Model	146.08	9	16.23	32.61	0.0006	significant
A-Time	41.72	1	41.72	83.84	0.0003	
B-Temperature	80.45	1	80.45	161.66	< 0.0001	
C-flow rate	11.71	1	11.71	23.53	0.0047	
AB	0.0110	1	0.0110	0.0222	0.8875	
AC	2.62	1	2.62	5.27	0.0701	
BC	1.46	1	1.46	2.94	0.1470	
A^2	0.0702	1	0.0702	0.1411	0.7226	
B^2	0.4975	1	0.4975	0.9997	0.3633	
C^2	7.24	1	7.24	14.55	0.0124	
Residual	2.49	5	0.4977			
Lack of Fit	0.3491	3	0.1164	0.1088	0.9474	not significant
Pure Error	2.14	2	1.07			
Cor Total	148.57	14				

Sugar yield

Source	Sum of Squares	df	Mean Square	F-value	*p*-value	
Model	1320.77	3	440.26	26.94	< 0.0001	significant
A-Time	78.44	1	78.44	4.80	0.0509	
B-Temperature	1241.27	1	1241.27	75.97	< 0.0001	
C-flow rate	1.07	1	1.07	0.0652	0.8031	
Residual	179.74	11	16.34			
Lack of Fit	165.93	9	18.44	2.67	0.3021	not significant
Pure Error	13.81	2	6.90			
Cor Total	1500.51	14				

β-*O*-4 linkages

Source	Sum of Squares	df	Mean Square	F-value	*p*-value	
Model	138.41	4	34.60	6.30	0.0085	significant
A-Time	7.68	1	7.68	1.40	0.2644	
B-Temperature	38.72	1	38.72	7.05	0.0241	
C-flow rate	48.71	1	48.71	8.86	0.0139	
AB	43.30	1	43.30	7.88	0.0186	
Residual	54.95	10	5.50			
Lack of Fit	51.33	8	6.42	3.55	0.2385	not significant
Pure Error	3.62	2	1.81			
Cor Total	193.36	14				

8.7 Time resolved sugar yields, beech

140 °C, average yield per fraction [mg per 1000 mg initial biomass]

t [min]	Fuc	Rha	Ara	Gal	Glc	Xyl	Man	GalA	GlcA
5	0.07	0.02	1.79	0.54	5.16	1.24	0.44	1.20	0.56
10	0.06	0.41	1.91	0.88	1.31	3.40	0.44	4.68	1.86
15	0.00	0.29	0.55	0.82	0.57	5.33	0.74	5.22	1.77
20	0.00	0.18	0.13	0.55	0.36	5.20	0.66	3.91	1.07
25	0.00	0.12	0.07	0.37	0.20	5.80	0.56	2.76	0.66
30	0.00	0.08	0.06	0.28	0.21	5.53	0.58	2.08	0.45
35	0.00	0.05	0.03	0.22	0.18	4.33	0.53	1.61	0.31
40	0.00	0.03	0.03	0.13	0.18	3.21	0.47	1.32	0.25
45	0.00	0.02	0.02	0.13	0.14	2.51	0.31	1.06	0.18
50	0.00	0.01	0.02	0.11	0.16	2.29	0.29	0.92	0.15
55	0.00	0.01	0.02	0.11	0.17	2.16	0.29	0.95	0.16
60	0.00	0.01	0.02	0.09	0.16	1.97	0.25	0.84	0.14
65	0.00	0.01	0.02	0.08	0.15	1.60	0.19	0.68	0.12
70	0.00	0.01	0.02	0.07	0.15	1.49	0.19	0.60	0.12
75	0.00	0.01	0.01	0.05	0.13	1.23	0.08	0.52	0.10
80	0.00	0.00	0.01	0.05	0.13	1.25	0.09	0.47	0.10
85	0.00	0.00	0.01	0.04	0.12	1.05	0.03	0.42	0.08
90	0.00	0.00	0.01	0.03	0.12	0.91	0.06	0.36	0.08

140 °C, std. deriv. [mg per 1000 mg initial biomass]

t [min]	Fuc	Rha	Ara	Gal	Glc	Xyl	Man	GalA	GlcA
5	0.06	0.03	0.99	0.29	1.01	0.46	0.05	0.76	0.37
10	0.01	0.12	0.61	0.31	0.28	1.51	0.42	2.29	0.78
15	0.00	0.09	0.18	0.07	0.21	1.56	0.54	1.63	0.37
20	0.00	0.15	0.09	0.03	0.12	1.24	0.49	1.00	0.02
25	0.00	0.08	0.05	0.03	0.03	0.69	0.39	0.63	0.04
30	0.00	0.03	0.03	0.02	0.03	1.12	0.01	0.32	0.05
35	0.00	0.03	0.03	0.02	0.01	0.79	0.12	0.25	0.05
40	0.00	0.03	0.02	0.09	0.02	0.85	0.09	0.21	0.05
45	0.00	0.02	0.02	0.02	0.01	0.82	0.07	0.10	0.04
50	0.00	0.02	0.02	0.02	0.03	0.83	0.07	0.12	0.03
55	0.00	0.01	0.02	0.01	0.02	0.51	0.06	0.17	0.02
60	0.00	0.02	0.02	0.03	0.01	0.59	0.07	0.05	0.04
65	0.00	0.01	0.01	0.02	0.02	0.39	0.03	0.18	0.03
70	0.00	0.01	0.02	0.03	0.01	0.53	0.05	0.07	0.03
75	0.00	0.01	0.01	0.02	0.02	0.33	0.06	0.14	0.03
80	0.00	0.00	0.01	0.02	0.01	0.44	0.07	0.14	0.03
85	0.00	0.00	0.01	0.02	0.02	0.31	0.04	0.09	0.02
90	0.00	0.00	0.01	0.02	0.03	0.29	0.05	0.07	0.02

160 °C, average yield per fraction [mg per 1000 mg initial biomass]

t [min]	Fuc	Rha	Ara	Gal	Glc	Xyl	Man	GalA	GlcA
5	0.10	0.94	3.63	1.80	8.96	7.36	1.54	6.89	1.88
10	0.03	1.03	1.62	2.77	2.98	27.80	3.91	10.87	1.69
15	0.00	0.44	0.54	1.25	1.57	17.29	2.76	5.99	0.67
20	0.00	0.15	0.39	0.58	1.32	11.77	1.76	2.90	0.35
25	0.00	0.17	0.41	0.17	0.88	5.77	0.98	1.55	0.23
30	0.00	0.04	0.03	0.13	0.80	3.34	0.47	1.15	0.12
35	0.00	0.02	0.02	0.08	0.67	2.84	0.32	0.65	0.11
40	0.00	0.00	0.02	0.06	0.71	2.23	0.27	0.49	0.08
45	0.00	0.00	0.01	0.04	0.62	1.74	0.22	0.36	0.06
50	0.00	0.00	0.01	0.03	0.83	1.72	0.18	0.29	0.05
55	0.00	0.00	0.00	0.02	0.63	1.30	0.13	0.24	0.04
60	0.00	0.00	0.01	0.02	0.73	1.32	0.14	0.25	0.05
65	0.00	0.00	0.00	0.02	0.76	1.19	0.13	0.22	0.05
70	0.00	0.00	0.00	0.02	0.65	0.96	0.08	0.18	0.04
75	0.00	0.00	0.01	0.02	0.66	0.87	0.08	0.16	0.04
80	0.00	0.00	0.00	0.01	0.70	0.87	0.07	0.17	0.04
85	0.00	0.00	0.00	0.01	0.66	0.73	0.01	0.12	0.03
90	0.00	0.00	0.00	0.01	0.63	0.62	0.06	0.11	0.03

160 °C, std. deriv. [mg per 1000 mg initial biomass]

t [min]	Fuc	Rha	Ara	Gal	Glc	Xyl	Man	GalA	GlcA
5	0.08	0.44	0.90	0.46	2.06	1.67	0.72	4.81	0.76
10	0.03	0.36	0.34	0.56	0.86	7.29	1.78	8.32	0.78
15	0.00	0.17	0.53	0.35	0.66	2.70	1.52	4.84	0.08
20	0.00	0.11	0.51	0.21	0.58	3.53	0.61	2.09	0.18
25	0.00	0.19	0.53	0.09	0.32	0.64	0.62	0.88	0.13
30	0.00	0.02	0.02	0.10	0.32	0.73	0.24	0.66	0.04
35	0.00	0.01	0.02	0.06	0.32	0.83	0.23	0.40	0.06
40	0.00	0.00	0.02	0.04	0.35	0.42	0.18	0.31	0.04
45	0.00	0.00	0.01	0.04	0.28	0.39	0.14	0.24	0.05
50	0.00	0.00	0.01	0.03	0.48	0.16	0.13	0.22	0.05
55	0.00	0.00	0.01	0.02	0.33	0.34	0.09	0.15	0.02
60	0.00	0.00	0.01	0.03	0.40	0.44	0.10	0.17	0.03
65	0.00	0.00	0.01	0.02	0.41	0.37	0.09	0.17	0.03
70	0.00	0.00	0.01	0.02	0.33	0.37	0.07	0.14	0.03
75	0.00	0.00	0.01	0.02	0.33	0.39	0.07	0.17	0.04
80	0.00	0.00	0.01	0.02	0.33	0.44	0.06	0.15	0.03
85	0.00	0.00	0.01	0.02	0.30	0.39	0.02	0.13	0.03
90	0.00	0.00	0.01	0.02	0.31	0.29	0.06	0.13	0.03

180 °C, average yield per fraction [mg per 1000 mg initial biomass]

t [min]	Fuc	Rha	Ara	Gal	Glc	Xyl	Man	GalA	GlcA
5	0.15	1.31	3.21	5.74	10.88	27.41	4.69	9.58	2.30
10	0.09	1.81	2.35	8.60	9.65	50.89	9.96	10.50	1.15
15	0.01	0.38	0.29	2.11	6.17	17.30	2.87	3.10	0.30
20	0.00	0.14	0.17	0.76	5.93	8.92	1.50	1.36	0.19
25	0.00	0.09	0.06	0.45	5.24	6.54	0.56	0.79	0.07
30	0.00	0.07	0.05	0.29	5.10	5.12	0.31	0.58	0.08
35	0.00	0.05	0.03	0.16	5.06	3.63	0.25	0.45	0.07
40	0.00	0.03	0.03	0.08	5.00	2.76	0.19	0.35	0.06
45	0.00	0.03	0.02	0.10	4.86	2.46	0.14	0.25	0.04
50	0.00	0.02	0.02	0.04	4.50	1.66	0.11	0.17	0.03
55	0.00	0.02	0.02	0.04	4.30	1.45	0.10	0.16	0.03
60	0.00	0.01	0.02	0.03	4.42	1.24	0.09	0.14	0.03
65	0.00	0.01	0.02	0.04	4.46	1.09	0.10	0.12	0.03
70	0.00	0.01	0.02	0.04	4.97	1.14	0.12	0.12	0.03
75	0.00	0.00	0.02	0.03	4.70	1.06	0.10	0.09	0.03
80	0.00	0.00	0.02	0.03	4.38	0.89	0.05	0.09	0.06
85	0.00	0.01	0.02	0.03	4.15	0.86	0.04	0.09	0.03
90	0.00	0.01	0.01	0.03	3.98	0.73	0.05	0.11	0.05

180 °C, std. deriv. [mg per 1000 mg initial biomass]

t [min]	Fuc	Rha	Ara	Gal	Glc	Xyl	Man	GalA	GlcA
5	0.10	0.73	0.82	4.48	4.29	13.06	2.97	3.90	0.75
10	0.06	0.68	0.70	6.47	2.65	9.98	4.59	4.56	0.53
15	0.02	0.08	0.06	1.78	2.16	3.95	1.16	0.57	0.06
20	0.01	0.09	0.09	0.67	2.89	1.93	0.62	0.17	0.11
25	0.01	0.07	0.04	0.46	2.68	1.87	0.36	0.08	0.04
30	0.00	0.05	0.03	0.29	2.69	1.51	0.19	0.08	0.04
35	0.00	0.04	0.02	0.10	2.86	1.30	0.18	0.08	0.05
40	0.00	0.04	0.02	0.08	2.96	0.78	0.14	0.05	0.05
45	0.00	0.04	0.01	0.04	2.57	1.10	0.10	0.08	0.04
50	0.00	0.02	0.01	0.03	2.46	0.64	0.10	0.05	0.03
55	0.00	0.02	0.01	0.03	2.30	0.69	0.10	0.06	0.03
60	0.00	0.02	0.01	0.02	2.44	0.55	0.09	0.07	0.03
65	0.00	0.01	0.00	0.02	2.49	0.54	0.07	0.03	0.03
70	0.00	0.01	0.01	0.02	2.93	0.54	0.09	0.05	0.03
75	0.00	0.00	0.00	0.02	2.63	0.55	0.07	0.07	0.02
80	0.00	0.00	0.00	0.02	2.56	0.58	0.06	0.04	0.02
85	0.00	0.01	0.01	0.02	2.22	0.51	0.05	0.03	0.02
90	0.00	0.01	0.01	0.02	2.28	0.48	0.06	0.02	0.01

8.8 Time resolved sugar yields, miscanthus

160 °C, average yield per fraction [mg per 1000 mg initial biomass]

t [min]	Fuc	Rha	Ara	Gal	Glc	Xyl	Man	GalA	GlcA
5	0.07	0.02	1.79	0.54	5.16	1.24	0.44	1.20	0.56
10	0.06	0.41	1.91	0.88	1.31	3.40	0.44	4.68	1.86
15	0.00	0.29	0.55	0.82	0.57	5.33	0.74	5.22	1.77
20	0.00	0.18	0.13	0.55	0.36	5.20	0.66	3.91	1.07
25	0.00	0.12	0.07	0.37	0.20	5.80	0.56	2.76	0.66
30	0.00	0.08	0.06	0.28	0.21	5.53	0.58	2.08	0.45
35	0.00	0.05	0.03	0.22	0.18	4.33	0.53	1.61	0.31
40	0.00	0.03	0.03	0.13	0.18	3.21	0.47	1.32	0.25
45	0.00	0.02	0.02	0.13	0.14	2.51	0.31	1.06	0.18
50	0.00	0.01	0.02	0.11	0.16	2.29	0.29	0.92	0.15
55	0.00	0.01	0.02	0.11	0.17	2.16	0.29	0.95	0.16
60	0.00	0.01	0.02	0.09	0.16	1.97	0.25	0.84	0.14
65	0.00	0.01	0.02	0.08	0.15	1.60	0.19	0.68	0.12
70	0.00	0.01	0.02	0.07	0.15	1.49	0.19	0.60	0.12
75	0.00	0.01	0.01	0.05	0.13	1.23	0.08	0.52	0.10
80	0.00	0.00	0.01	0.05	0.13	1.25	0.09	0.47	0.10
85	0.00	0.00	0.01	0.04	0.12	1.05	0.03	0.42	0.08
90	0.00	0.00	0.01	0.03	0.12	0.91	0.06	0.36	0.08

160 °C, std. deriv. [mg per 1000 mg initial biomass]

t [min]	Fuc	Rha	Ara	Gal	Glc	Xyl	Man	GalA	GlcA
5	0.00	0.57	0.84	0.16	0.27	9.09	1.78	1.80	1.20
10	0.00	0.23	0.29	0.66	0.71	20.69	3.37	2.42	0.14
15	0.00	0.00	0.46	0.25	0.28	3.21	0.70	0.13	0.09
20	0.00	0.00	0.07	0.06	0.38	2.05	0.38	0.41	0.13
25	0.00	0.00	0.08	0.04	0.39	1.01	0.50	0.19	0.04
30	0.00	0.00	0.05	0.04	0.44	1.37	0.36	0.17	0.04
35	0.00	0.00	0.05	0.03	0.46	1.47	0.27	0.18	0.04
40	0.00	0.00	0.03	0.03	0.53	1.28	0.24	0.11	0.03
45	0.00	0.00	0.03	0.03	0.47	1.02	0.22	0.08	0.03
50	0.00	0.00	0.03	0.03	0.51	0.75	0.16	0.05	0.04
55	0.00	0.00	0.02	0.03	0.53	0.67	0.17	0.05	0.02
60	0.00	0.00	0.02	0.03	0.55	0.71	0.10	0.05	0.03
65	0.00	0.00	0.02	0.03	0.55	0.47	0.02	0.04	0.03
70	0.00	0.00	0.02	0.03	0.46	0.43	0.02	0.04	0.03
75	0.00	0.00	0.02	0.00	0.51	0.39	0.02	0.06	0.03
80	0.00	0.00	0.02	0.00	0.52	0.35	0.01	0.04	0.03
85	0.00	0.00	0.02	0.00	0.54	0.29	0.02	0.04	0.03
90	0.00	0.00	0.02	0.00	0.43	0.22	0.01	0.04	0.03